THE STUDY OF CREEP IN MACHINE ELEMENTS USING FINITE ELEMENT METHODS

by

MARC ANTON WEBER
B.Sc. (Eng)(Mech) UCT

A thesis submitted in partial fulfillment of the requirements for the degree of Master of Science in Engineering

Department of Mechanical Engineering

University of Cape Town

November 1989

DECLARATION

This is to certify that the results, calculations and any other work presented in this thesis are essentially my own work, and that no part of it has been submitted for a degree at any other university.

Signed by candidate

November 1989

Dedication

I would like to dedicate this thesis to my parents, my brother and my sister, who stood behind me all the way, and without whose support I would never have made it this far.

ACKNOWLEDGEMENTS

I acknowledge, and sincerely appreciate, the help of the following people :

Professor R K Penny, under whose supervision this thesis was conducted, for his interest and support,

the CSIR's Division of Materials Science and Technology, for their support and collaboration,

fellow colleagues at the Center for Research into Computational and Applied Mechanics and the Department of Mechanical Engineering, for their willing assistance,

Helmutt Bowles, for fruitful discussions, and

the Foundation for Research and Development for their financial assistance.

ABSTRACT

In this thesis a simplified analysis procedure is developed, in which creep laws are decoupled from damage laws, for the purpose of constructing methods of use in the early stages of high temperature design. The procedure is based on the creep and damage laws proposed by Kachanov and Rabotnov. The creep laws are normalised with respect to a convenient normalising stress. As a consequence of this normalisation, the dependence of the creep law on the stress constant, the time and temperature functions, and the actual load level is removed. In addition, if the reference stress of the component is chosen as the normalising stress, the creep law becomes insensitive to the stress exponent. The non-dimensional creep laws are then implemented in a standard finite element scheme, from which the results of a stationary state creep analysis are then in non-dimensional form. In order to estimate rupture times, the maximum stationary stresses in a component are used together with the damage laws. Conservative failure criteria are derived from the creep and damage laws to extend the method to residual life assessment and damage monitoring. The procedure is illustrated and tested against simple examples and case studies.

TABLE OF CONTENTS

NOMENCLATURE

A, K, B	Creep, damage constant
E	Elastic constant (modulus)
m, k	Creep, damage stress exponent
r, p	Damage exponent
n	Time exponent
a	Hardening parameter
t, τ	Real, distorted time
$\dot{(\ )}$	Differentiation w. r. t. distorted time
ω	Damage
σ, Σ	Dimensional, non-dimensional stress
ε, λ	Strain, normalised strain
u, U	Dimensional, non-dimensional displacement
σ_o, ε_o	Normalising stress, strain
$\bar{\sigma}$, $\bar{\varepsilon}$	Reference stress, strain
α	Reference stress parameter
γ	Upper bound deformation parameter
Γ	Life fraction parameter
R_i	i^{th} failure criterion factor

Subscripts

c	Creep strain component
cd	Coupled creep/damage strain component
el	Elastic value
ss	Stationary value
N	Nominal value
β	Hayhurst equivalent stress
th, sh, mh	Time, strain, mixed hardening

Superscripts

r, z	r, z component
I	Maximum principal value
*	von Mises equivalent value

1 INTRODUCTION

Ever since the first successful steam engine was build by James Watt at the end of the eighteenth century, the operating temperatures of man's engines and industrial plants have continually increased. Engineering materials working at these extreme temperatures do not behave in the normal linear-elastic manner, and the problem of *Creeping Materials* was encountered. This problem could not be solved by the usual elastic material models and new theories had to be developed.

In the beginning of the twentieth century various empirical material models were developed through which simple problems could be solved analytically. In the latter half of the century, it was the development of the computer which extended the earlier methods to more complex problems. A great deal of empiricism remained however, while the solution schemes grew in complexity. The question can be asked whether this empiricism is compatible with the developments in numerical modeling techniques : rarely are the so-called *material constants* in the *constitutive relationships* known exactly. Nor are the operating temperature and loading patterns fixed. Nevertheless, the structure must be analysed, and because the input to the analysis is uncertain, the analysis will be run and re-run as more information becomes available. In many organisation this puts a large strain on the available computing facilities.

This has created the need for a creep analysis procedure which is independent of, or insensitive to inputs like material parameters and loads, yet which has rigour underlying its simplicity.

PROBLEM STATEMENT

The objective of this work is to develop a creep analysis procedure which simplifies the current methods. The method must be be based on rigour, and acceptable to the current knowledge about creep behaviour. The procedure must be able to predict creep deformations, creep rupture and remaining life, and must be able to do so with the minimum number of computer simulations. The information from the computer

simulation must be available to the user without having to re-run the simulation. Last, but not least, the procedure must complement current design practice, and must form part of the acceptable design procedure.

This thesis first surveys the literature on which the method is based. The theory of the method is developed in Sections 3 and 4. The procedure itself is described and discussed in Sections 5 and 6. The method is applied in Section 7 to some simple problems for which previous solutions exist. The method is shown to be *applicable* in three short case studies in Section 8. Lastly, some conclusions are drawn in Section 9. Appendix D reflects the results to the courses that were completed as a co-requirement towards an M.Sc. Degree.

2 SURVEY OF THE LITERATURE

2.1 OUTLINE OF THE PROBLEM

A component subjected to small loads at ambient temperatures will deform elastically. This means that the original size of the component will be recovered when the load is removed. However, if the applied load is high enough, part of the deformations become permanent and cannot be recovered when the load is removed. This is known as a *permanent set*, and the component is said to behave *plastically* (Hill,1964). The criterion which determines whether plasticity behaviour has been reached is a so-called *yield criterion*. A number of such yield criteria have been postulated, notably the *Tresca criterion*, and the more widely used *von Mises criterion*. The implication of these criteria is that a component will behave elastically as long as the stresses in the component do not exceed the yield criterion, and that no plastic (or permanent) strains will then be present after the load is removed.

It has been observed however, that if the temperature is higher than ambient then some materials show a tendency to develop permanent deformations even though the stresses in the component are below any known yield criterion. The permanent deformations accumulate with time, until they became excessive and sometimes a component can fail due to mismatch. To compound the problem, it has been observed that components also fail by sudden rupture after a finite time and strain accumulation. This problem became known as *Creep*. From a study of simple tensile specimens at elevated temperatures it is possible to obtain so-called *creep curves* which show the creep deformations with time. One such typical creep curve is shown in Figure 2.1.

The creep curve shows three well-defined regions :

- the *primary stage* in which the deformation rate decreases with time,
- the *secondary stage* during which the deformation rate is nominally constant, and
- the *tertiary stage* in which the deformation rate increases rapidly until final rupture occurs.

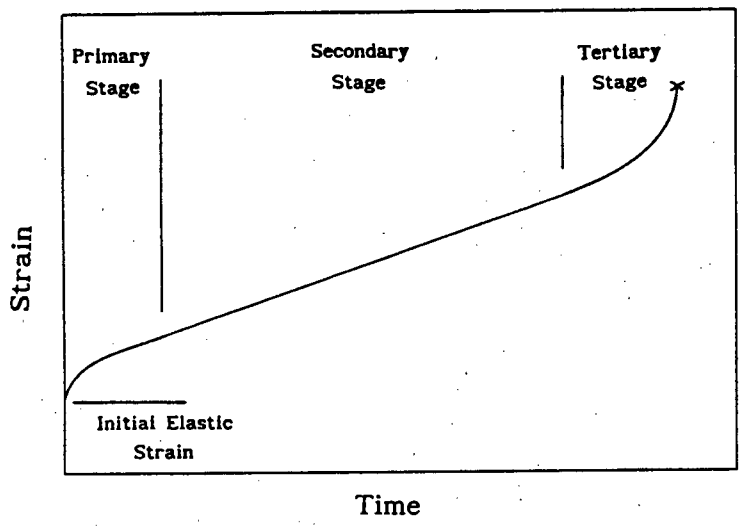

Figure 2.1 : Generalised creep curve

At the turn of the century, the first studies of this phenomenon were begun (Andrade,1910), and the subject has been extensively covered in subsequent years (Norton,1929; Sully,1949; Kennedy,1962; Hult,1966; Rabotnov,1969; Penny and Marriott,1971; Kraus,1980). Due to the complexity of the creep process, the problem remains however, and has in fact become of major importance in those industries where there is a continuing drive towards higher operating temperatures : gas turbine engines, chemical and power generation plants, etcetera.

Worthwhile strides have been made in the metallurgical field and many high temperature alloys have been developed which can withstand higher temperatures whilst limiting the creep strain accumulation and extending the useful life of the component. (Superalloys II,1984).

At the same time, mathematical models to simulate the creep behaviour have been developed and these are used extensively in the design of new components where creep is thought to be a possible cause of failure. The models take the form of constitutive relationships, and range from fairly simple empirical equations showing the relationship between strain accumulation, stress, temperature, and time for uniaxial specimens under steady loading and temperature to increasingly complex relationships, applicable to multiaxial stress and strain states and which include all the aspects of the creep process.

The early efforts aimed at deriving constitutive relationships that reproduced the observed behaviour in tensile creep tests. They disregarded the tertiary stage and concentrated on strain accumulation. Initially, it was assumed that the creep deformation under constant uniaxial stress depends on stress, time and temperature. The most general creep law is therefore (Penny and Marriott,1971) :

$$\varepsilon_c = f(\sigma,t,T) \tag{2.1}$$

In order to simplify this equation, it is useful to separate the variables as follows :

$$\varepsilon_c = f_1(\sigma)\ f_2(t)\ f_3(T) \tag{2.2}$$

The separate stress and time functions have been accepted in most of the work on creep. Much less research has centered on the temperature function and some workers (Dorn,1955) have combined the time and temperature functions.

2.2 THE STRESS FUNCTION

The function $f_1(\sigma)$ has been chosen in many different ways, most of which are empirical. Kennedy (1962) gives a full summary. The most common forms are given below :

(i)	$f_1 = K\ \sigma^m$	Norton (1929)
(ii)	$f_1 = A\ \sinh(\sigma/\sigma_o)$	McVetty (1943)
(iii)	$f_1 = B\ \left[\exp(\sigma/\sigma_o) - 1\right]$	Soderberg (1936)
(iv)	$f_1 = C\ \exp(\sigma/\sigma_o)$	Dorn (1955)
(v)	$f_1 = D_1\ \sigma^{m1} + D_2\ \sigma^{m2}$	Johnson et al. (1963)
(vi)	$f_1 = A\ \left[\sinh(\sigma/\sigma_o)\right]^m$	Garofalo (1965)

where K, A, B, C, D_1, D_2, m, m_1, and m_2 are material constants.

The most commonly used stress function is the power law proposed by Norton. Its simplicity in application to stress analysis is perhaps the main reason for this, but one of the main advantages over the other formulations is that $f_1(\sigma) = K\sigma^m$ has the same *shape* regardless of the magnitude of stress. This means that under proportional load changes the stress distributions are independent of the magnitude of the load (Penny and Marriott,1971).

Dorn (1955) has shown that the power law fits experimental data best at low stresses while the exponential laws are more accurate at high stresses. All the laws approximate to the same shape however, and it has been argued (Penny and Marriott,1971) that the power law should be chosen from expedience as it will approach the other laws to within the usual limits of experimental scatter.

2.3 THE TIME FUNCTION

Many different time functions have been proposed, most of which are based on empiricism. The most notable are :

(i)	$f_2 = \left(1 + b\, t^{1/3}\right) \exp(kt - 1)$	Andrade (1910)
(ii)	$f_2 = F\, t^n \quad (\frac{1}{2} \leq n \leq \frac{1}{3}$ usually)	Bailey (1935)
(iii)	$f_2 = G\left(1 - e^{-at}\right) + Ht$	McVetty (1943)
(iv)	$f_2 = \sum a_i\, t^{ni}$	Graham and Walles (1955)

where b, k, F, n, G, a, H are material constants.

These empirical relations are based on observations from steady load experimental data, and should be used with caution when used outside the context of the experiment, especially when dealing with varying stress histories.

2.4 THE TEMPERATURE FUNCTION

The effect of temperature is twofold. An increase in temperature will affect material constants like Young's modulus and the constants m and K in Norton's power law. The second effect of temperature changes is to alter the material structure.

If T_m is the absolute melting temperature, it is found that creep below $0.4T_m$ in most metals is governed by a slip process, similar to instantaneous plasticity. Dislocations encounter obstacles in the form of grain boundaries and this causes continual strain hardening and decreasing strain rates (Penny and Marriott,1971).

At temperatures above $0.4T_m$ the increased thermal activity provides dislocations with higher mobility and allows them to climb over obstacles. In the temperature region of $0.4T_m$ to $0.5T_m$ this is possible by a process known as *cross slip* involving the screw component of dislocations (Hayhurst,1970). At temperatures above $0.5T_m$ temperature-induced diffusion allows recovery, causing dislocations to climb over obstacles by diffusing away from them. This mechanism can destroy the effects of strain hardening and the secondary stage is reached when strain hardening and recovery are balanced (Sully,1949).

The difficulty is to quantify recovery processes. The most notable work in this field is by Dorn (1955) who suggested that temperature dependence should appear in the form, $e^{-Q/RT}$, where Q is the activation energy, R is Boltzmann's constant and T is the absolute temperature. This form is fundamental to all rate processes. Dorn found that creep data at various temperatures can all be plotted by a single curve if creep strain is plotted against a single parameter, $t\, e^{-Q/RT}$. Figure 2.2 shows a reproduction of Dorn's results.

A generalised expression for the creep law is then :

$$\varepsilon_c = f(t\, e^{-Q/RT})\, f_1(\sigma) \qquad (2.3)$$

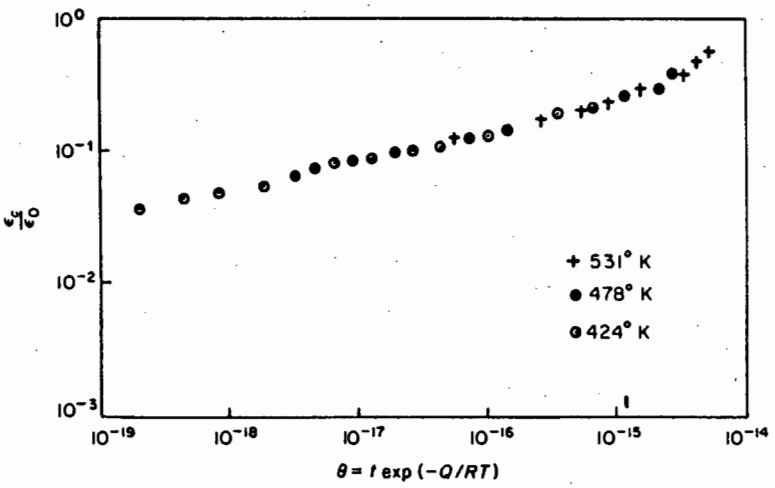

Figure 2.2 : Creep curves of aluminium at various temperatures and constant stress (Dorn,1955)

The function f can be assumed to be a power law (Penny and Marriott,1971) :

$$\varepsilon_c = (t\ e^{-Q/RT})^n\ f_1(\sigma) \qquad (2.4)$$

This formulation is particularly useful. It is separable in the form of equation (2.2) and is acceptable in the light of basic studies of uniaxial creep behaviour. In separated form the equation is :

$$\varepsilon_c = K\ e^{-Q/RT}\ \sigma^m\ t^n \qquad (2.5)$$

2.5 VARIABLE STRESS CREEP

Equation (2.5) is derived from the observation of creep data from constant load (or stress) and constant temperature uniaxial creep tests. The effect of variable loading under creep conditions is to produce complex deformation behaviour. Many theories, derived mainly from hypothetical considerations, have attempted to describe this behaviour. However, they predict widely different behaviour for the same stress histories. Obviously not all hypotheses can be correct, and experimental evidence shows that no theory is completely satisfactory. To list all proposed theories would be beyond the scope of this work, and only the *Time Hardening*, *Strain Hardening*, and *Mixed Hardening* theories will be discussed here. A more complete discussion can be

found in Penny and Marriott (1971) and Kraus (1980).

2.5.1 TIME HARDENING

The simplest of the hardening hypotheses is the time hardening hypothesis. The creep strain rate is assumed to be a function of stress, time and temperature :

$$\frac{d\varepsilon_c}{dt} = f(\sigma,t,T) \tag{2.6}$$

Figure 2.3 from Penny and Marriott (1971) summarises time hardening behaviour under variable stress conditions. Equation (2.6) can be separated for isothermal conditions :

$$\frac{d\varepsilon_c}{dt} = f_1(\sigma)\,\frac{d}{dt}\left[f_2(t)\right]\,f_3(T) \tag{2.7}$$

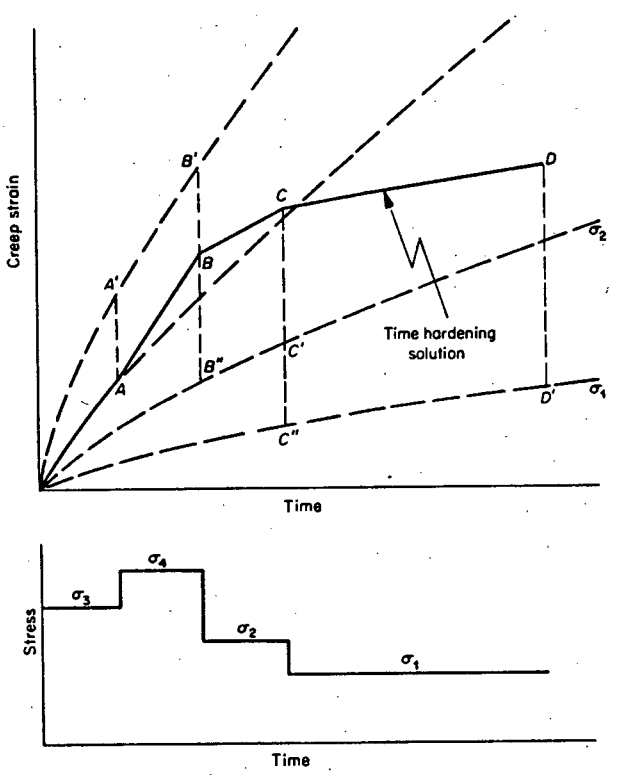

Figure 2.3 : Strain history predicted from Time Hardening theory (Penny and Marriott,1971)

2.5.2 STRAIN HARDENING

This hypothesis assumes the creep strain rate to be a function of stress, temperature, and accumulated creep strain :

$$\frac{d\varepsilon_c}{dt} = g(\sigma,\varepsilon_c,T) \tag{2.7}$$

or in separated form, for constant temperature conditions :

$$\frac{d\varepsilon_c}{dt} = g_1(\sigma)\ g_2(\varepsilon_c)\ g_3(T) \tag{2.8}$$

Equation (2.8) can be simplified if g_1 and g_2 are assumed to be of the form :

$$g_1(\sigma) = n\ K^{1/n}\ e^{-Q/nRT}\ \sigma^{m/n} \tag{2.9}$$

$$g_2(\varepsilon_c) = \varepsilon_c^{(n-1)/n} \tag{2.10}$$

where n is the time exponent derived from experimental data. Then, substituting (2.9) and (2.10) into (2.8) :

$$\frac{d\varepsilon_c}{dt} = n\ K^{1/n}\ e^{-Q/nRT}\ \sigma^{m/n}\ \varepsilon_c^{(n-1)/n} \tag{2.11}$$

Strain hardening behaviour is summarised in Figure 2.4 from Penny and Marriott (1971).

2.5.3 MIXED HARDENING

Neither the time- nor the strain hardening hypothesis tend to give completely satisfactorily results over a range of materials. A compromise in the form of an intermediate theory between strain- and time hardening has been proposed by Johnson et al. (1963). The creep strain rate is a function of strain,

time, temperature and accumulated creep strain :

$$\frac{d\varepsilon_c}{dt} = h(\sigma, t, T, \varepsilon_c) \tag{2.12}$$

which can be separated for isothermal conditions :

$$\frac{d\varepsilon_c}{dt} = h_1(\sigma) \frac{d}{dt}\left[h_2(t)\right] h_3(T)\, h_4(\varepsilon_c) \tag{2.13}$$

Payne (1979) proposed a mixed hardening law of form :

$$\frac{d\varepsilon_c}{dt} = n\, K^a\, e^{-Qa/RT}\, \sigma^{ma}\, t^{na-1}\, \varepsilon_c^{1-a} \tag{2.14}$$

This formulation is particularly useful because for a = 1 the time hardening formulation results while for a = 1/n the strain hardening formulation follows. Figure 2.5 from Penny and Marriott (1971) shows creep strain behaviour for a variable stress history when mixed hardening is assumed.

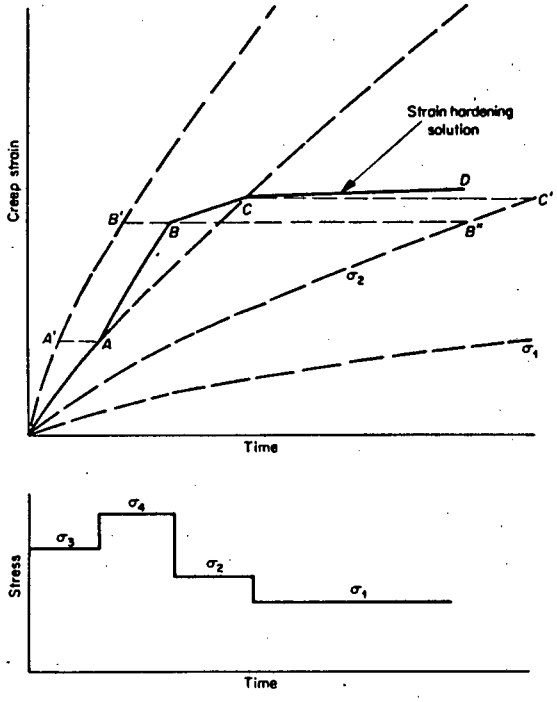

Figure 2.4 : Strain history predicted from Strain Hardening theory

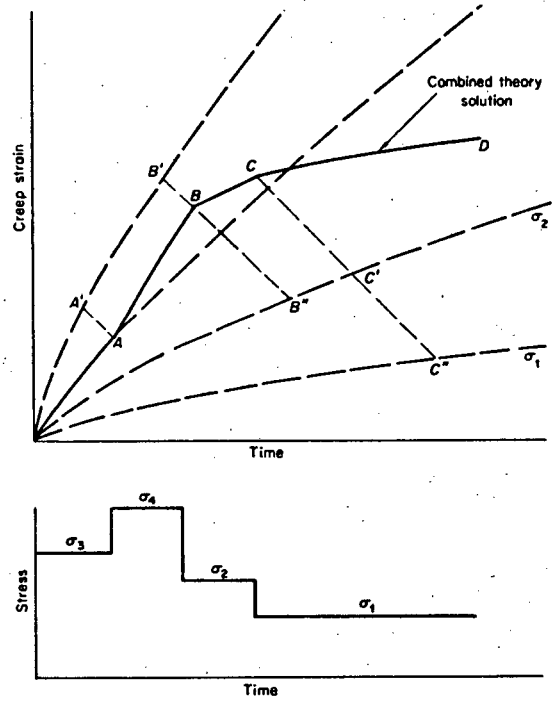

Figure 2.5 : Strain history predicted from Mixed Hardening theory

2.6 MULTIAXIAL STRESS STATES

Mathematical models of material behaviour are useful only when they can be used to predict the stress and strain behaviour of complicated geometries under complex loads for which it would be too expensive to build prototypes. The constitutive relationships derived above for uniaxial stress states have to be extended to multiaxial stress states.

Most of the work in creep is analogous to the development of the theories of instantaneous plasticity. This theory uses the concept of an *equivalent stress*, caused by the multiaxial stress system, which produces a certain *magnitude* of strain. In creep an equivalent stress, σ^*, and an equivalent strain increment, $\Delta\varepsilon^*$, are defined which represent the combined action of a stress system σ_{ij} in producing a corresponding strain increment system $\Delta\varepsilon_{ij}$. For a Norton power relationship :

$$\Delta\varepsilon^* = K\,\sigma^{*m}\,\Delta t \tag{2.15}$$

and

$$\sigma^* = \sigma^*(\sigma_x, \sigma_y, \sigma_z, \sigma_{xy}, \sigma_{xz}, \sigma_{yz}) \tag{2.16}$$

$$\Delta\varepsilon^* = \Delta\varepsilon^*(\Delta\varepsilon_x, \Delta\varepsilon_y, \Delta\varepsilon_z, \Delta\varepsilon_{xy}, \Delta\varepsilon_{xz}, \Delta\varepsilon_{yz}) \tag{2.17}$$

Analogous to instantaneous plasticity theory, the equivalent stress σ^* is usually chosen to take the form of the von Mises yield criterion.

A *Flow Rule* determines how the deformation is distributed between the three directions of the strain system. It is convenient to derive the flow rule from a *Plastic Potential Function*, $\psi(\sigma_{ij})$, which is a scalar function of stress. The creep strain increment is expressed in the form (Prandtl,1924; Drucker,1967) :

$$d\varepsilon_{ij,c} = \frac{d\psi}{d\sigma_{ij}}\,d\lambda \tag{2.18}$$

where $d\lambda$ is a constant which can vary during a load history and is related to the equivalent strain increment $d\varepsilon^*$ by (Hill,1964) :

$$d\lambda = \frac{d\varepsilon^*}{\sqrt{\frac{2}{3}\frac{d\psi}{d\sigma_{mn}}\frac{d\psi}{d\sigma_{mn}}}} \tag{2.19}$$

Isotropic multiaxial creep laws will be derived later.

2.7 CREEP RUPTURE

The constitutive relationships derived above describe the creep strain behaviour during the primary and secondary stages of the creep process. They have no means however of predicting rupture times or rupture strains, as they would allow creep strains to accumulate indefinitely. Creep, of course, does not continue indefinitely. At some finite strain and time rupture will occur, and in the design of components it is the possibility of failure due to sudden rupture which is more serious than the failure due to excessive deformation. It is for this reason that experimental work is mostly concerned with the measurement of rupture times, and less with deflection measurement.

The common form of representing rupture data is by plotting logarithms of constant uniaxial stress versus logarithms of time to rupture for different values of constant temperature. This is not ideal since most design problems concern multiaxial states of varying stress and/or temperatures. However, most testing facilities would not be able to cope with experimental work of such complexity in a field where even simple experiments show a considerable amount of scatter. Realising this, the limited data must be used to solve three important problems, namely :

- rupture prediction under conditions of variable stress and temperature,
- rupture prediction in multiaxial stress systems from uniaxial data, and
- rupture prediction of long term service conditions from short term experimental data.

This work is primarily concerned with the first two problems. It will be beneficial first to describe briefly the mechanisms of creep rupture.

2.7.1 MECHANISMS OF CREEP RUPTURE

Two distinct modes of creep rupture exist. At high stress and low temperature the deformation is ductile. Fracture occurs after large deformations and is similar to failure due to extensive plastic deformation. The primary cause of deformation is slip due to the movement of dislocations. Grain boundaries form barriers against continued slip (Sully,1949), and the major components of deformation occur within the grains. Final fracture is caused by the propagation of transgranular cracks inwards from the surface. This type of creep behaviour is characterised by large ductile deformations in all stages of creep and by transgranular cracks.

At higher temperatures, usually above half the melting temperature, slip is accompanied by diffusion due to the increased thermal activation energy. This diffusion causes grain boundaries to become a source of weakness rather than strength, and sliding on the grain boundaries occurs. The most important effect of grain boundary sliding is the formation of voids. These voids may be formed at the intersection of grain boundaries, a mechanism which requires a certain minimum amount of stress. Voids can also be formed at ledges in the grain boundary. These ledges open up to form cavities under the action of sliding at very low stresses. The cavities will grow due to the diffusion process. This leads to a gradual degradation of the material, and to final brittle rupture when the voids have enlarged to macrocracks which are governed by fracture mechanics behaviour (Rabotnov,1969).

It has been observed that voids tend to concentrate at grain boundaries normal to the applied tensile stress. It can be assumed from this that the criterion for rupture is probably related to the maximum tensile stress in uniaxial states (Penny and Marriott,1971) and the maximum principal stress in multiaxial states (Hayhurst,1970). This mode of creep rupture is characterised by small deformations in the primary and secondary stages of creep, and by brittle behaviour with cracks initiated within the material. Figure 2.6 shows a generalised representation of the two failure modes.

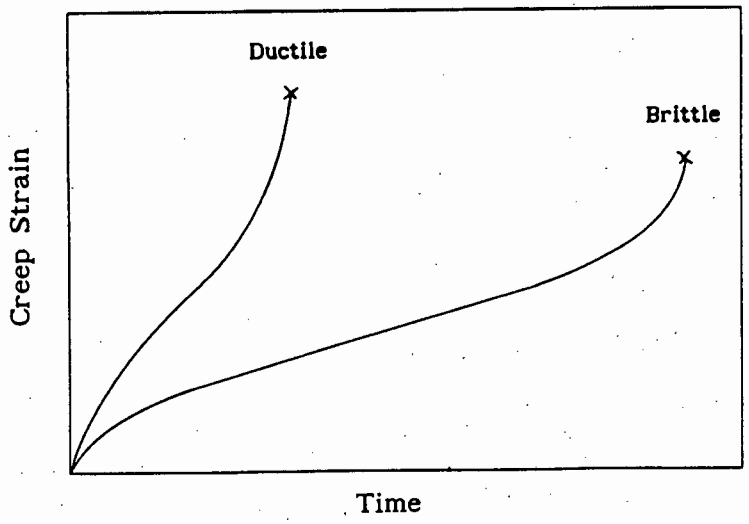

Figure 2.6 : Creep curves for ductile and brittle failure modes

The fact that different rupture mechanisms exist at different combinations of stress and temperature implies that it would be too restricting to assume that a linear relationship exists between log(stress) and log (rupture). In fact, most experiments over wide ranges of stress and temperature confirm that this is not the case. Many log(stress) versus log(rupture time) curves show a kink in the curve corresponding to separate ductile and brittle behaviour (Greenwood et al.,1980; Needham and Gladman,1980). This is shown in Figure 2.7 (from Needham and Gladman). Some long term creep curves show a point of inflexion which would confirm that it is unreasonable to expect a finite life at zero stress (Wickens et al.,1980; Bennewitz,1963).

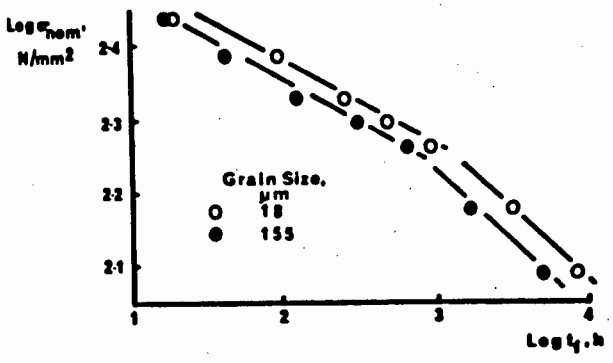

Figure 2.7 : Plot of log(stress) vs log(rupture time) for Cr-Mo steel (Needham and Gladman,1980)

It is outside the scope of the present work to discuss this problem in detail except to note that constitutive models using *constant* material parameters will apply only over limited ranges of stress and temperature and that care must be taken when extrapolating from short term, high stress data to long term, low stress design parameters. A more detailed discussion of the problem can be found in Penny and Marriott (1971).

2.7.2 VARIABLE STRESS HISTORIES

When a uniaxial component under steady loads and temperatures is designed, it is relatively easy to perform rupture tests in order to find the rupture and deformation characteristics. However, when a component is subjected to varying loads and temperatures, experimental verification becomes difficult and expensive, especially if the stress and/or temperature histories are not known exactly. A practical approach to this problem was proposed by Robinson (1938), and is known as the *Life Fraction Rule*. No attempt to justify the method was made, but, in the absence of other methods, it has proven to be reliable in the case of varying temperature (Goldhoff,1965), but not as successful in the case of varying stress histories (Woodford,1973).

The method postulates that the amount of creep damage under steady conditions is proportional to the fraction of the total rupture life under these conditions. *Creep Damage* is a quantification of the amount of material degradation in the component. The Life Fraction Rule then follows :

$$\omega_1 = \frac{t_1}{t_{R1}} \tag{2.20}$$

where ω_1 is the damage under conditions σ_1 and T_1,
t_1 is the period spend at σ_1 and T_1, and
t_{R1} is the rupture life for σ_1 and T_1.

A second amount of damage ω_2 is incurred during period t_2 at stress σ_2 and temperature T_2 for which the rupture life is t_{R2} :

$$\omega_2 = \frac{t_2}{t_{R2}} \tag{2.21}$$

It is now assumed that all amounts of damage are independent of each other. The total damage ω is calculated by summing the damage from each period :

$$\omega = \sum \omega_1 = \sum \frac{t_1}{t_{R1}} \tag{2.22}$$

Rupture occurs when the total damage is equal to one.

The Life Fraction Rule has been refined for brittle fracture by Kachanov (1958), and extended by Rabotnov (1969). Kachanov also approached the problem of rupture prediction under variable loads from the viewpoint that the material is continually degrading. He tried to link the quantification of this degradation, the creep damage, to the rupture mechanism present in the material, namely the growth of voids. Damage is defined as the reduction in the amount of material available for carrying the applied load. Therefore the nominal stress increases, causing local stress redistribution and this explains the accelerated strain rates in the tertiary section of the creep curve. To explain the concept, consider a tensile specimen of initial cross-section A_o and at constant load P. The growth of voids along grain boundaries normal to the tensile load causes the load carrying area to reduce with time. Kachanov proposed that the area, A_t, after some time t is :

$$A_t = A_o(1 - \omega) \tag{2.23}$$

The initial stress σ_o at the cross-section caused by the load is :

$$\sigma_o = \frac{P}{A_o} \tag{2.24}$$

After time t, the stress σ_t will have increased :

$$\sigma_t = \frac{P}{A_t} = \frac{P}{A_o(1-\omega)} = \frac{\sigma_o}{(1-\omega)} \tag{2.25}$$

Kachanov assumed that the time variation of damage is a function of stress, and in particular a power law was assumed to correspond with the usual Norton power law for creep deformation :

$$\frac{d\omega}{dt} = B\,\sigma_t^k \tag{2.26}$$

where B and k are material constants dependent on temperature. Substituting equation (2.25) into (2.26) :

$$\frac{d\omega}{dt} = B\left[\frac{\sigma_\circ}{(1-\omega)}\right]^k \tag{2.27}$$

subject to the conditions that $\omega = 0$ at $t = 0$ and $\omega = 1$ at $t = t_R$.

For constant stress (2.27) integrates to give the rupture life t_{Ro} at steady stress $\sigma_\circ$:

$$t_{Ro} = \frac{1}{B(1+k)\sigma_\circ^k} \tag{2.28}$$

Under variable nominal stress $\sigma_\circ(t)$, integration of (2.27) gives :

$$\int_0^1 (1-\omega)^k\, d\omega = B\int_0^{t_R} [\sigma_\circ(t)]^k\, dt \tag{2.29}$$

where t_R is the rupture life under varying stress, whence

$$\int_0^{t_R} B(1+k)[\sigma_\circ(t)]^k\, dt = 1 \tag{2.30}$$

From (2.30), the time to rupture t_{Ro} due to a steady stress of $\sigma_\circ(t)$ throughout the life is :

$$t_{Ro} = \frac{1}{B(1+k)[\sigma_\circ(t)]^k} \tag{2.31}$$

Substituting (2.31) into (2.30) :

$$\int_0^{t_R} \frac{1}{t_{Ro}}\, dt = 1 \qquad (2.32)$$

which is the Life Fraction Rule in its continuous integral form.

Kachanov's theory predicts a straight line plot of log(stress) versus log(rupture time). This makes the theory useful when considering problems over well-defined stress and temperature regions.

The theory was further refined by Rabotnov (1969) who coupled the material degradation equations with the strain accumulation equations :

$$\frac{d\varepsilon_c}{dt} = n\, A\, \frac{\sigma_N^m}{(1-\omega)^p}\, t^{n-1} \qquad (2.33)$$

and

$$\frac{d\omega}{dt} = n\, B\, \frac{\sigma_N^k}{(1-\omega)^r}\, t^{n-1} \qquad (2.34)$$

where A, B, n, m, k, r, and p are material constants dependent on temperature and σ_N is the nominal stress. Rabotnov's method will be used in this work, and will be discussed in greater depth later.

Continuum damage concepts in the modeling of material degradation have been extended into other fields, notably that of fatigue and creep-fatigue interaction (Chaboche,1988; Bogdanoff and Kozin,1984). These models are however of increasing complexity and are not compatible with the objects of this work.

The Kachanov/Rabotnov postulates can be extended to multiaxial states of stress and strain as will be shown in a later section. They can thus be used to solve general problems involving both varying loads and temperatures as well as complex geometries. Its drawback is however that the constitutive model is highly stress sensitive whilst also predicting a large amount of

stress redistribution throughout the life of the component. As a result powerful computers are required to implement the model successfully into a structural analysis program. Nevertheless the method has been used with success in both finite difference and finite element type structural analysis programs (Hayhurst,1970; Payne,1979; Sieburg,1989).

A second, far simpler approach to predicting rupture in complex geometries is the *Reference Stress Method.* This method results from attempts to relate component behaviour to a single tensile test (Soderberg,1941). Schulte (1951) noted that at certain points within a beam cross-section the elastic and stationary state stresses were identical. By performing a tensile test at this stress, which he assumed would remain constant with time, Schulte was able to make accurate predictions of beam deflections.

The *Reference Stress* was then defined as a representative stress level which links multiaxial component behaviour to uniaxial experiments. It was observed that the reference stress was insensitive to the creep exponent m (Mackenzie,1968). Finding the reference stress remained difficult as closed form solutions were required, until Sim (1968) proposed a method which accepted numerical solutions as well. This method, as well as a second method proposed by Sim, is described in detail in a later section.

The validity of the reference stress technique to predict component behaviour from uniaxial data has been shown using the energy theorem by Matsuda and Fujikawa (1980). The reference stress method has also been checked in a number of test programs (Kraus,1976; Hyde and Webster,1980; Henderson and Ferguson,1980). The reference stress technique was initially confined to constant loads and temperatures. However, through the use of time variation functions, the method has been extended to include varying stress and temperature histories (Penny and Marriott,1971).

The reference stress technique has also been used quite successfully in the prediction of rupture of components. The hypothesis here is that the deformations and rupture times of the simple tension test at the reference stress can be related to the deformations and rupture time of the full-scale component. The CEGB, for instance, has included the reference stress method in its code of practice, R5 (Ainsworth,1989). Other workers have noted however that analytically derived reference stresses may lead to conservative

rupture time estimates (Henderson and Ferguson,1980). This conservatism is of course preferable in the development of codes of practice.

2.8 FINITE ELEMENT METHODS

The *Finite Element Method* (FEM), originally developed for the structural analysis of complex geometries, has become one of the most powerful means of solving structural problems. It has gained acceptance in the structural engineering world mainly because of its ability to solve otherwise unsolvable problems and as a consequence of the rapid increases in computer power in recent years.

Several texts have been written on the Finite Element Method, notably by Zienkiwicz (1977). The initial linear-elastic solution capabilities of the method have been extended to solution schemes for non-linear problems such as plasticity and creep, as well as many other problems.

This work is not concerned with developments in FEM as the method is merely used as a solution scheme for creep problems. The method is therefore not discussed in detail, but for completeness a brief description of a typical creep solution scheme is given in Appendix A.

2.9 RESIDUAL LIFE ASSESSMENT

The prediction of the residual life of components which have been operating under creep conditions for extended periods has become a vital element of the structural analysis of power plant. This is the consequence of rapidly increasing replacement costs and all utilities' wish to avoid retiring components or plant unnecessarily. There are many examples of components which have been allowed to operate long beyond the intended life (Davidson et al.,1985). This has confirmed that codes of practice such as BS5500 and ASME are overly conservative. Nevertheless, components still have a limited life and the problem is to predict *safely* how long that life is.

One of the main difficulties of residual life predictions is that the state of material degradation in a component is highly dependent on the stress and

temperature history of the component. In the case of plant designed thirty or more years ago this information is often not available, or at least not complete. A number of methods have been developed to overcome this problem. Initially, a sample of the component was examined metallurgically and the extent of material degradation was determined from a quantative study of the cracks found (Penny,1974; Harth and Sherlock,1985). This method was unsatisfactory however, as it was semi-destructive, and samples could often not be taken from the high stress and high damage regions.

More recently, the technique of *replicas* has partially solved these shortcomings (Viswanathan,1985). Here a replica of the surface microstructure is taken and examined. The method is non-destructive, but can be used only to the surface microstructure. The very recent advances in non-destructive flaw detection (X-Ray fractography and holography) should be able to overcome these problems.

In the cases where the loading and temperature histories have been recorded, the usual approach is to use these histories together with some constitutive model that takes into account material degradation as well as previous experience. Different utilities have developed such programs (Cane et al., 1985; Iwadate et al.,1985; Simonen and Jaske,1985; Davidson et al.,1985; Mlynarski and Taler,1988; Seshadri,1988; Viswanathan et al.,1988), most of which are based on the use of computers. Utilities also perform actual prototype tests to verify life prediction programs (Hepworth and Williams,1987; Price and Alberry,1988; Gooch,1988). Of late however there has been a call to reduce the complexity of these programs, and also to use a uniform approach (Jaske,1985). Specifically, life prediction methods should be easy to use and should use parametric calculations. The results of these calculations can be summarised in a handbook of case studies to provide guidelines for applying life-assessment technology.

3 DERIVATION OF NORMALISED CREEP EQUATIONS

The design process is one which, ideally, follows a step-by-step path towards a final solution. The first, and probably most important, step is the *problem statement.* The problem statement will reflect how the designer (and designer here can mean a team) views the problem, and how he will set about solving it.

Any structural design problem involving creep and damage is by its very nature highly complex. The number of unknown parameters is usually large, and these will include uncertain loading and temperature patterns. During the initial design stages especially, the designer will not know the precise material behaviour, or may not have chosen a particular material yet. In the latter case the designer will want to know how different materials will affect the performance of the component, and thus make rational decisions on what material will have the best characteristics under the expected load and temperature patterns.

The first task facing the designer is to find bounds to the unknown parameters. In doing this he will draw on his intuition and experience, and will make some simplifying assumptions. The next step is to see how the unknown parameters affect the design. It would be pointless to spend great effort on determining the exact characteristics of a particular parameter if it is found later that this parameter has little influence on the design or, if the parameter itself is subject to high variability.

In most problems involving creep and damage, the shape of the component will be dictated by other factors. In the design of blades for turbine engines for instance, the geometry of the blade is governed by aerodynamic considerations. In pipework, the size of the pipe is dependent on the fluid flow and the thermodynamic aspects of the component. As a general rule, the designer will decide on a number of possible design solutions, and will want to discover how they behave under the expected loading before he enters the detailing stage. The objective of the exercise is to delete the obviously bad solutions and to improve on the better ones.

One approach would be to build prototypes, and to perform hardware tests on these models. This method is usually considered to be too expensive,

especially in the initial design stages. The current trend is to model the component numerically. This method requires the availability of powerful computers, but recent advances in this field have made this possible.

The most widely used tool in the field of numerical structural design is the Finite Element Method of analysis. This method, although time-saving when compared to earlier methods, still requires significant amounts of computing time, especially when the problem under consideration is complex and follows non-linear material behaviour. If also the loading is uncertain, then the required number of analyses, and therefore the total computing time may become unduly large.

The aim of the designer must be to limit as far as possible the number of computer analyses, and to make the best possible use of any data resulting from a single analysis. This objective is especially important if a range of materials (with a range of material behaviours) and a range of loadings are being analysed.

One possible way of achieving this is to parameterize the analysis, so that the data from a single analysis can be applied to a range of material responses and/or loading patterns.

If we limit our present approach to stationary state creep analyses, then the usual creep model assumes the creep strain to be a function of stress, time, temperature and previously accumulated creep strain :

$$\varepsilon_c = f(\sigma,t,T,\varepsilon_c) \tag{3.1}$$

This expression is then simplified by assuming that separate stress, time, temperature and strain functions exist :

$$\varepsilon_c = f_1(\sigma)\ f_2(t)\ f_3(T)\ f_4(\varepsilon_c) \tag{3.2}$$

For isothermal conditions, equation (3.2) can be differentiated with respect to time to give :

$$\frac{d\varepsilon_c}{dt} = f_1(\sigma)\,\frac{d}{dt}\left[f_2(t)\right]\,f_3(T)\,f_4(\varepsilon_c) \tag{3.3}$$

3.1 Derivation of uniaxial normalised creep equations

As shown earlier, equation (3.3) can be simplified even further by assuming time or strain hardening behaviour. For the present derivations mixed hardening will be assumed, but the constitutive relationships will be cast in such a way that it will be easy to revert to time or strain hardening assumptions. From Payne (1979) the separate functions in equation (3.3) can be written as follows :

$$\frac{d\varepsilon_c}{dt} = n\,K^a\,e^{-Qa/RT}\,\sigma^{ma}\,t^{na-1}\,\varepsilon_c^{1-a} \tag{3.4}$$

where K, Q, R, m, and n are material constants dependent on temperature. The factor a determines the extent of mixed hardening. If a = 1, the material follows a time hardening behaviour :

$$\frac{d\varepsilon_c}{dt} = n\,K\,e^{-Q/RT}\,\sigma^{m}\,t^{n} \tag{3.5}$$

If a = 1/n, the material follows a strain hardening behaviour :

$$\frac{d\varepsilon_c}{dt} = n\,K^{1/n}e^{-Q/nRT}\,\sigma^{m/n}\,\varepsilon_c^{(n-1)/n} \tag{3.6}$$

Mixed hardening occurs for $1 < a < 1/n$.

For stationary state creep, the total strain consists of the sum of the elastic strain and the creep strain :

$$\varepsilon = \varepsilon_e + \varepsilon_c \tag{3.7}$$

The uniaxial, mixed hardening strain rate equation then becomes :

$$\frac{d\varepsilon}{dt} = \frac{1}{E}\frac{d\sigma}{dt} + n\,K^a\,e^{-Qa/RT}\,\sigma^{ma}\,t^{na-1}\,\varepsilon_c^{1-a} \tag{3.8}$$

If now the stresses and strains are normalised as follows :

$$\Sigma = \frac{\sigma}{\sigma_\circ} \;;\quad \lambda = \frac{\varepsilon}{\varepsilon_\circ} \;;\quad E = \frac{\sigma}{\varepsilon} = \frac{\sigma_\circ}{\varepsilon_\circ} \tag{3.9}$$

where $\sigma_\circ$ is some conveniently chosen normalising stress, then equation (3.8) becomes :

$$\varepsilon_\circ\frac{d\lambda}{dt} = \varepsilon_\circ\frac{d\Sigma}{dt} + n\,K^a\,e^{-Qa/RT}\,\sigma_\circ^{ma}\,\varepsilon_\circ^{1-a}\,\Sigma^{ma}\,\lambda_c^{1-a}\,t^{na-1} \tag{3.10}$$

Simplifying :

$$\frac{d\lambda}{dt} = \frac{d\Sigma}{dt} + n\,E^a\,K^a\,e^{-Qa/RT}\,\sigma_\circ^{(m-1)a}\,t^{na-1}\,\Sigma^{ma}\,\lambda_c^{1-a} \tag{3.11}$$

Now apply a time transformation from t to a *distorted time* parameter τ :

$$\frac{d\lambda}{d\tau}\frac{d\tau}{dt} = \frac{d\Sigma}{d\tau}\frac{d\tau}{dt} + n\left(E\,K\,e^{-Q/RT}\,\sigma_\circ^{m-1}\right)^a t^{na-1}\,\Sigma^{ma}\,\lambda_c^{1-a} \tag{3.12}$$

Then let

$$\frac{d\tau}{dt} = n\left(E\,K\,e^{-Q/RT}\,\sigma_\circ^{m-1}\right)^a t^{na-1} \tag{3.13}$$

whence

$$\int_0^\tau d\tau = \int_0^t n\left(E\,K\,e^{-Q/RT}\,\sigma_\circ^{m-1}\right)^a t^{na-1}\,dt \tag{3.14}$$

To simplify the equations, assume that the parameters inside the bracket within the integral are time independent, then :

$$\tau = \frac{1}{a}\left(E\ K\ e^{-Q/RT}\ \sigma_{\circ}^{m-1}\ t^{n}\right)^{a} \qquad (3.15)$$

From (3.15) and for the time hardening assumption (i.e. a = 1) :

$$\tau_{th} = E\ K\ e^{-Q/RT}\ \sigma_{\circ}^{m-1}\ t^{n} \qquad (3.16)$$

Then in the general case of mixed hardening, substituting (3.16) into (3.15) :

$$\tau_{mh} = \frac{1}{a}\left(\tau_{th}\right)^{a} \qquad (3.17)$$

and for strain hardening behaviour (i.e. a = 1/n) :

$$\tau_{sh} = n\left(\tau_{th}\right)^{1/n} \qquad (3.18)$$

The subscripts *th*, *sh*, and *mh* refer to time, strain, and mixed hardening respectively.

Substituting (3.13) into (3.12), the normalised mixed hardening uniaxial strain rate is obtained :

$$\frac{d\lambda}{d\tau} = \frac{d\Sigma}{d\tau} + \Sigma^{ma}\ \lambda_{c}^{1-a} \qquad (3.19)$$

For a time hardening assumption equation (3.19) reduces to :

$$\frac{d\lambda}{d\tau} = \frac{d\Sigma}{d\tau} + \Sigma^{m} \qquad (3.20)$$

Similarly, for a strain hardening assumption :

$$\frac{d\lambda}{d\tau} = \frac{d\Sigma}{d\tau} + \Sigma^{m/n}\ \lambda_{c}^{(n-1)/n} \qquad (3.21)$$

3.2 CREEP IN MULTIAXIAL STRESS STATES

Equation (3.19) applies only to uniaxial cases. It is however relatively easy to derive similarly normalised equations for multiaxial cases. This derivation is shown in Appendix B, and only the underlying assumptions and main features of converting the uniaxial creep to a multiaxial creep law are listed here.

In the conversion from uniaxial to multiaxial states it is assumed that the hypotheses and concepts which have been proposed in the development of the theory of instantaneous plasticity apply here (Soderberg,1941; Penny and Marriott,1971). Two basic problems have to be resolved.

In instantaneous plasticity theory the concept of a yield criterion defines the equivalent effect of a multiaxial stress system to produce a certain magnitude of strain. In the case of stationary state creep, an equivalent stress and an equivalent creep strain increment can be defined (Johnson et al.,1963) :

$$\sigma^* = \sigma^*\left(\sigma_x,\ \sigma_y,\ \sigma_z,\ \tau_{xy},\ \tau_{xz},\ \tau_{yz}\right) \tag{3.22}$$

and

$$\Delta\varepsilon^* = \Delta\varepsilon^*\left(\Delta\varepsilon_x,\ \Delta\varepsilon_y,\ \Delta\varepsilon_z,\ \Delta\varepsilon_{xy},\ \Delta\varepsilon_{xz},\ \Delta\varepsilon_{yz}\right) \tag{3.23}$$

where σ^* and $\Delta\varepsilon^*$ define the combined action of the stress system σ_{ij} in producing a corresponding strain increment $\Delta\varepsilon_{ij}$.

For consistency, the equivalent stress and strain increment are usually chosen to reduce to the appropriate values of stress and strain increment in the uniaxial case. This means that for the usual exponential creep law, equation (3.3) would become :

$$\Delta\varepsilon^* = f_1(\sigma^*)\ \frac{d}{dt}\left[f_2(t)\right]\ f_3(T)\ f_4(\varepsilon^*)\ \Delta t \tag{3.24}$$

The form of the equivalent stress σ^* is, as in the case of instantaneous plasticity, usually assumed to be the same as the von Mises yield criterion. For isotropic materials σ^* is then defined by :

$$\sigma^* = \sqrt{\frac{1}{2} S_{ij} S_{ij}} \tag{3.25}$$

with S_{ij} defined later.

This assumption is entirely intuitive and is preferred in most cases simply because it works reasonably well (Penny and Marriott, 1971).

The second problem in the conversion from uniaxial to multiaxial cases is to define the manner in which the deformations caused by the stress system σ_{ij} are distributed between the three directions. An analogy with instantaneous plasticity is again taken, and, for isotropic materials which exhibit volume constancy and coincidence of the principal axes of stress and strain, the following so-called *Flow Rules* can be defined (Penny and Marriott,1971) :

$$\Delta\varepsilon_x = d\lambda \left[\sigma_x - \frac{\sigma_y + \sigma_z}{2}\right], \text{ etc,} \tag{3.26}$$

where $d\lambda$ defines the magnitude of deformation and is a function of σ^*.

In order to unify the above concepts, it is convenient to derive the flow rules from a *Plastic Potential Function* (Drucker,1967). This will allow the use of an associated yield criterion thought to be the most appropriate in a given situation. The plastic potential function $\psi(\sigma_{ij})$ is a scalar function of stress and is associated with a particular yield criterion. The creep strain increment is then expressed in the form (Prandtl,1924) :

$$d\varepsilon_{ij,c} = \frac{d\psi}{d\sigma_{ij}} d\lambda \tag{3.27}$$

where $d\lambda$ is a constant related to the equivalent strain increment $d\varepsilon^*$:

$$d\lambda = \frac{d\varepsilon^*}{\sqrt{\frac{2}{3} \frac{d\psi}{d\sigma_{mn}} \frac{d\psi}{d\sigma_{mn}}}} \tag{3.28}$$

and $d\lambda$ can vary during a load history. Equation (3.27) then becomes :

$$d\varepsilon_{ij,c} = \frac{d\psi}{d\sigma_{ij}} \frac{d\varepsilon^*}{\sqrt{\frac{2}{3}\frac{d\psi}{d\sigma_{mn}}\frac{d\psi}{d\sigma_{mn}}}} \tag{3.29}$$

In this study, the von Mises yield criterion will be used. This choice is supported by experimental evidence (Johnson et al.,1963) as well as tradition (Soderberg,1941; Penny and Marriott,1971). The plastic potential function associated with the von Mises yield criterion is :

$$\psi(\sigma_{ij}) = \frac{(\sigma^*)^2}{3} \tag{3.30}$$

Using equation (3.30) in (3.29), the creep strain increments are then given by :

$$d\varepsilon_{ij,c} = \frac{3}{2}\frac{d\varepsilon^*}{\sigma^*} S_{ij} = d\varepsilon^* \frac{d\sigma^*}{d\sigma_{ij}} \tag{3.31}$$

where $S_{ij} = \frac{d\psi}{d\sigma_{ij}}$, known as the *Stress Deviator*.

From equation (3.3) the mixed hardening law for equivalent creep can be written :

$$d\varepsilon^* = f_1(\sigma^*) \frac{d}{dt}\left[f_2(t)\right] f_3(T)\, f_4(\varepsilon^*)\, dt \tag{3.32}$$

so that

$$d\varepsilon_{ij,c} = f_1(\sigma^*) \frac{d\sigma^*}{d\sigma_{ij}} \frac{d}{dt}\left[f_2(t)\right] f_3(T)\, f_4(\varepsilon^*)\, dt \tag{3.33}$$

If the separate functions f_1, f_2, f_3, and f_4 are assumed to be the same as for the uniaxial case, equation (3.33) becomes :

$$\frac{d\varepsilon_{ij,c}}{dt} = n\, K^a\, e^{-Qa/RT}\, \sigma^{*ma}\, t^{na-1}\, \varepsilon_c^{*1-a}\, \frac{d\sigma^*}{d\sigma_{ij}} \tag{3.34}$$

This equation can be normalised as before, and the time base can be similarly transformed. The normalised mixed hardening multiaxial creep strain rate law then becomes :

$$\frac{d\lambda_{ij,c}}{d\tau} = \Sigma^{*ma}\, \lambda^{*1-a}\, \frac{d\Sigma^*}{d\Sigma_{ij}} \tag{3.35}$$

The normalised multiaxial creep strain rate law is derived in more detail in Appendix B. The time hardening version of equation (3.35) is :

$$\frac{d\lambda_{ij,c}}{d\tau} = \Sigma^{*m}\, \frac{d\Sigma^*}{d\Sigma_{ij}} \tag{3.36}$$

while the strain hardening version is :

$$\frac{d\lambda_{ij,c}}{d\tau} = \Sigma^{*m/n}\, \lambda^{*(n-1)/n}\, \frac{d\Sigma^*}{d\Sigma_{ij}} \tag{3.37}$$

The implications of normalising the creep law and distorting the time scale are multifold ; firstly, if the normalising stress and strain are of the same magnitude as the expected stresses and strains, the normalised values of both the stresses and strains will be close to unity which will enhance the numerical stability and reduce rounding errors. The second major implication is that the strain rate law is no longer dependent on the temperature function, nor on the stress constant and the elastic modulus. In the case of the mixed and strain hardening versions, the strain rate law is dependent only on the stress exponent m and the time exponent n. In the case of the time hardening version, this dependence is reduced to the stress exponent m.

For steady loads and uniaxial configurations, the mixed (and strain) hardening deformations are the same as the time hardening deformations. In these cases it is necessary only to calculate deformations using the time hardening assumption, and the mixed hardening deformations can be calculated from them.

From equation (3.35), for the time hardening assumption and for the uniaxial case :

$$\int_0^{\lambda_c} d\lambda_c = \int_0^{\tau} \Sigma^m \, d\tau \tag{3.38}$$

whence

$$\lambda_{c_{th}} = \Sigma^m \, \tau_{th} \tag{3.39}$$

where subscript c indicates creep strain.

From equation (3.35), for the uniaxial case :

$$\int_0^{\lambda_c} \lambda_c^{a-1} \, d\lambda_c = \int_0^{\tau} \Sigma^{ma} \, d\tau \tag{3.40}$$

whence

$$\lambda_{c_{mh}} = a \, \Sigma^m \, \tau_{mh}^{1/a} \tag{3.41}$$

Using equation (3.17), equation (3.41) reduces to :

$$\lambda_{c_{mh}} = \Sigma^m \, \tau_{th} = \lambda_{c_{th}} \tag{3.42}$$

This simplifies the creep analysis in some limited cases, two notable ones being uniaxial specimens and turbine blades if the strains along the length of the blade are dominant. This simplification is not possible in multiaxial cases, and in these cases it is necessary to use the hardening behaviour thought to be most appropriate to the material. The reason for this is given below.

Integrating equation (3.36) leads to :

$$\lambda_{ij,c_{th}} = \Sigma^{*m} \frac{d\Sigma^*}{d\Sigma_{ij}} \, \tau_{th} \tag{3.43}$$

which, using the normalised form of equation (3.31) can be modified to :

$$\frac{d\lambda^*_{th}}{d\lambda_{ij}} \lambda_{ij,c_{th}} = \Sigma^{*m} \tau_{th} \tag{3.44}$$

Equation (3.37) can be integrated to :

$$\lambda^*_{mh} = \Sigma^{*m} \tau_{th} \tag{3.45}$$

If time and mixed hardening are equivalent, $\lambda^*_{th} = \lambda^*_{mh} = \lambda^*$ and $\lambda_{ij,c_{th}} = \lambda_{ij,c_{mh}} = \lambda_{ij,c}$. Equating (3.44) and (3.45), we obtain :

$$\frac{d\lambda^*}{\lambda^*} = \frac{d\lambda_{ij,c}}{\lambda_{ij,c}} \tag{3.46}$$

This would imply for instance, that :

$$\frac{d\lambda_{x,c}}{\lambda_{x,c}} = \frac{d\lambda_{y,c}}{\lambda_{y,c}} \tag{3.47}$$

which would not generally be the case.

4 DERIVATION OF NORMALISED CREEP/DAMAGE EQUATIONS

The equations derived in the previous section described the deformations occurring in a component during the period of stress redistribution (the primary stage) and during the stationary state (secondary stage). These creep laws predict that the component, once it has achieved stationary state, will continue to accumulate creep deformation indefinitely. The rate of the creep deformation remains constant with time. The deformation history for this case is shown in Figure 4.1.

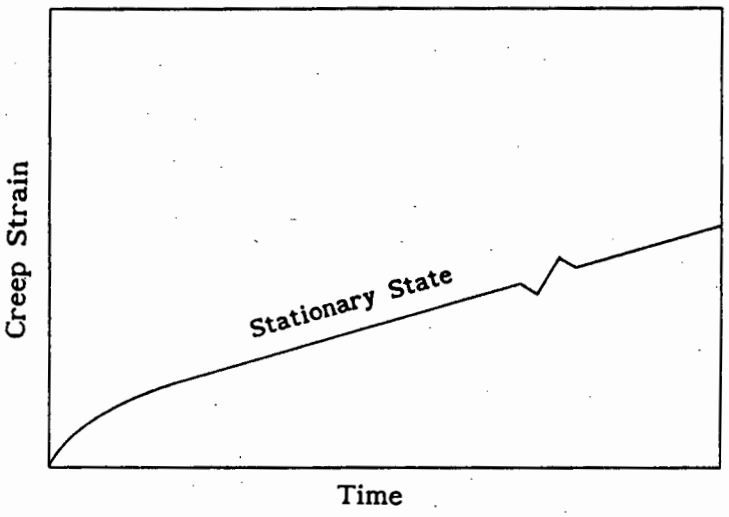

Figure 4.1 : Deformation history assuming stationary state creep

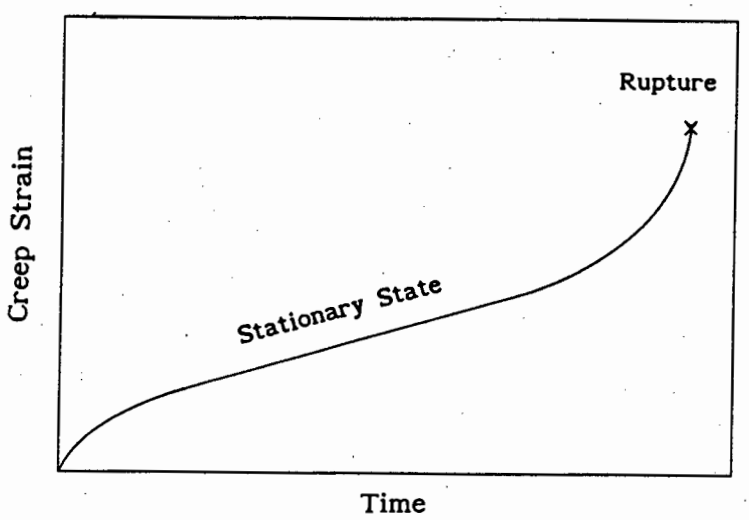

Figure 4.2 : Deformation history under creep/damage behaviour

This deformation history of course does not reflect reality. After a definite time, the component will fail, and the deformation rate just prior to failure is far from constant ; the deformation rate is continually increasing in the tertiary stage. Figure 4.2 shows a more realistic picture of the deformation history of a component subjected to creep.

An earlier section has described various approaches to predicting deformations in the tertiary stage, and to predicting the time of rupture. For the purpose of this thesis, the initial hypothesis by Kachanov (1958), and its modifications by Rabotnov (1969) shall be used. Kachanov assumed the existence of a damage parameter, ω, which grows from a value of zero at first loading to a value of one at failure. The damage parameter relates the load bearing area at time t, A_t, to the initial load bearing area A_o :

$$A_t = A_o (1 - \omega) \tag{4.1}$$

The phenomenon underlying this relationship is the fact that during the life of a component under creep conditions, voids grow at the grain boundaries of the component which reduce the load bearing area of the component. It is then possible to derive for the uniaxial case an expression for the stress at time t, σ_t, in terms of the nominal initial stress, σ_o :

$$\sigma_t = \frac{\sigma_o}{1 - \omega} \tag{4.2}$$

Towards the end of the life of the component, as ω tends to one, the stresses in the component will tend to infinity. This explains to a certain extent the sudden fracture exhibited by most components and materials.

Rabotnov proposed that the equations governing creep strain rates and damage rates should be similar to the stationary state creep strain rate equations. For the purpose of an example, consider a simple uniaxial isothermal time hardening creep law of the form :

$$\varepsilon_c = A \sigma^m t^n \tag{4.3}$$

where A is a constant dependent on temperature which combines the constants in equation (3.4). The corresponding creep strain rate equation is :

$$\frac{d\varepsilon_c}{dt} = n\ A\ \sigma_N^m\ t^{n-1} \tag{4.4}$$

where σ_N indicates the nominal stationary state stress.

If the effects of damage accumulation are to be included, Rabotnov modified equation (4.4) to :

$$\frac{d\varepsilon_{cd}}{dt} = n\ A\ \frac{\sigma_N^m}{(1-\omega)^p}\ t^{n-1} \tag{4.5}$$

and

$$\frac{d\omega}{dt} = n\ B\ \frac{\sigma_N^k}{(1-\omega)^r}\ t^{n-1} \tag{4.6}$$

where A, B, m, n, k, p, and r are material constants dependent on temperature. Subscript *c* refers to creep without the inclusion of damage accumulation and subscript *cd* refers to creep coupled to damage accumulation. The material constants can be estimated from uniaxial creep test data if the following information is available :

- a set of creep curves showing the minimum creep strain rate and rupture strains and times over a range of stresses, and
- a log(stress) versus log(rupture time) plot.

A method for extracting these constants from experimental data is shown in Appendix C.

Considering total strain rates, equations (4.4), (4.5), and (4.6) become :

$$\frac{d\varepsilon}{dt} = \frac{1}{E}\frac{d\sigma_N}{dt} + n\ A\ \sigma_N^m\ t^{n-1} \tag{4.7}$$

$$\frac{d\varepsilon_d}{dt} = \frac{1}{E}\frac{d\sigma_N}{dt} + n\ A\ \frac{\sigma_N^m}{(1-\omega)^p}\ t^{n-1} \tag{4.8}$$

and

$$\frac{d\omega}{dt} = n\ B\ \frac{\sigma_N^k}{(1-\omega)^r}\ t^{n-1} \tag{4.9}$$

where subscript d refers to strains including the effects of damage.

The stresses and strains can be normalised as follows :

$$\Sigma = \frac{\sigma}{\sigma_\circ}\ ;\quad \lambda = \frac{\varepsilon}{\varepsilon_\circ}\ ;\quad E = \frac{\sigma}{\varepsilon} = \frac{\sigma_\circ}{\varepsilon_\circ} \tag{4.10}$$

where $\sigma_\circ$ is some conveniently chosen normalising stress. Equations (4.7), (4.8), and (4.9) then become :

$$\frac{d\lambda}{dt} = \frac{d\Sigma_N}{dt} + n\ A\ E\ \sigma_\circ^{m-1}\ t^{n-1}\ \Sigma_N^m \tag{4.11}$$

$$\frac{d\lambda_d}{dt} = \frac{d\Sigma_N}{dt} + n\ A\ E\ \sigma_\circ^{m-1}\ t^{n-1}\ \frac{\Sigma_N^k}{(1-\omega)^p} \tag{4.12}$$

and

$$\frac{d\omega}{dt} = n\ B\ \sigma_\circ^k\ \frac{\Sigma_N^k}{(1-\omega)^r}\ t^{n-1} \tag{4.13}$$

Transforming the time base from t to τ, equations (4.11), (4.12), and (4.13) become :

$$\frac{d\lambda}{d\tau}\frac{d\tau}{dt} = \frac{d\Sigma_N}{d\tau}\frac{d\tau}{dt} + n\ A\ E\ \sigma_\circ^{m-1}\ t^{n-1}\ \Sigma_N^m \tag{4.14}$$

$$\frac{d\lambda_d}{d\tau}\frac{d\tau}{dt} = \frac{d\Sigma_N}{d\tau}\frac{d\tau}{dt} + n\ A\ E\ \sigma_\circ^{m-1}\ t^{n-1}\ \frac{\Sigma_N^k}{(1-\omega)^p} \tag{4.15}$$

and

$$\frac{d\omega}{d\tau}\frac{d\tau}{dt} = \frac{n\ B\ \sigma_\circ^m\ t^{n-1}}{C}\ C\ \frac{\Sigma_N^k}{(1-\omega)^r} \tag{4.16}$$

where C is some constant that will be defined later. Letting :

$$\frac{d\tau}{dt} = n\ A\ E\ \sigma_{\circ}^{m-1}\ t^{n-1} \tag{4.17}$$

we obtain by integrating, for A, E, and $\sigma_{\circ}$ independent of time :

$$\tau = A\ E\ \sigma_{\circ}^{m-1}\ t^{n} \tag{4.18}$$

Letting :

$$\frac{d\tau}{dt} = \frac{n\ B\ \sigma_{\circ}^{m-1}\ t^{n-1}}{C} = n\ A\ E\ \sigma_{\circ}^{m-1}\ t^{n-1} \tag{4.19}$$

we obtain an expression for the constant C :

$$C = \frac{B\ \sigma_{\circ}^{1+k-m}}{A\ E} \tag{4.20}$$

Substituting (4.19) into (4.14), (4.15), and (4.16), and using $\dot{(\ )}$ to represent $(d/d\tau)$, we obtain :

$$\dot{\lambda} = \dot{\Sigma}_{N} + \Sigma_{N}^{m} \tag{4.21}$$

$$\dot{\lambda}_{d} = \dot{\Sigma}_{N} + \frac{\Sigma_{N}^{m}}{(1-\omega)^{p}} \tag{4.22}$$

and

$$\dot{\omega} = C\ \frac{\Sigma_{N}^{k}}{(1-\omega)^{r}} \tag{4.23}$$

Using similar principles to the stationary state case, equations (4.21) and (4.22) can be converted to multiaxial stress and strain states :

$$\dot{\lambda}_{ij,c} = \Sigma^{*m}\ \frac{d\Sigma^{*}}{d\Sigma_{ij}} \tag{4.24}$$

and

$$\dot{\lambda}_{ij,cd} = \frac{\Sigma^{*m}}{(1-\omega)^p} \frac{d\Sigma^*}{d\Sigma_{ij}} \tag{4.25}$$

The damage equation is modified using a principle proposed by Hayhurst (1970) :

$$\dot{\omega} = C \frac{\Sigma_\beta^k}{(1-\omega)^r} \tag{4.26}$$

where Σ_β is the Hayhurst equivalent stress :

$$\Sigma_\beta = \beta \Sigma^* + (1-\beta) \Sigma^I \tag{4.27}$$

where $0 \leq \beta \leq 1$ and Σ^* and Σ^I are the Mises equivalent and maximum principal stress respectively.

Equation (4.26) can be integrated to give :

$$\int_0^\omega (1-\omega)^r \, d\omega = \int_0^\tau C \, \Sigma_\beta^k \, d\tau \tag{4.28}$$

whence

$$(1-\omega) = \left[1 - (1+r) \, C \, \Sigma_\beta^k \, \tau \right]^{1/1+r} \tag{4.29}$$

When $\omega = 1$, rupture occurs at $\tau = \tau_R$, and :

$$\tau_R = \frac{1}{(1+r) \, C \, \Sigma_\beta^k} \tag{4.30}$$

Substituting (4.30) into (4.29) we obtain :

$$(1 - \omega) = (1 - \Gamma)^{1/1+r} \tag{4.31}$$

where $\Gamma = \tau/\tau_R$ is a life fraction measure. Using (4.18) :

$$\Gamma = \frac{\tau}{\tau_R} = \left(\frac{t}{t_R} \right)^n \tag{4.32}$$

Equations (4.24) and (4.25) give expressions for the creep strain rates :

$$\dot{\lambda}_{ij,c} = \Sigma^{*m} \frac{d\Sigma^*}{d\Sigma_{ij}} \tag{4.33}$$

$$\dot{\lambda}_{ij,cd} = \frac{\Sigma^{*m}}{(1-\omega)^p} \frac{d\Sigma^*}{d\Sigma_{ij}} \tag{4.34}$$

Integrating (4.33) results :

$$\lambda_{ij,c} = \Sigma^{*m} \frac{d\Sigma^*}{d\Sigma_{ij}} \tau \tag{4.35}$$

whilst integrating (4.34) gives :

$$\int_0^{\lambda_{ij,cd}} d\lambda_{ij,cd} = \int_0^{\tau} \frac{\Sigma^{*m}}{(1-\omega)^p} \frac{d\Sigma^*}{d\Sigma_{ij}} d\tau \tag{4.36}$$

Substituting (4.26) into (4.36) gives :

$$\int_0^{\lambda_{ij,cd}} d\lambda_{ij,cd} = \int_0^{\omega} \frac{1}{C} \frac{\Sigma^{*m}}{\Sigma_\beta^k} \frac{d\Sigma^*}{d\Sigma_{ij}} (1-\omega)^{r-p} \, d\omega \tag{4.37}$$

whence

$$\lambda_{ij,cd} = \frac{1}{C\ (1+r-p)} \frac{\Sigma^{*m}}{\Sigma_\beta^k} \frac{d\Sigma^*}{d\Sigma_{ij}} \left[1 - (1-\omega)^{1+r-p} \right] \tag{4.38}$$

Using (4.32), equation (4.35) can be modified to read :

$$\lambda_{ij,c} = \tau_R \, \Sigma^{*m} \frac{d\Sigma^*}{d\Sigma_{ij}} \, \Gamma \tag{4.39}$$

whence

$$\lambda_{ij,c} = K \, \Gamma \tag{4.40}$$

where

$$K = \tau_R \, \Sigma^{*m} \frac{d\Sigma^*}{d\Sigma_{ij}} = \frac{1}{C \, (1+r)} \frac{\Sigma^{*m}}{\Sigma_\beta^k} \frac{d\Sigma^*}{d\Sigma_{ij}} = \dot{\lambda}_{ij,c} \, \tau_R \tag{4.41}$$

Using (4.32), and substituting (4.41) into (4.38) there results :

$$\lambda_{ij,cd} = \eta \, K \left[1 - (1 - \Gamma)^{1/\eta} \right] \tag{4.42}$$

where

$$\eta = \frac{1+r}{1+r-p} \tag{4.43}$$

By differentiating (4.40) and (4.42) with respect to Γ the creep strain rates with and without damage are :

$$\frac{d\lambda_{ij,c}}{d\Gamma} = K \tag{4.44}$$

and

$$\frac{d\lambda_{ij,cd}}{d\Gamma} = K \, (1 - \Gamma)^{(1-\eta)/\eta} \tag{4.45}$$

When attempting to predict the deformation and rupture characteristics of a component of material following the Kachanov/Rabotnov characteristics, the strain and damage behaviour must be coupled. This means that equations (4.25) and (4.26) are used interactively, and the deformation and rupture behaviour follows equations (4.42) and (4.45). This is the mathematically correct implementation of the Kachanov/Rabotnov relationships. The method has been used and tested by several workers, among which Hayhurst (1970), Payne (1979), and Sieburg (1989). The method is however numerically complex and is time-consuming even when powerful computers are used. The numerical complexity, together with the high stress dependence of equations (4.25) and (4.26) result in numerical instabilities which make the forward integration

process slow.

When prohibitive computer costs and time make this method an unattractive proposition, then the material degradation is uncoupled for the purpose of the stress analysis. The analysis is then based on equation (4.24) and equations (4.40) and (4.44) are used to predict the deformation behaviour. If this course of action is taken, the analysis will not be capable of predicting rupture characteristics directly. However, prudent manipulation of the results of the analysis, namely the stationary state stresses, interpreted with the use of equations (4.20) and (4.30), is likely to provide a method of component assessment which is particularly useful at the early stages of design when its leanness in computer processing time makes it economically viable. This method was suggested by Odqvist (1966) who suggested that the stresses throughout the life of a structure may well be approximated by the stationary state stresses. The method was used by Boyle and Spence (1980) in their creep analysis of some complex piping components.

5 DECOUPLED CREEP/RUPTURE ANALYSIS

5.1 OUTLINE OF PROCEDURE

The object of the structural analysis method which is described here is to make as efficient use as possible of available structural analysis programs to solve problems covering a wide range of materials, loads and temperatures. The loads are assumed to be constant with time, but the method can be extended to include varying load and temperature histories.

The proposed method is capable of parametrically predicting deformation behaviour as well as rupture characteristics. This means that a knowledge of the actual material behaviour or of the actual load level is *not* required before the structural analysis. This makes the method particularly suited to the initial design stages when the designer is usually still uncertain about the values of most material and load parameters, but would like to find out quickly how those parameters would affect the design.

The method is independent of the actual size of the component as long as geometrically similar components are used. This will be useful for problems where the load levels and material parameters are set and where the size of the component is the main variable in the design.

The method is based on the Kachanov/Rabotnov constitutive model which includes the effects of material degradation. Assuming that the stresses throughout the life of the component can be approximated by the stationary state (Odqvist,1966), it is possible to decouple the effects of material degradation from the stress analysis. This means that it is necessary only to perform a stationary state creep analysis, using a creep law of the form :

$$\frac{d\varepsilon_c}{dt} = f_1(\sigma)\,\frac{d}{dt}\left[f_2(t)\right]\,f_3(T)\,f_4(\varepsilon_c) \qquad (5.1)$$

The rupture characteristics are then calculated using the stationary state stresses. The advantage of the method compared to a stress analysis where

deformation and degradation are coupled is that the computer time required for the stress analysis is considerably less. The main disadvantage of the method is that in some cases the rupture times predicted from maximum stationary state stresses will be unconservative and in some cases it will be conservative.

In statically determinate components (a notched rod for instance), the predicted rupture times are unconservative because the high local stresses during the tertiary stage are not taken into account. It will be shown later that in simple problems the error is small and within the usual range of experimental scatter.

In statically indeterminate components (a plate with a hole under equibiaxial tension for instance), the rupture times estimated from maximum stationary stresses will be conservative : although voids will grow initially at the high stress locations, the component is able to shed the high stresses due to local damage to the less damaged regions, thus extending the life of the component.

For some statically indeterminate components (pipes with internal pressure for instance), the stationary stresses at a so-called *Skeletal Point* can be used to predict rupture times. The skeletal point is that location in a component where the stationary state stresses are independent of the stress exponent m. The existence of a skeletal point in pipes was first noticed by Soderberg (1941), and has resulted in the *Mean Diameter Formula* for thick walled pipes (Penny and Marriott,1971).

Several conservative failure criteria are developed in Section 6 to minimise the effects of any unconservatism. They are also derived parametrically and are independent of the load level and insensitive to the material parameters. The failure criteria are aimed at Residual Life predictions.

5.2 STATIONARY STATE ANALYSIS

The stationary state analysis is the basis to the solution of the problem. Any structural analysis program capable of solving non-linear creep behaviour can be used. For the purpose of this work the commercial non-linear finite

element program ABAQUS Version 4.7 (Hibbitt et al,1988) was used. This program has a build-in creep routine, but a separate creep subroutine was developed mainly to allow the output of some non-standard parameters (such as the instantaneous creep strain rate).

The constitutive creep relationship used was the mixed hardening power law relationship :

$$\frac{d\varepsilon_c}{dt} = n\, K^a\, e^{-Qa/RT}\, \sigma^{ma}\, t^{na-1}\, \varepsilon_c^{1-a} \tag{5.2}$$

or, in multiaxial form

$$\frac{d\varepsilon_{ij,c}}{dt} = n\, K^a\, e^{-Qa/RT}\, \sigma^{*ma}\, t^{na-1}\, \varepsilon^{*1-a}\, \frac{d\sigma^*}{d\sigma_{ij}} \tag{5.3}$$

For the creep/rupture calculations the time hardening version of equation (5.3) was used :

$$\frac{d\varepsilon_{ij,c}}{dt} = n\, K\, e^{-Q/RT}\, \sigma^{*m}\, t^{n-1}\, \frac{d\sigma^*}{d\sigma_{ij}} \tag{5.4}$$

This equation was normalised and transformed with respect to time to :

$$\dot{\lambda}_{ij,c} = \Sigma^{*m}\, \frac{d\Sigma^*}{d\Sigma_{ij}} \tag{5.5}$$

where

$$\Sigma = \frac{\sigma}{\sigma_\circ} \quad ; \quad \lambda = \frac{\varepsilon}{\varepsilon_\circ} \quad ; \quad E = \frac{\sigma}{\varepsilon} = \frac{\sigma_\circ}{\varepsilon_\circ} \tag{5.6}$$

and $\sigma_\circ$ is some conveniently chosen normalising stress and $(\dot{}) = (d/d\tau)$ where

$$\tau = \int_0^t n\, K\, E\, e^{-Q/RT}\, \sigma_\circ^{m-1}\, t^{n-1}\, dt \tag{5.7}$$

Appealing to the insensitivity of the creep structural analysis to the stress exponent m if the reference stress is used as a normalising stress (Sim,1968) the constitutive relationship in equation (5.4) is independent of material parameters K, E, and n and is insensitive to m.

If a Norton power law stress function is used, the shape of the stress distributions is independent of the actual load (Penny and Marriott,1971). This means that the reference stress is directly related to the load (Sim and Penny,1971) and it is then possible to define a reference stress parameter α such that :

$$\bar{\sigma} = \frac{1}{\alpha} P \tag{5.8}$$

where $\bar{\sigma}$ is the reference stress at load P. This relationship is a constant function for a particular geometry with a particular load type, but holds for all similar geometries and for any value of the load. It is now possible to normalise the load value, P, used for the stationary state analysis to a load parameter, θ :

$$\theta = \frac{P}{\bar{\sigma}} = \frac{P}{\frac{1}{\alpha} P} = \alpha \tag{5.9}$$

The normalised load parameter for the load value is then identical for all load values. This implies that only a single analysis is required to find the stationary state behaviour for a range of loads at a particular stress exponent. A similar analysis at a different stress exponent should produce similar stationary state behaviour. Lastly, it implies that, if the load is assumed to be in units of stress, a normalised analysis of this kind is independent of the size of the component, as long as geometrically similar scaling is used.

The ramifications of the method are that the number of computer runs necessary to cover a wide range of variables is reduced to a single set of runs covering the usual range of possible stress exponents (i.e. $3 \leq m \leq 9$ for units of Nm^{-2} and hours). A second consequence is that, because the number of computer runs is few, the normalised results can be tabulated, and the computer analysis need not be re-run to obtain non-dimensional results for, say, a different

load.

Real Time responses for a wide variety of loads and material responses can be calculated using the *Time Distortion* caused by the time transformation of the normalising process (equation (5.7)). The concept of a distorted time is illustrated in Figure 5.1 (from Penny and Marriott,1971).

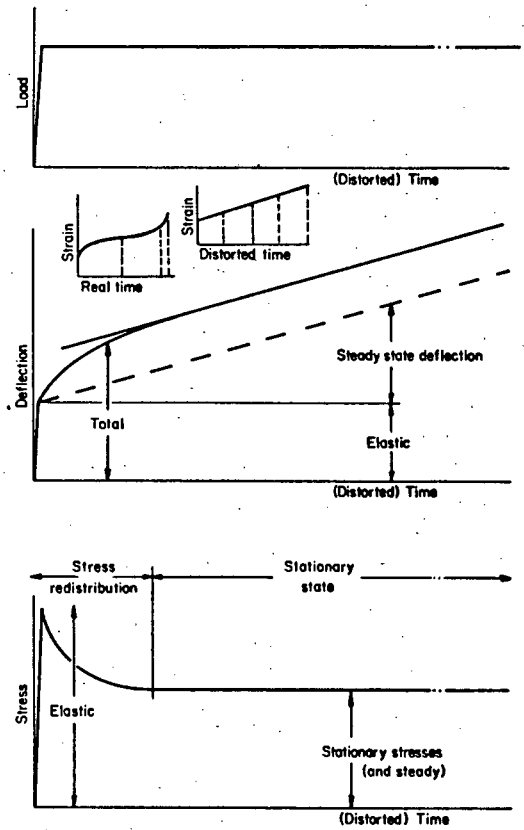

Figure 5.1 : Schematic representation of strain accumulation and stress redistribution following elastic loading (Penny and Marriott, 1971)

Using the reference stress of the component as the normalising stress, equation (5.7) can be conveniently rewritten as :

$$\tau = \frac{\int_0^t n\, K\, e^{-Q/RT}\, \bar{\sigma}^m\, t^{n-1}\, dt}{\bar{\sigma} / E} \qquad (5.10)$$

whence

$$\tau = \frac{\text{creep strain in time t at stress } \bar{\sigma}}{\text{elastic strain at stress } \bar{\sigma}} \qquad (5.11)$$

as noted in Penny and Marriott (1971).

Values for equation (5.11) can be calculated if the constants in (5.10) are known, or can be read from a creep curve at the reference stress if these constants are not known.

Methods for calculating the stationary state behaviour of components are well known (Penny and Marriott,1971; Kraus,1980) and will only be summarised here. The stationary state differs from the steady state analysis in that it includes the effect of *Stress Redistribution* after first loading. Figure 5.1 illustrates this difference.

It is easier to perform a stationary state analysis in most cases, and whether this achieved through finite difference or finite element methods, the basic process remains the same :

1. Solve the initial elastic or elastic/plastic problem ($\tau = 0$),

2. Use the stresses from step 1 to calculate creep terms at $\tau = 0$; solve the rate problem to evaluate stress and strain rates,

3. Over a time interval $\Delta\tau$ evaluate new stresses by integrating forward :

$$\Sigma_{\tau+\Delta\tau} = \Sigma_{\tau} + \dot{\Sigma}_{\tau}\,\Delta\tau, \text{ etc,}$$

4. Repeat steps 2 and 3 until a state of stationarity is reached to within prescribed tolerances of $\dot{\Sigma} = 0$,and $\dot{\lambda}$ is constant.

When the governing equations are normalised as shown earlier, the stresses, strains, and deformations will be non-dimensional and will refer to the transformed time parameter τ. To obtain dimensional values, the stresses, strains and deformations are calculated using equation (5.6), while the time parameter is transformed to real time using equation (5.10) or (5.11).

5.3 CALCULATION OF REFERENCE STRESS

The problem is now to find the relationship between the reference stress and the load for the geometry of the component under investigation. Sim (1968) proposed two simple methods which have found general acceptance (Kraus,1976; Matsuda and Fujikawa,1980). The simplest method is based on the assumption that as $m \rightarrow \infty$:

$$\bar{\sigma}_{m\rightarrow\infty} = \frac{P}{P_{collapse}} \sigma_y \tag{5.12}$$

which is an upper bound on the reference stress. $P_{collapse}$ is the collapse load for a perfectly plastic material. Values of $P_{collapse}$ for a large number of notched geometries have been summarised by Miller (1988). From equation (5.8) :

$$\alpha = \frac{P_{collapse}}{\sigma_y} \tag{5.13}$$

The second method appeals to the insensitivity of the deformation rate to the stress exponent m. Assuming a power law relationship, any stationary state creep deformation, u_c, can be expressed as :

$$u_c = u_c\left(\sigma^m, \text{ dimensions } \right) f_2(t) \tag{5.14}$$

Differentiating and choosing a convenient normalising stress σ_o, a non-dimensional rate equation can be derived, where $\dot{(\ )} = (d/d\tau)$:

$$\dot{U}_c = \dot{U}_c\left[\left(\frac{\sigma}{\sigma_o} \right)^m \right] \tag{5.15}$$

whence

$$\dot{u}_c = \sigma_o^m \, g(\text{dimensions}) \, \dot{U}_c\left[\left(\frac{\sigma}{\sigma_o} \right)^m \right] \frac{d}{dt}\left[f_2(t) \right] \tag{5.16}$$

Here $f_2(t)$ is the usual time function, g(dimensions) is a purely linear function of the dimensions, and $\dot{U}_c$ is the non-dimensional creep rate predicted by the numerical analysis. In general $\dot{U}_c$ will vary with the stress exponent m, and the degree of variation depends on the choice of σ_o. Letting :

$$\bar{\sigma} = \chi \sigma_o \tag{5.17}$$

where $\bar{\sigma}$ is the reference stress and χ is a constant to be determined. Then , since the stress analysis is insensitive to the stress exponent m :

$$\dot{U}_c = \dot{U}_c\left[\left(\frac{\sigma}{\bar{\sigma}}\right)^{m1}\right] = \dot{U}_c\left[\left(\frac{\sigma}{\bar{\sigma}}\right)^{m2}\right] \tag{5.18}$$

Substituting (5.17) into (5.18) and noting that $\dot{U}_c$ is a homogeneous m-degree function of σ :

$$\frac{1}{\chi^{m1}} \dot{U}_c\left[\left(\frac{\sigma}{\sigma_o}\right)^{m1}\right] = \frac{1}{\chi^{m2}} \dot{U}_c\left[\left(\frac{\sigma}{\sigma_o}\right)^{m2}\right] \tag{5.19}$$

Computing $\dot{U}_c$ for an arbitrary choice of σ_o at two values of m, we can find two stationary state deformation rates $\left(\dot{U}_c\right)_{m1}$ and $\left(\dot{U}_c\right)_{m2}$. Using equation (5.19) an expression for χ can be obtained :

$$\chi = \left[\frac{\left(\dot{U}_c\right)_{m1}}{\left(\dot{U}_c\right)_{m2}}\right]^{1/(m1-m2)} \tag{5.20}$$

Noting that a normalising stress parameter α_o can be defined such that :

$$\sigma_o = \frac{1}{\alpha_o} P \tag{5.21}$$

then, using equations (5.8), (5.17), (5.20), and (5.21), the reference stress parameter, α, can be found :

$$\alpha = \frac{\alpha_o}{\chi} \tag{5.22}$$

Non-dimensional initial and stationary stresses obtained for different normalising stresses can be related as follows. For a particular load P, the initial stress will be σ_{el} and the stationary stress σ_{ss}. Choose two normalising stresses $\sigma_o^{(1)}$ and $\sigma_o^{(2)}$ such that :

$$\sigma_o^{(1)} = \frac{P}{\alpha^{(1)}} \tag{5.23}$$

and

$$\sigma_o^{(2)} = \frac{P}{\alpha^{(2)}} \tag{5.24}$$

Then for initial non-dimensional stresses $\Sigma_{el}^{(1)}$ and $\Sigma_{el}^{(2)}$:

$$\sigma_{el} = \Sigma_{el}^{(1)} \sigma_o^{(1)} = \Sigma_{el}^{(2)} \sigma_o^{(2)} \tag{5.25}$$

Then, using (5.24), and rearranging :

$$\Sigma_{el}^{(1)} = \frac{\alpha_o^{(1)}}{\alpha_o^{(2)}} \Sigma_{el}^{(2)} \tag{5.26}$$

Similar relationships can be derived for the non-dimensional stationary stresses.

5.4 STATIONARY STATE RESULTS

A generalised plot of the non-dimensional deformation of a component versus distorted time for a range of stress exponents is shown in Figure 5.2 . This allows the definition of upper and lower bound solutions where the lower bound solution corresponds to the steady state solution, whilst the upper bound is defined by the stationary state deformation behaviour at a high value of stress exponent (usually m = 9 or m = 11; Sim and Penny,1971).

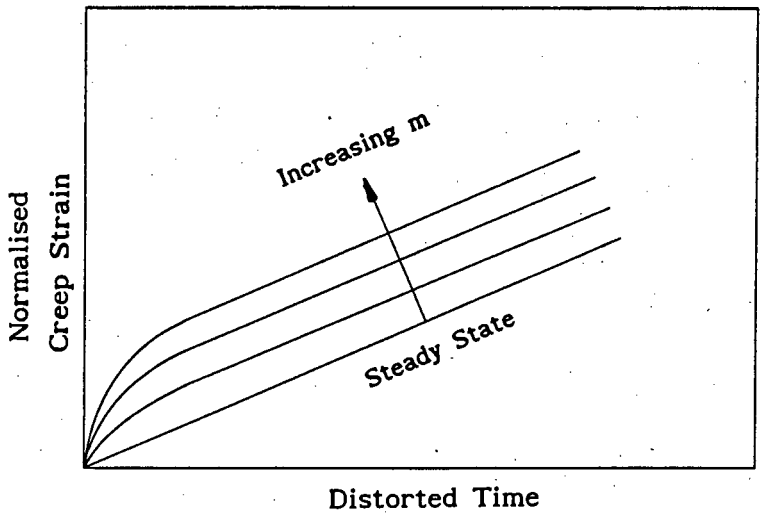

Figure 5.2 : Generalised non-dimensional creep curves

The non-dimensional deformation U can then be bounded by :

$$U_l = U^e + \frac{dU^{ss}}{d\tau}\,\tau \tag{5.27}$$

and

$$U_u = (1 + \gamma)\,U^e + \frac{dU^{ss}}{d\tau}\,\tau \tag{5.28}$$

whence, using (5.27) :

$$U_u = \gamma\,U^e + U_l \tag{5.29}$$

with the terms as defined in Figure 5.3.

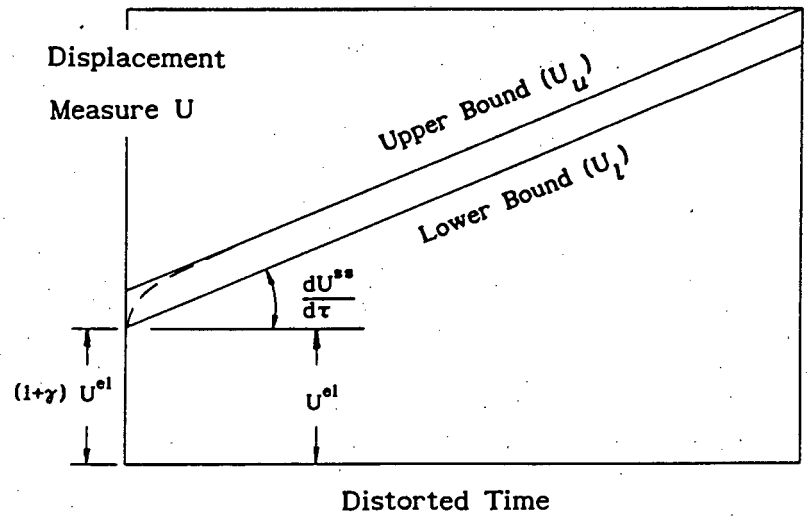

Figure 5.3 : Schematic representation of deformation characteristics

A generalised plot of the non-dimensional stresses in a component versus distorted time for a range of stress exponents is shown in Figure 5.4 . These non-dimensional stresses can be used to calculate distorted rupture times using equations derived earlier, namely :

$$\tau_R = \frac{1}{(1+r)\ C\ \Sigma_\beta^k} \tag{5.30}$$

where k and r are material constants,

$C = \frac{B\ \bar{\sigma}^{1+k-m}}{A\ E}$, and

Σ_β is the Hayhurst equivalent stress.

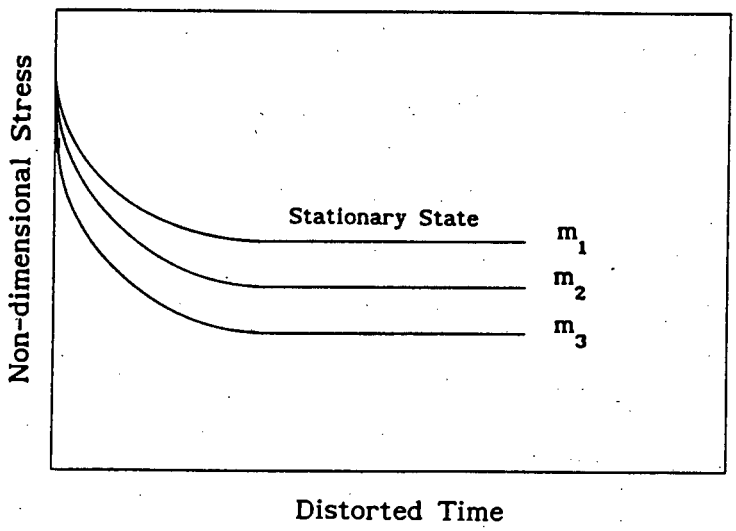

Figure 5.4 : Generalised stress relaxation curve

Two approaches are possible ; firstly, by using maximum elastic stresses to calculate the Hayhurst equivalent stress. This approach is overly conservative (Penny and Marriott,1971) and the second approach, using the maximum stationary state stresses, is preferred. The distorted rupture time can be reverted to a *real* rupture time using equation (5.10) or (5.11). Note however that a knowledge of the material constants is necessary to calculate C and therefore the distorted rupture time.

As argued earlier, the second approach leads to both conservative and unconservative rupture estimates, depending on whether the component is

statically determinate or indeterminate. The method must therefore be used prudently, and it must be realised that the proposed method is a *time-saver* in the initial design stages.

A number of problems was studied, which will be discussed later. For illustration, a typical table of results, obtained for a plate with a circular hole under equibiaxial tension, is included here. The plate was modeled using 150 quadratic plane stress elements. The finite element mesh, shown in Figure 5.5, was subjected to mesh sensitivity tests to achieve optimum results, and the stresses found were checked against analytical and other numerical solutions.

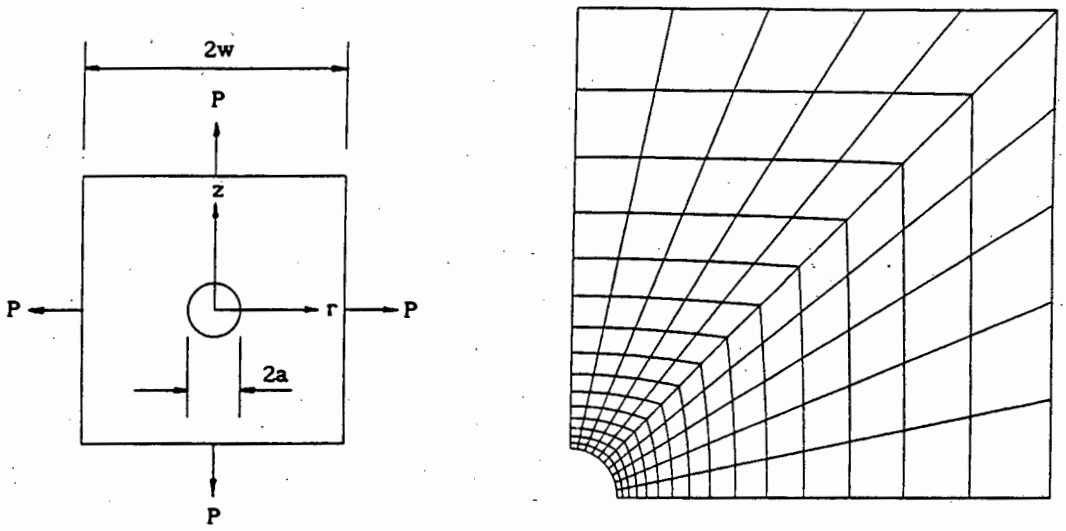

Figure 5.5 : Plate with circular hole : geometry and mesh details

Table 5.1 shows the maximum stresses and strain measures, both at the initial and stationary state times, as well as the approximate positions where they occur. As a first check, it can be seen from the table that the initial tangential stress at the hole edge is approximately twice the load, α, as predicted by analytical solutions (Faupel and Fisher,1981). The stationary stress at the hole edge approaches α as the stress exponent m is increased. This is consistent with the results of Penny and Hayhurst (1969).

By judicious data management much more information can be extracted from the finite element analysis. Examples of this are, in Figure 5.6, a plot of normalised tangential strain versus distorted time at various positions along the r-axis, and , in Figure 5.7, a plot of non-dimensional maximum principal stress versus distorted time at the same positions. Both plots are for stress

exponents m = 5. Note that the finite element program expects the initial elastic loading to take a finite time, and that this time is conveniently chosen to be one distorted time unit. This time is neglected when distorted time is reverted to real time.

Plate with hole : equibiaxial tension ; a/w = 1/10 ; α = 0.9565						
	m = 1	m = 3	m = 5	m = 7	m = 9	m = 11
Σ^{*}_{el}	1.928 (1.0)	1.928 (1.0)	1.928 (1.0)	1.928 (1.0)	1.928 (1.0)	1.928 (1.0)
Σ^{*}_{ss}	1.930 (1.0)	1.313 (1.0)	1.184 (1.0)	1.127 (1.0)	1.095 (1.0)	1.075 (1.0)
Σ^{I}_{el}	1.933 (1.0)	1.933 (1.0)	1.933 (1.0)	1.933 (1.0)	1.933 (1.0)	1.933 (1.0)
Σ^{I}_{ss}	1.936 (1.0)	1.318 (1.0)	1.221 (1.4)	1.191 (1.6)	1.177 (1.6)	1.168 (1.6)
Σ^{z}_{el}	1.933 (1.0)	1.933 (1.0)	1.933 (1.0)	1.933 (1.0)	1.933 (1.0)	1.933 (1.0)
Σ^{z}_{ss}	1.936 (1.0)	1.318 (1.0)	1.221 (1.4)	1.191 (1.6)	1.177 (1.6)	1.168 (1.6)
Σ^{r}_{el}	0.957 (10)	0.957 (10)	0.957 (10)	0.957 (10)	0.957 (10)	0.957 (10)
Σ^{r}_{ss}	0.958 (10)	0.957 (10)	0.957 (10)	0.957 (10)	0.957 (10)	0.956 (10)
λ^{z}_{el}	1.930	1.930	1.930	1.930	1.930	1.930
γ	-	0.139	0.239	0.301	0.377	0.389
$\dot{\lambda}^{z}_{ss}$	1.930	2.221	2.278	2.263	2.214	2.164
λ^{r}_{el}	-0.571	-0.571	-0.571	-0.571	-0.571	-0.571
γ	-	0.513	0.743	0.862	0.892	1.009
$\dot{\lambda}^{r}_{ss}$	-0.925	-1.081	-1.035	-1.101	-1.083	-1.053
U^{r}_{el}	1.930	1.930	1.930	1.930	1.930	1.930
γ	-	0.157	0.255	0.317	0.341	0.366
$\dot{U}^{r}_{ss}$	1.930	2.262	2.323	2.312	2.346	2.226
τ_{ss}	-	$\propto$ 2.6	$\propto$ 2.0	$\propto$ 1.9	$\propto$ 1.8	$\propto$ 1.7
Note : Locations given in brackets are approximate values along the r-axis All strain measures are taken at edge of hole (i.e. r = 1.0)						

Table 5.1 : Plate with hole under equibiaxial tension ; maximum non-dimensional stresses and strains

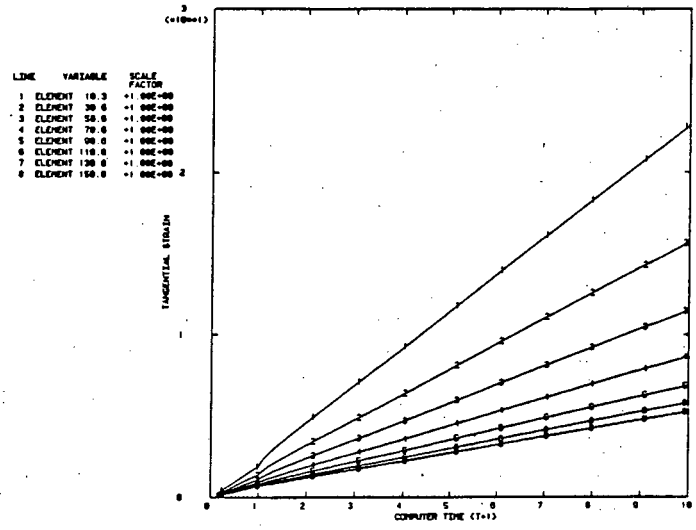

Figure 5.6 : Plot of normalised tangential strain versus distorted time

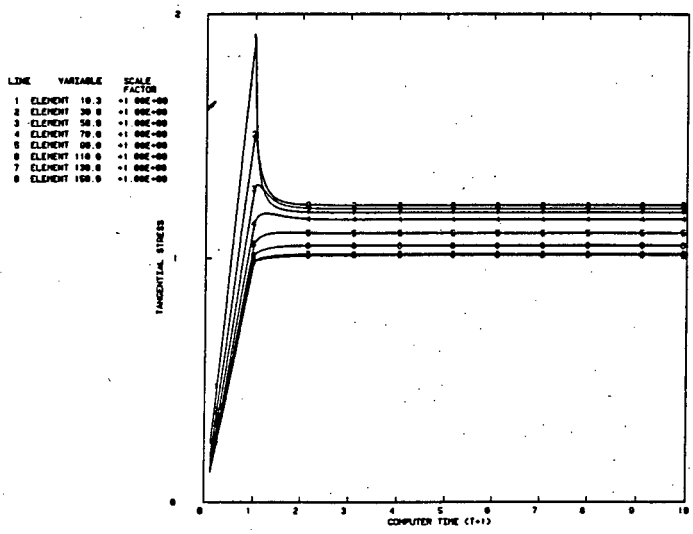

Figure 5.7 : Plot of non-dimensional maximum principal stress versus distorted time

If a knowledge of elastic and/or stationary stresses throughout the component is required , a *Contour Plot* is a standard option in most finite element programs. Figure 5.8 shows a contour plot of elastic non-dimensional maximum Principal stresses and Figure 5.9 shows the stationary state values. By changing the contour levels using equation (5.6), the contour plots can be easily converted to dimensional stress plots without re-running the stress analysis.

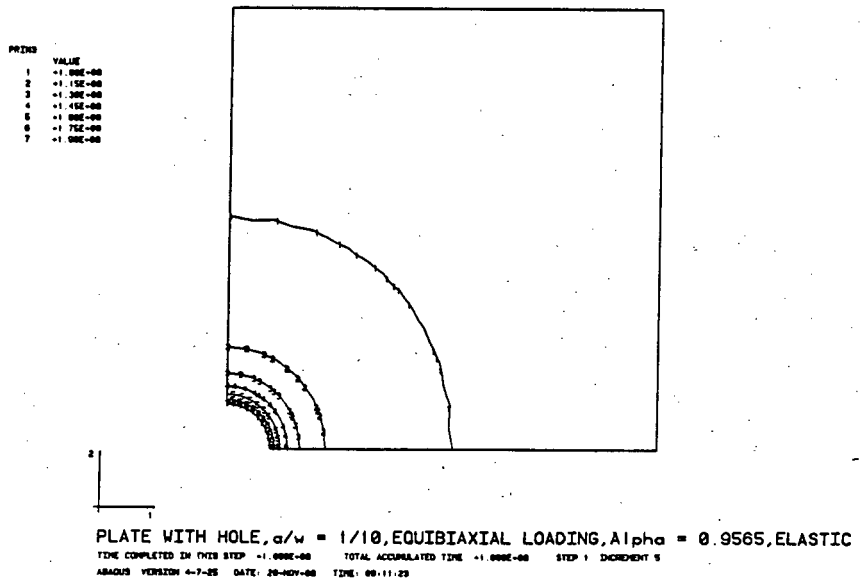

Figure 5.8 : Contour plot of elastic non-dimensional principal stress

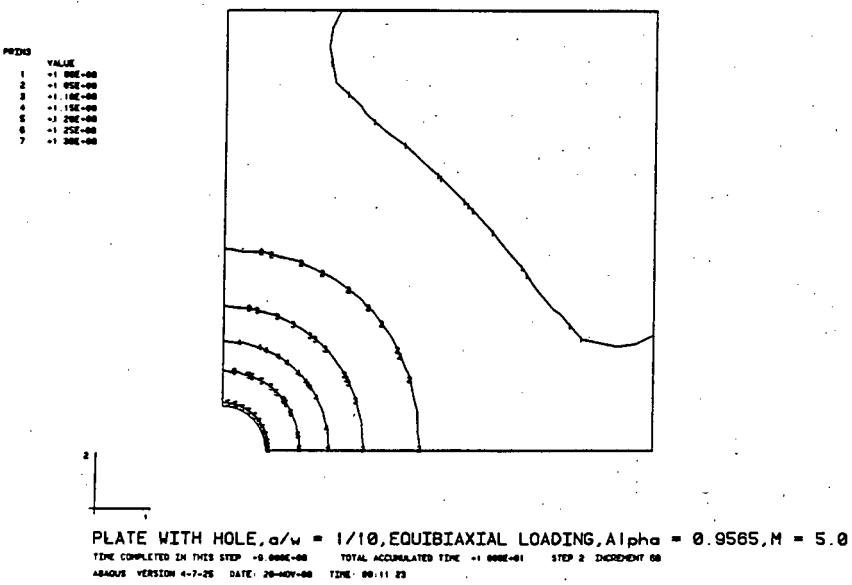

Figure 5.9 : Contour plot of stationary non-dimensional principal stress

The stationary stresses in the plate were further manipulated. Figure 5.10 shows the variation of the stationary state tangential stress (Σ^z_{ss}) at the hole edge with the stress exponent m. The linear relation of Σ^z_{ss} with the inverse of m corresponds well with Nadai (1963) and Calladine (1963). As $m \rightarrow \infty$ (i.e. at $1/m = 0$) the tangential stress at the hole edge tends to α, confirming the results of Penny and Hayhurst (1969).

The spatial variation along the r-axis of the stationary state tangential

stress, and the influence of the stress exponent m is shown in Figure 5.11. The maximum stationary state occurs some distance away from the hole edge, and the locus of maximum values moves inwards as the stress exponent increases. This corresponds to the results of Penny and Hayhurst (1969). It also implies that damage cracks can be expected to initiate some distance within the plate, a conclusion which seems to be confirmed by Hayhurst's experiments (1970). A skeletal point occurs at r = 2.7, and its value of Σ^z_{ss} = 1.13 corresponds to the findings of Penny and Hayhurst.

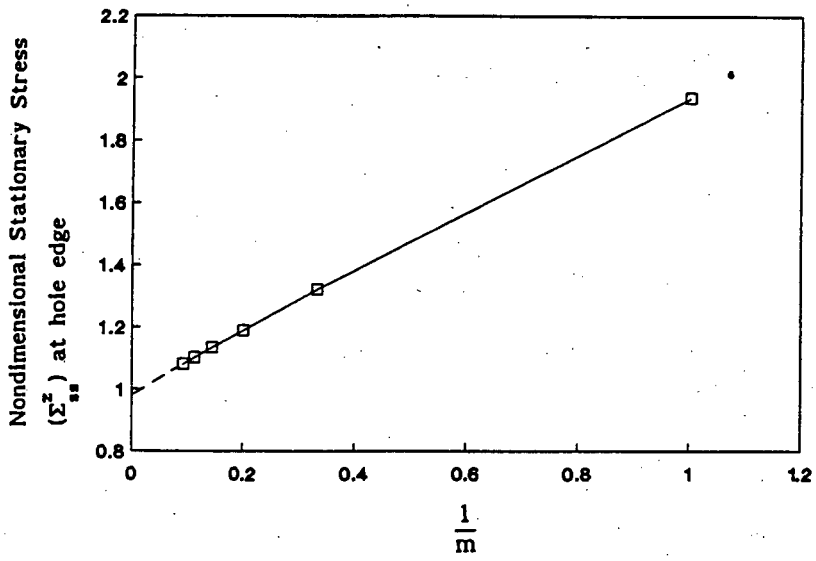

Figure 5.10 : Plot of stationary tangential stress at hole edge versus inverse of stress exponent m

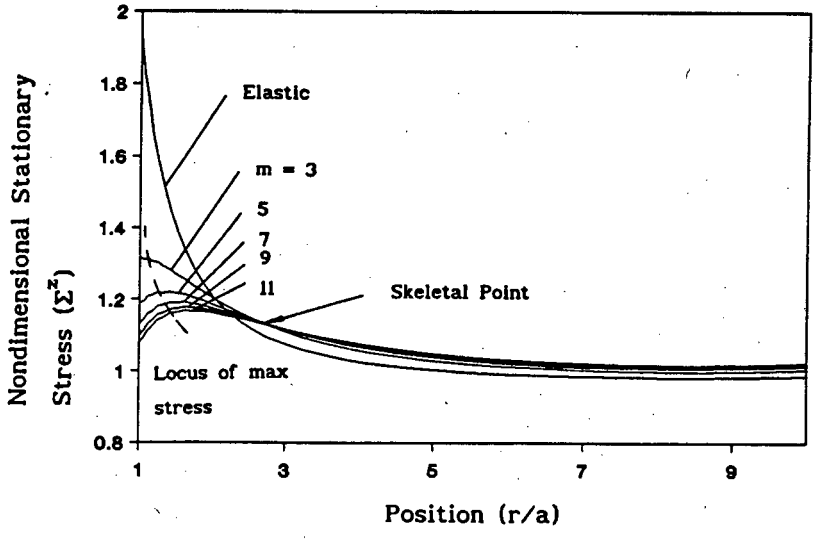

Figure 5.11 : Plot of stationary tangential stresses along r-axis

6 COMPONENT FAILURE CRITERIA AND RESIDUAL LIFE PREDICTION

The proposed method of creep deformation and rupture time prediction is particularly suitable for the initial design. As a residual life prediction method however, it has serious shortcomings. Firstly, as discussed earlier, the method can be conservative or unconservative, depending on the structural determinacy of the component. Secondly, it is only possible to predict an expended life based on constant load design data. The last shortcoming may be overcome if the proposed method is extended using a Life Fraction approach together with a typical load history. It is rarely possible to check the effects of the actual load history, as this load history is generally not known.

A solution will be proposed here which is suited to residual life prediction and which is based on the actual load history and the creep deformation of a component. The method is based on the coupled creep deformation and material degradation laws proposed by Rabotnov (1969), and assumes that it is possible to monitor the gross deformation of components at regular intervals. The method links actual deformation to the deformations predicted by stationary state analyses, and extracts information about the expended life from these data.

The formulation of the method is based on the normalised creep and creep/damage equations derived earlier (equations (4.24), (4.25), and (4.26)) :

$$\dot{\lambda}_{ij,c} = \Sigma^{*m} \frac{d\Sigma^*}{d\Sigma_{ij}} \tag{6.1}$$

$$\dot{\lambda}_{ij,cd} = \frac{\Sigma^{*m}}{(1-\omega)^p} \frac{d\Sigma^*}{d\Sigma_{ij}} \tag{6.2}$$

and

$$\dot{\omega} = C \frac{\Sigma_\beta^k}{(1-\omega)^r} \tag{6.3}$$

From equation (6.3) it is possible to derive an expression for the damage ω in terms of Γ, the life fraction measure :

$$\omega = 1 - (1 - \Gamma)^{1/1+r} \tag{6.4}$$

where r is usually assumed to be $r \simeq k \simeq p$ (Penny,1974). This relation is shown in Figure 6.1 for a range of values of r.

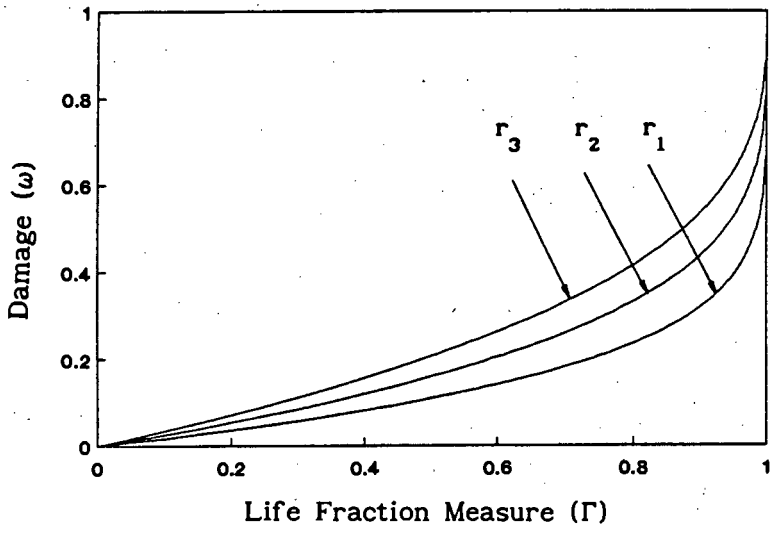

Figure 6.1 : Plot of damage versus life fraction measure

From this it appears that the damage is relatively insensitive to r for high values of r. From (6.1), (6.2), (6.3), and (6.4) it is possible to derive :

$$\lambda_{1j,c} = K\,\Gamma \tag{6.5}$$

$$\lambda_{1j,cd} = \eta\,K\left[1 - (1 - \Gamma)^{1/\eta}\right] \tag{6.6}$$

$$\frac{d\lambda_{1j,c}}{d\Gamma} = K \tag{6.7}$$

and

$$\frac{d\lambda_{1j,cd}}{d\Gamma} = K\,(1 - \Gamma)^{(1-\eta)/\eta} \tag{6.8}$$

where $$\eta = \frac{1 + r}{1 + r - p} \simeq 1 + r \quad \text{for } r \simeq p$$

and

$$K = \frac{1}{C\ (1+r)} \frac{\Sigma^{*m}}{\Sigma_\beta^k} \frac{d\Sigma^*}{d\Sigma_{1j}} = \tau_R\ \Sigma^{*m} \frac{d\Sigma^*}{d\Sigma_{1j}} = \dot{\lambda}_{1j,c}\ \tau_R$$

Figure 6.2 shows a generalised representation of stationary and damaged strain measures for a range of values of η as a function of the life fraction measure. Note that the strain measures (equations (6.5) and (6.6) respectively) are normalised with respect to $\lambda_{1j,c}$. Again the damaged strain measures are insensitive to r (or η) at high values.

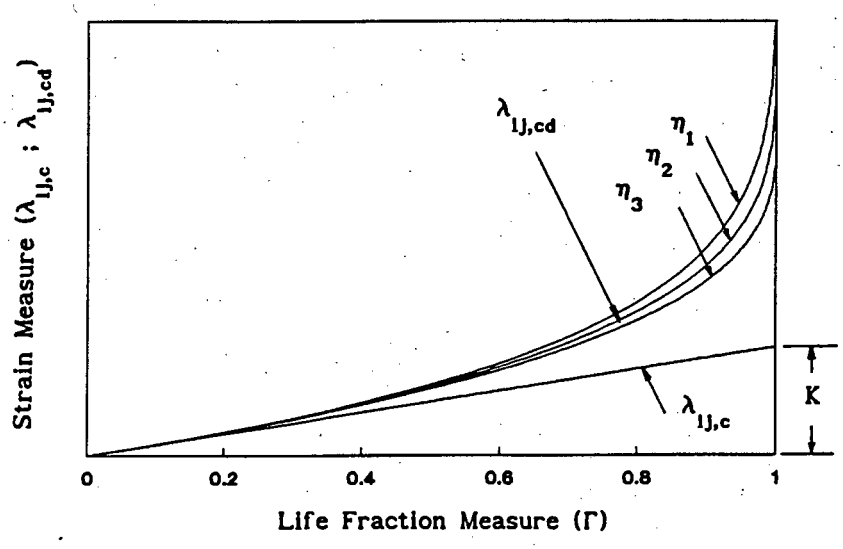

Figure 6.2 : Generalised representation of stationary and damaged strain measures as functions of the life fraction measure

The above discussion leads to the development of three failure criteria which can be used to calculate component retirement times from the gross deformation or gross deformation rate. The three failure criteria are represented schematically in Figure 6.3. The failure criteria allow the designer to choose a level of conservatism thought appropriate.

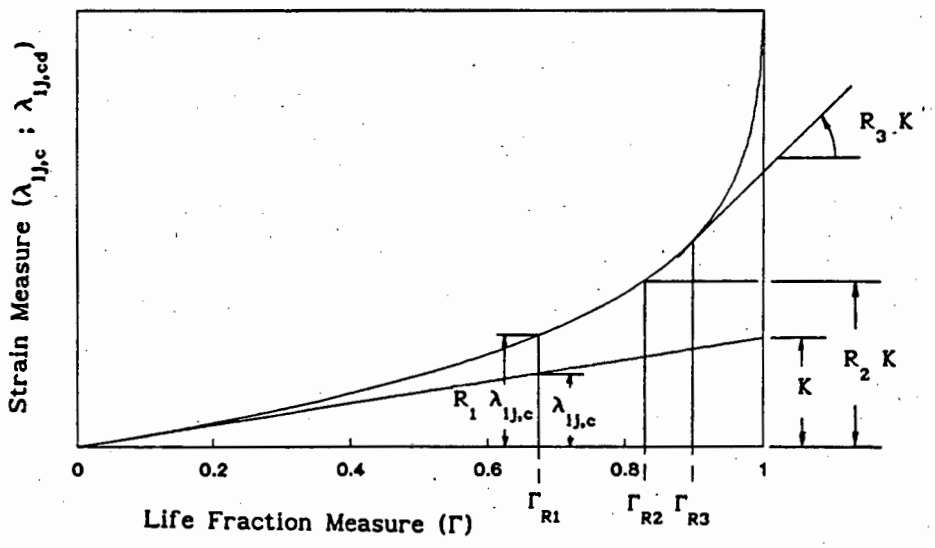

Figure 6.3 : Schematic representation of failure criteria based on strain measures

The first failure criteria links actual deformations to stationary state deformations. An acceptable value of creep strain which includes contributions from the *hardened* (stationary) and the *softened* (damage accumulated) state is chosen as a proportion R_1 of the hardened state, known from a computer simulation or from actual minimum strain rates. Then :

$$\lambda_{ij,cd} = R_1 \, \lambda_{ij,c} \tag{6.9}$$

and, using equations (6.5) and (6.6) :

$$\eta \left[1 - \left(1 - \Gamma_{R1} \right)^{1/\eta} \right] = R_1 \, \Gamma_{R1} \tag{6.10}$$

Equation (6.10) cannot be solved explicitly, but various retirement life fractions corresponding to different values of R_1 and different values of η are plotted in Figure 6.4 .

The second failure criterion relates actual deformations to the stationary state deformation at rupture. The creep/damage strain is allowed to achieve a proportion R_2 ($1 \leq R_2 \leq \eta$) of the stationary state strain at rupture. Then :

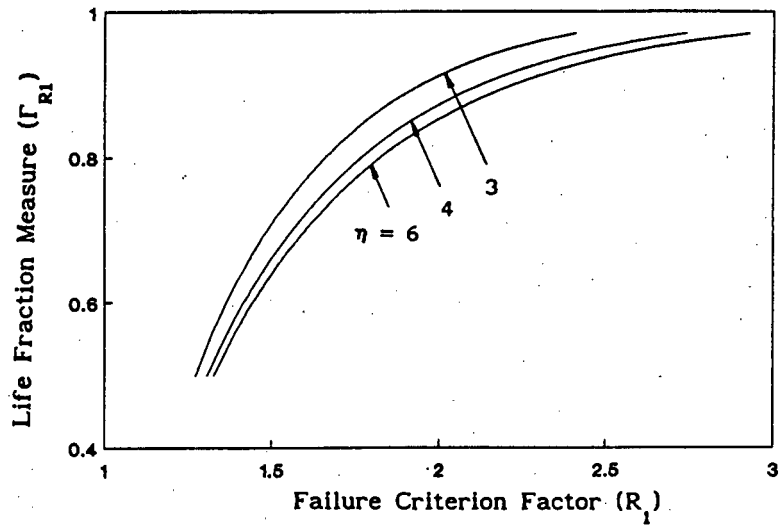

Figure 6.4 : Variation of life fraction using first failure criterion

$$\lambda_{ij,cd} = R_2 \, \lambda_{ij,c}{}_{\tau=\tau_R} \tag{6.11}$$

whence, using equations (6.5) and (6.6) :

$$\eta \left[1 - \left(1 - \Gamma_{R2} \right)^{1/\eta} \right] = R_2 \tag{6.12}$$

Equation (6.12) can be solved analytically, but a graphical representation is more convenient to use. This is shown in Figure 6.5 .

The last failure criterion links actual deformation rates to the stationary state deformation rate. An average measured deformation rate is related to the predicted or measured stationary state rate by a factor R_3 :

$$\dot{\lambda}_{ij,cd} = R_3 \, \dot{\lambda}_{ij,c} \tag{6.13}$$

and, using equations (6.5) and (6.6) :

$$\Gamma_{R3} = 1 - R_3^{\eta(1-\eta)^{-1}} \tag{6.14}$$

This relationship is shown in Figure 6.6.

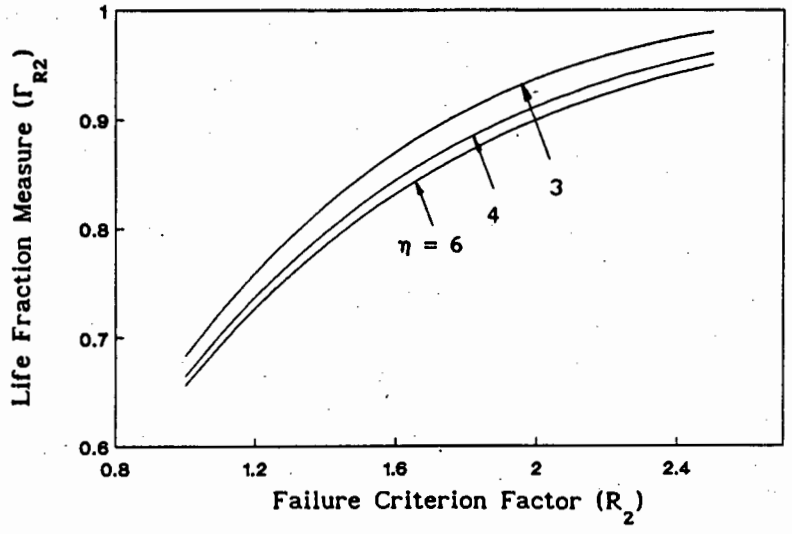

Figure 6.5 : Variation of life fraction using second failure criterion

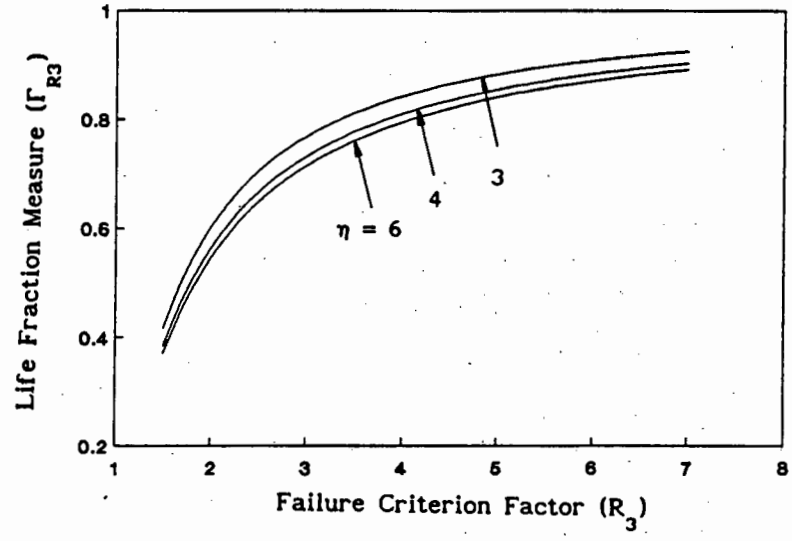

Figure 6.6 : Variation of life fraction using third failure criterion

The method allows the user to determine the expended life of a component from a comparison of the actual deformation to the deformation predicted from a stationary state analysis or to actual stationary state deformations. More useful though is the inverse method, where the designer chooses a safe retirement life fraction and corresponding failure ratios, and monitors the deformation of a component throughout its life until the failure ratios have been achieved. This approach also allows the designer to choose rational inspection intervals : if from previous inspections a certain safe life fraction remains, the next inspection must occur well within the remaining

life of the component. Inspection intervals can then be allowed to vary throughout the life of the component.

At this stage, the method is hypothetical, and will need to be backed up by experimental work, especially on multiaxial components. An ideal application, and a possible means for verification, is pipework. Should experimental work verify this method, or provide indications of how to modify it, a fast and simple procedure for in situ damage monitoring will result.

7 PROBLEMS STUDIED AND RESULTS

A number of problems was studied by the stationary state analysis. In some cases a complete creep/damage analysis was performed. The objective of this exercise was to verify the proposed methods against as many checks as possible, as well as to illustrate the methods. The geometries that were modeled are a uniaxial creep specimen, an hourglass specimen, a circular rod with a circumferential notch, a plate with a circular hole under uni- and equibiaxial tension, pipes under internal pressure of three different internal-to-external radius ratios , and a pressure vessel containing a radial branch. The stationary state stresses and strain measures that resulted for these problems are discussed in this section. The following section will present three case studies covering complete creep/damage analyses.

The finite element program used in all cases was ABAQUS Version 5.7 (Hibbitt et al.,1988) installed on a VAX 6230. ABAQUS is a commercial F.E.M. program that is particularly suited to non-linear analyses. 8-noded quadratic solid elements were used primarily, and the mesh geometries were subjected to mesh sensitivity analyses in order to optimise the results. Where possible, results were compared with analytical solutions, and errors were found to be less than 3%. Use was also made of the standard load and strain accumulation tolerancing capabilities of ABAQUS to prevent instability and numerical errors. Little difference was found between using implicit or explicit integration schemes. All runs were allowed to continue well into the stationary state in order to find accurate values for the stationary state deformation rates.

The first step in each problem was to find the relationship between the reference stress and the load, i.e. to quantify the reference stress parameter α. This was achieved by using the second method developed by Sim (1968), described in Section 5.3. The regions of high stress and strain were identified from contour plots and attention was focused on these regions. The problem was then run over a range of stress exponents ($m = 1 \rightarrow 11$), and all the relevant data was extracted from the finite element analysis.

7.1 UNIAXIAL CREEP SPECIMEN AND HOURGLASS SPECIMEN

The uniaxial specimen is a model of a typical creep specimen. It was chosen to verify the deformations predicted by the stationary state analysis when using material constants gathered from experimental data. The mesh and geometry characteristics of this specimen are shown in Figure 7.1. An hourglass specimen was also modeled after it was observed that considerable differences existed between strains and strain rates measured across the gauge length and across the cross-head ends. The geometry of the hourglass specimen were taken from Taira (1973) ; the geometry and mesh details are shown in Figure 7.2. Lastly, the gauge length of the uniaxial creep specimen was varied to study the effect on the measurement of strains and strain rates.

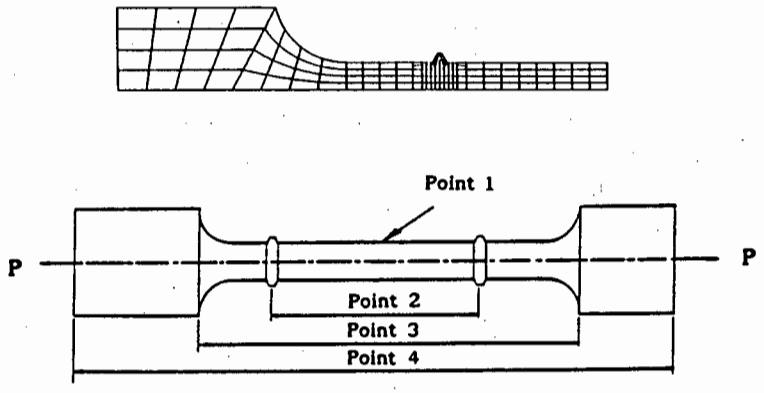

Figure 7.1 : Uniaxial creep specimen ; geometry and mesh details

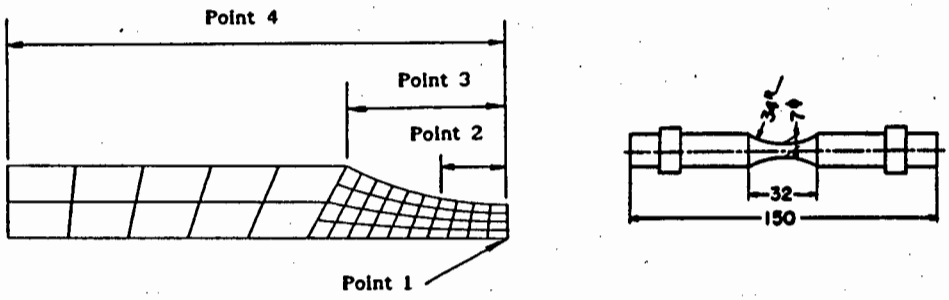

Figure 7.2 : Hourglass specimen ; geometry and mesh details

Figure 7.3 shows the variation of the elastic strain measurement with gauge length for the uniaxial creep specimen. Figure 7.4 shows the variation of

creep strain rate measurement with gauge length at different stress exponents m. Note here that all strains and strain rates have been normalised with respect to the true strain and strain rate at the mid-section (point 1), and that gauge length ratio relates the gauge length of the analysis to the gauge length of the original creep specimen.

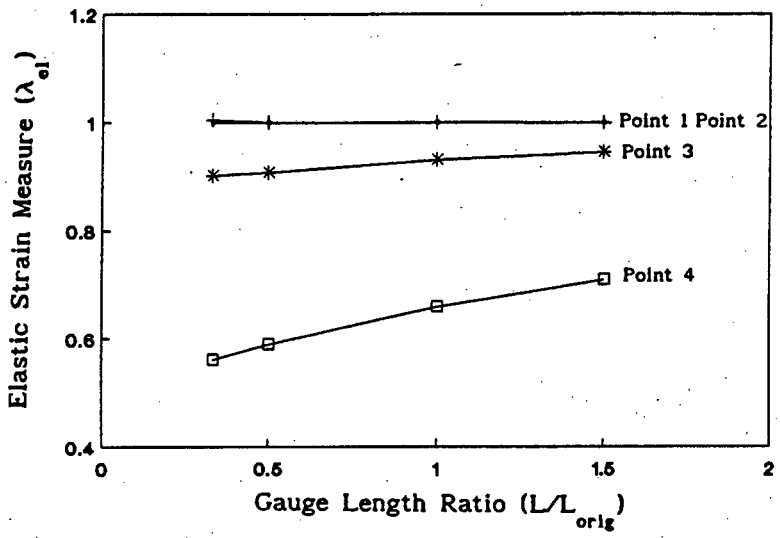

Figure 7.3 : Variation of elastic strain with gauge length at different measurement locations

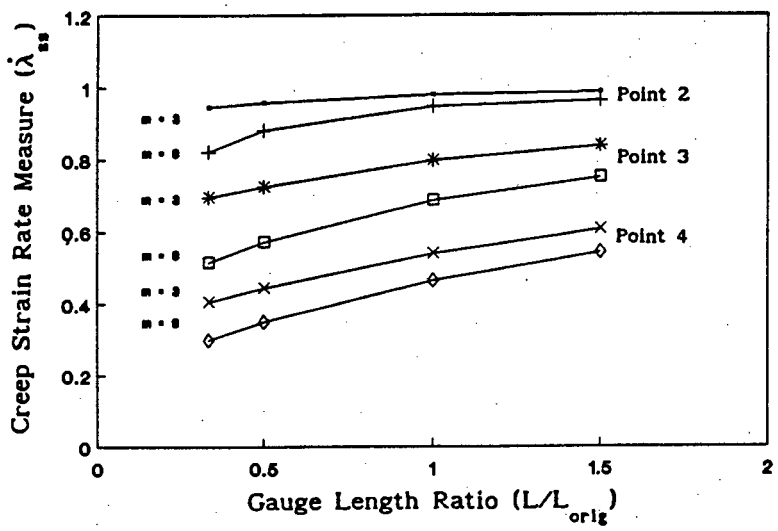

Figure 7.4 : Variation of creep strain rate with gauge length at different measurement locations and for different stress exponents

From all these plots it can be concluded that strains and strain rates calculated from displacements across the shoulders and the cross-head will be

in considerable error. The gauge length as a ratio of the diameter is also an important factor in the design of specimens from which displacements and strains are measured.

Similar analyses were done for the hourglass specimen. Figure 7.5 shows the variation of creep strain rate with stress exponent m at various possible extensometer locations. From here it is obvious that a uniaxial specimen with a long stem of constant diameter will perform better when creep strains and strain rates are measured.

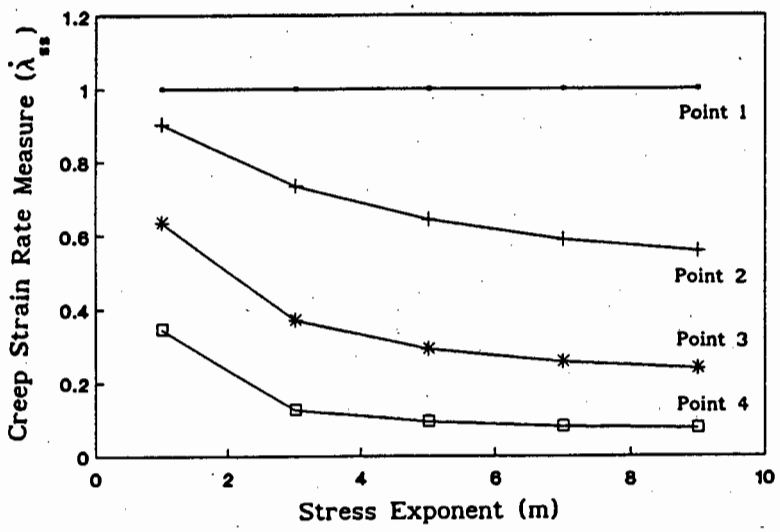

Figure 7.5 : Variation of creep strain rate with measurement location

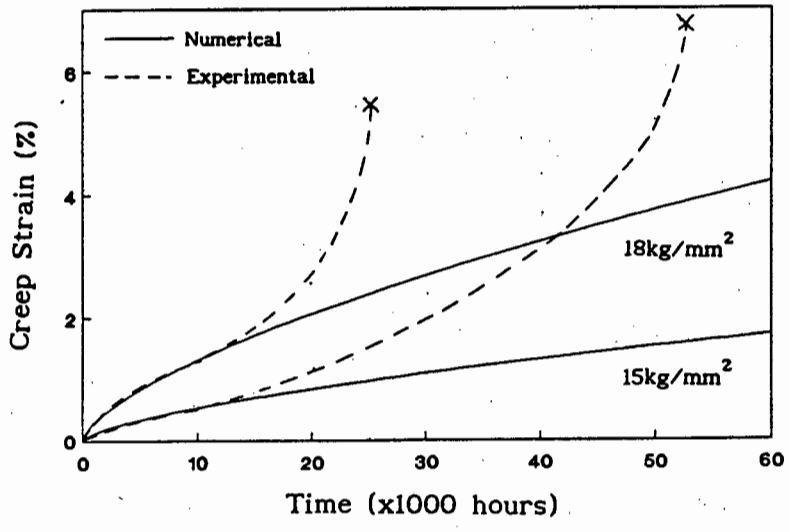

Figure 7.6 : Comparison of creep deformation from uniaxial creep specimen with experimental results

Figure 7.10 shows how the creep deformation predicted by the stationary state analysis differs from the creep deformation of the test from which the material data was acquired. The material constants are derived in Appendix C from long term tests by Krisch (1963).

7.2 CIRCULAR ROD WITH CIRCUMFERENTIAL NOTCH

The geometry of this component was used by Sieburg (1989) in a stress analysis which coupled the creep deformation with material degradation. This component will be used in Case Study 1 in the following section where the predicted life from the present analysis will be compared with the predicted life from the Sieburg analysis.

Geometry and mesh details are shown in Figure 7.7. Table 7.1 gives the maximum stress and strain measures for a range of stress exponents. Note that the non-dimensional stationary state stresses decrease with stress exponent. The upper bound deformation parameter γ occurs for stress exponent m = 11. Figure 7.8 shows the variation of initial and stationary maximum principal stress with postion along the r-axis. It can be seen that the maximum stationary state principal stress moves inwards relative to the maximum elastic principal stress. This was also found by Sieburg. The skeletal point is close to the position of maximum stationary state principal stress.

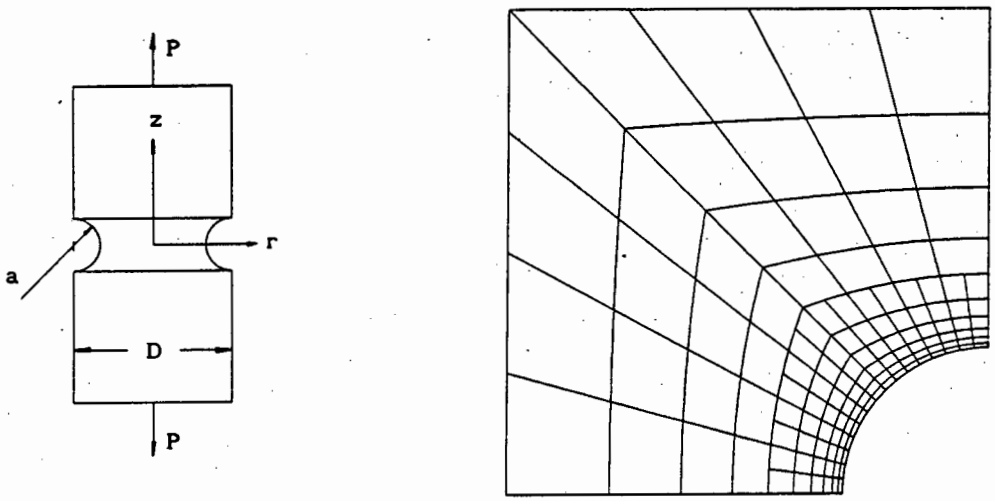

Figure 7.7 : Notched rod ; geometry and mesh details

Circular rod with circumferential notch ; D = 2.0 ; d = 1.4 ; α = 0.7076						
	m = 1	m = 3	m = 5	m = 7	m = 9	m = 11
Σ^{*}_{el}	2.512 (0.7)	2.512 (0.7)	2.512 (0.7)	2.512 (0.7)	2.512 (0.7)	2.512 (0.7)
Σ^{*}_{ss}	2.392 (0.7)	1.460 (0.7)	1.266 (0.7)	1.181 (0.7)	1.133 (0.7)	1.102 (0.7)
Σ^{I}_{el}	2.787 (0.7)	2.787 (0.7)	2.787 (0.7)	2.787 (0.7)	2.787 (0.7)	2.787 (0.7)
Σ^{I}_{ss}	2.720 (0.7)	1.802 (0.6)	1.790 (0.6)	1.800 (0.6)	1.799 (0.6)	1.790 (0.6)
Σ^{z}_{el}	2.787 (0.7)	2.787 (0.7)	2.787 (0.7)	2.787 (0.7)	2.787 (0.7)	2.787 (0.7)
Σ^{z}_{ss}	2.720 (0.7)	1.802 (0.6)	1.790 (0.6)	1.800 (0.6)	1.799 (0.6)	1.790 (0.6)
λ^{z}_{el}	2.579 (0.7)	2.579 (0.7)	2.579 (0.7)	2.579 (0.7)	2.579 (0.7)	2.579 (0.7)
γ	-	0.270	0.703	0.995	1.215	1.263
$\dot{\lambda}^{z}_{ss}$	2.259	2.919	3.013	2.989	2.877	2.759
Note : Locations given in brackets are approximate values along the r-axis						

Table 7.1 : Notched rod ; maximum non-dimensional stresses and strains

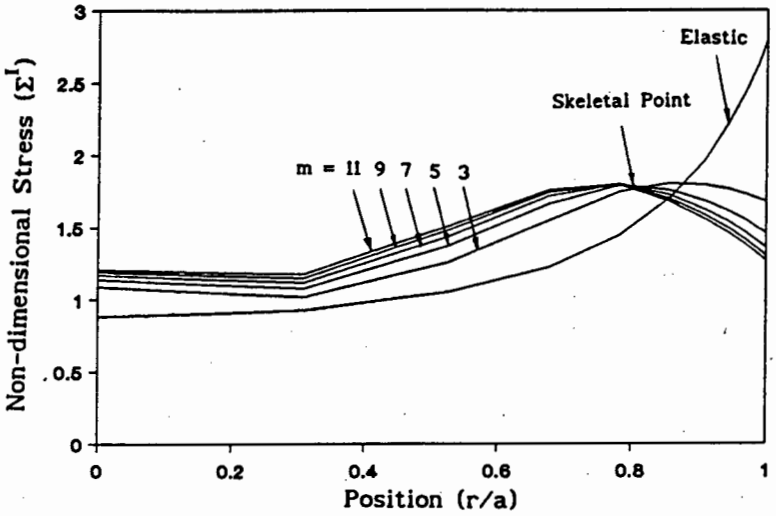

Figure 7.8 : Variation of non-dimensional principal stresses along r-axis

7.3 PLATE WITH CIRCULAR HOLE

The plate with a circular hole was studied by Penny and Hayhurst (1969) and Hayhurst (1970). Figure 5.5 gives geometry and mesh details. The results for the equibiaxial tension case have been discussed earlier. Table 7.2 gives

maximum stresses and strain measures for a range of stress exponents in the uniaxial tension case. The initial tangential stress at the hole edge is 3% too high when compared to the analytically predicted value (i.e. three times the load α) (Faupel and Fisher,1981). The plate with hole under equibiaxial tension will be studied in more depth in Case Study 2 where comparisons will be made with numerical and experimental work of Hayhurst and Penny.

Plate with hole : uniaxial tension ; a/w = 1/10 ; α = 0.8285						
	m = 1	m = 3	m = 5	m = 7	m = 9	m = 11
Σ^{*}_{el}	2.551 (1.0)	2.551 (1.0)	2.551 (1.0)	2.551 (1.0)	2.551 (1.0)	2.551 (1.0)
Σ^{*}_{ss}	2.556 (1.0)	1.556 (1.0)	1.327 (1.0)	1.221 (1.0)	1.159 (1.0)	1.119 (1.0)
Σ^{I}_{el}	2.562 (1.0)	2.562 (1.0)	2.562 (1.0)	2.562 (1.0)	2.562 (1.0)	2.562 (1.0)
Σ^{I}_{ss}	2.572 (1.0)	1.556 (1.0)	1.335 (1.0)	1.246 (1.1)	1.202(1.25)	1.172(1.25)
Σ^{z}_{el}	2.562 (1.0)	2.562 (1.0)	2.562 (1.0)	2.562 (1.0)	2.562 (1.0)	2.562 (1.0)
Σ^{z}_{ss}	2.572 (1.0)	1.556 (1.0)	1.335 (1.0)	1.246 (1.1)	1.202(1.25)	1.172(1.25)
λ^{z}_{el}	2.555	2.555	2.555	2.555	2.555	2.555
γ	-	0.516	0.710	1.188	1.380	1.630
$\dot{\lambda}^{z}_{ss}$	2.465	3.614	3.989	3.904	3.662	3.340
U^{z}_{el}	2.557	2.557	2.557	2.557	2.557	2.557
γ	-	0.083	0.261	0.361	0.392	0.427
$\dot{U}^{z}_{ss}$	2.557	2.664	2.576	2.139	1.844	1.568
Note : Locations given in brackets are approximate values along the r-axis Values for λ^{z} taken at r = 1.0 ; z = 0.0 (used for finding α) Values for U^{z} taken at r = 0.0 ; z = 1.0						

Table 7.2 : Plate with hole under uniaxial tension ; maximum non-dimensional stresses and strain measures

7.4 PIPE UNDER INTERNAL PRESSURE

Pipes under internal pressure were studied by Sim and Penny (1971) who covered a wide variety of internal-to-external radius ratios. Here three different

internal-to-external radius ratios X_o will be analysed, namely X_o = 0.9, 0.7, and 0.5. Figure 7.9 shows generalised geometry and mesh details for the three cases. Tables 7.3, 7.4, and 7.5 list the maximum stresses and strain measures for different stress exponents for X_o = 0.9, X_o = 0.7, and X_o = 0.5 respectively. Figures 7.10, 7.11, and 7.12 show the initial and stationary maximum principal stress distribution along the r-axis for X_o = 0.9, X_o = 0.7, and X_o = 0.5 respectively. All plots show skeletal points occurring in the middle of the pipe, as is predicted by Soderberg (1941).

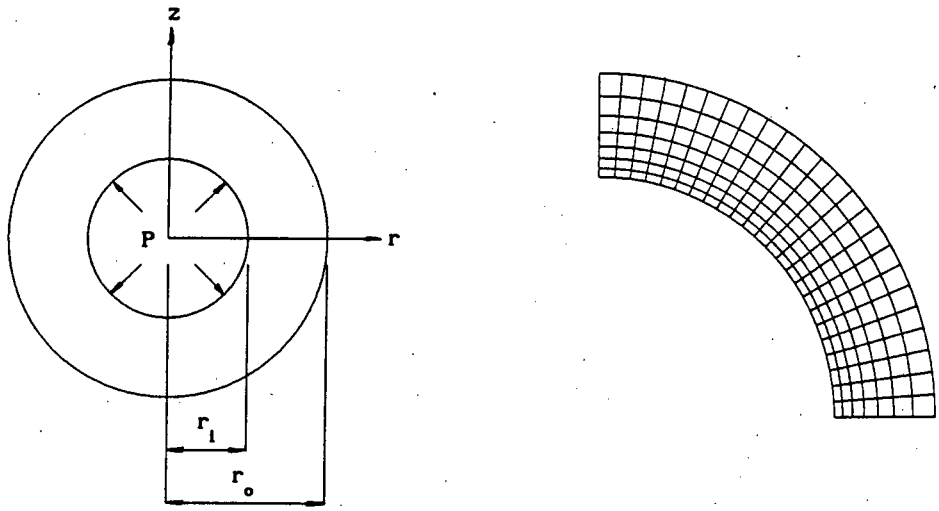

Figure 7.9 : Pipe under internal pressure ; geometry and mesh details

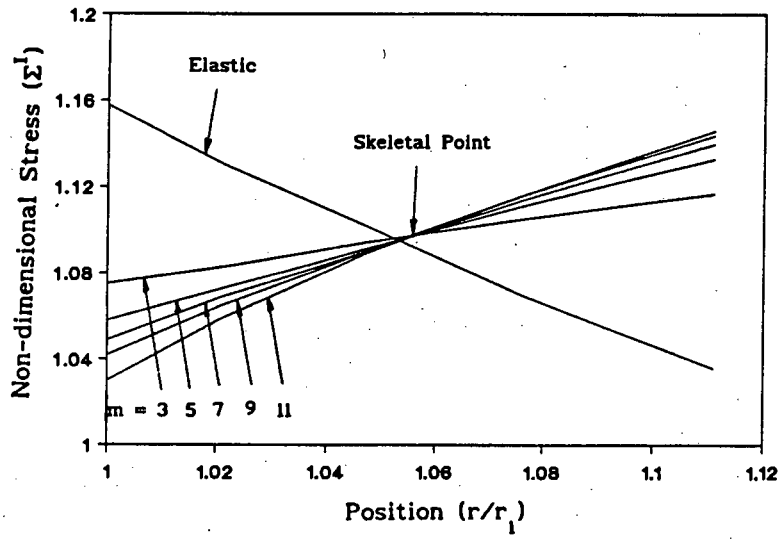

Figure 7.10 : Pipe (X_o = 0.9) ; variation of principal stress along r-axis

Thin pipe under internal pressure ; r_i/r_o = 0.9 ; α = 0.1215						
	m = 1	m = 3	m = 5	m = 7	m = 9	m = 11
Σ^{*}_{el}	1.121 (0.9)	1.121 (0.9)	1.121 (0.9)	1.121 (0.9)	1.121 (0.9)	1.121 (0.9)
Σ^{*}_{ss}	1.107 (0.9)	1.034 (0.9)	1.020 (0.9)	1.012 (0.9)	1.009 (0.9)	1.000 (0.9)
Σ^{I}_{el}	1.158 (0.9)	1.158 (0.9)	1.158 (0.9)	1.158 (0.9)	1.158 (0.9)	1.158 (0.9)
Σ^{I}_{ss}	1.159 (0.9)	1.117 (1.0)	1.133 (1.0)	1.140 (1.0)	1.144 (1.0)	1.147 (1.0)
Σ^{z}_{el}	1.158 (0.9)	1.158 (0.9)	1.158 (0.9)	1.158 (0.9)	1.158 (0.9)	1.158 (0.9)
Σ^{z}_{ss}	1.159 (0.9)	1.117 (1.0)	1.133 (1.0)	1.140 (1.0)	1.144 (1.0)	1.147 (1.0)
Σ^{r}_{el}	-0.121(0.9)	-0.121(0.9)	-0.121(0.9)	-0.121(0.9)	-0.121(0.9)	-0.121(0.9)
Σ^{r}_{ss}	-0.119(0.9)	-0.119(0.9)	-0.119(0.9)	-0.118(0.9)	-0.116(0.9)	-0.117(0.9)
λ^{z}_{el}	1.085 (0.9)	1.085 (0.9)	1.085 (0.9)	1.085 (0.9)	1.085 (0.9)	1.085 (0.9)
γ	0.040	0.055	0.084	0.092	0.099	0.106
$\dot{\lambda}^{z}_{ss}$	0.953	0.952	0.948	0.947	0.947	0.946
U^{r}_{el}	0.976 (0.9)	0.976 (0.9)	0.976 (0.9)	0.976 (0.9)	0.976 (0.9)	0.976 (0.9)
γ	0.023	0.074	0.081	0.088	0.110	0.117
$\dot{U}^{r}_{ss}$	0.864	0.859	0.858	0.857	0.856	0.854
U^{r}_{el}	0.923 (1.0)	0.923 (1.0)	0.923 (1.0)	0.923 (1.0)	0.923 (1.0)	0.923 (1.0)
γ	0.035	0.050	0.057	0.081	0.089	0.096
$\dot{U}^{r}_{ss}$	0.777	0.776	0.775	0.772	0.772	0.771
Note : Locations given in brackets are values along the r-axis						

Table 7.3 : Pipe (X_o = 0.9) ; maximum non-dimensional stresses and strains

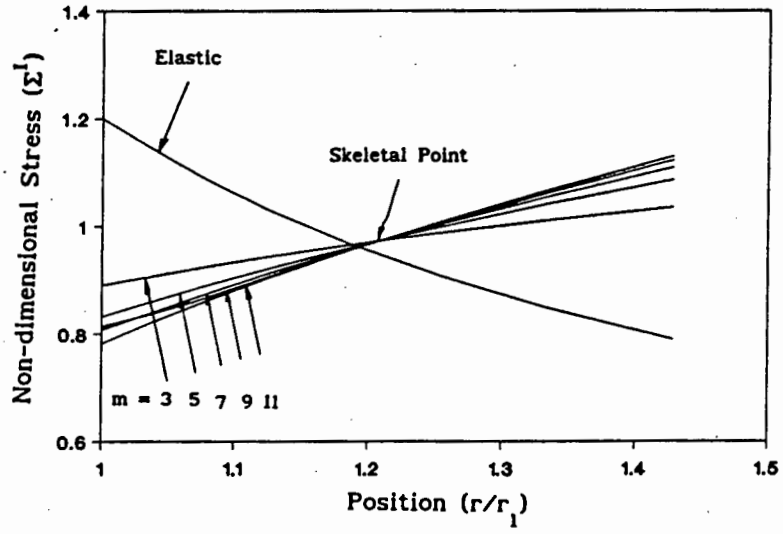

Figure 7.11 : Pipe (X_o = 0.7) ; variation of principal stress along r-axis

Pipe under internal pressure ; r_i/r_o = 0.7 ; α = 0.4106						
	m = 1	m = 3	m = 5	m = 7	m = 9	m = 11
Σ^*_{el}	1.401 (0.7)	1.401 (0.7)	1.401 (0.7)	1.401 (0.7)	1.401 (0.7)	1.401 (0.7)
Σ^*_{ss}	1.394 (0.7)	1.120 (0.7)	1.070 (0.7)	1.049 (0.7)	1.070 (0.7)	1.027 (0.7)
Σ^I_{el}	1.200 (0.7)	1.200 (0.7)	1.200 (0.7)	1.200 (0.7)	1.200 (0.7)	1.200 (0.7)
Σ^I_{ss}	1.206 (0.7)	1.035 (1.0)	1.086 (1.0)	1.109 (1.0)	1.122 (1.0)	1.130 (1.0)
Σ^z_{el}	1.200 (0.7)	1.200 (0.7)	1.200 (0.7)	1.200 (0.7)	1.200 (0.7)	1.200 (0.7)
Σ^z_{ss}	1.206 (0.7)	1.035 (1.0)	1.086 (1.0)	1.109 (1.0)	1.122 (1.0)	1.130 (1.0)
Σ^r_{el}	-0.410(0.7)	-0.410(0.7)	-0.410(0.7)	-0.410(0.7)	-0.410(0.7)	-0.410(0.7)
Σ^r_{ss}	-0.403(0.7)	-0.403(0.7)	-0.403(0.7)	-0.403(0.7)	-0.422(0.7)	-0.403(0.7)
λ^z_{el}	1.249 (0.7)	1.249 (0.7)	1.249 (0.7)	1.249 (0.7)	1.249 (0.7)	1.249 (0.7)
γ	0.035	0.073	0.136	0.162	0.188	0.239
$\dot{\lambda}^z_{ss}$	1.195	1.207	1.199	1.195	1.191	1.182
U^r_{el}	0.874 (0.7)	0.874 (0.7)	0.874 (0.7)	0.874 (0.7)	0.874 (0.7)	0.874 (0.7)
γ	0.035	0.059	0.125	0.142	0.190	0.231
$\dot{U}^r_{ss}$	0.844	0.853	0.848	0.845	0.840	0.835
U^r_{el}	0.703 (1.0)	0.703 (1.0)	0.703 (1.0)	0.703 (1.0)	0.703 (1.0)	0.703 (1.0)
γ	0.054	0.105	0.125	0.135	0.186	0.206
$\dot{U}^r_{ss}$	0.590	0.594	0.593	0.592	0.588	0.585
Note : Locations given in brackets are values along the r-axis						

Table 7.4 : Pipe (X_o = 0.7) ; maximum non-dimensional stresses and strains

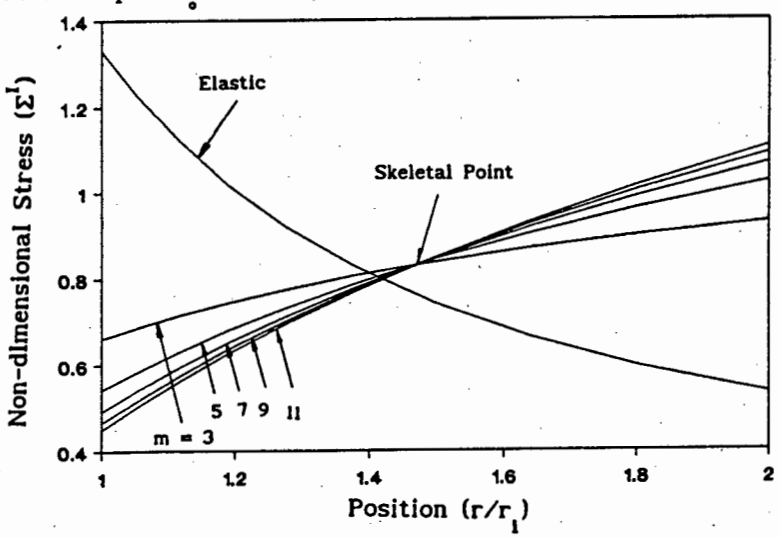

Figure 7.12 : Pipe (X_o = 0.5) ; variation of principal stress along r-axis

Thick pipe under internal pressure ; r_1/r_o = 0.5 ; α = 0.798						
	m = 1	m = 3	m = 5	m = 7	m = 9	m = 11
$\Sigma^{\bullet}_{el}$	1.844 (0.5)	1.844 (0.5)	1.844 (0.5)	1.844 (0.5)	1.844 (0.5)	1.844 (0.5)
$\Sigma^{\bullet}_{ss}$	1.842 (0.5)	1.245 (0.5)	1.141 (0.5)	1.099 (0.5)	1.076 (0.5)	1.061 (0.5)
Σ^{I}_{el}	1.331 (0.5)	1.331 (0.5)	1.331 (0.5)	1.331 (0.5)	1.331 (0.5)	1.331 (0.5)
Σ^{I}_{ss}	1.349 (0.5)	0.930 (1.0)	1.024 (1.0)	1.066 (1.0)	1.090 (1.0)	1.106 (1.0)
Σ^{z}_{el}	1.331 (0.5)	1.331 (0.5)	1.331 (0.5)	1.331 (0.5)	1.331 (0.5)	1.331 (0.5)
Σ^{z}_{ss}	1.349 (0.5)	0.930 (1.0)	1.024 (1.0)	1.066 (1.0)	1.090 (1.0)	1.106 (1.0)
Σ^{r}_{el}	-0.795(0.5)	-0.795(0.5)	-0.795(0.5)	-0.795(0.5)	-0.795(0.5)	-0.795(0.5)
Σ^{r}_{ss}	-0.776(0.5)	-0.776(0.5)	-0.776(0.5)	-0.776(0.5)	-0.776(0.5)	-0.776(0.5)
λ^{z}_{el}	1.535 (0.5)	1.535 (0.5)	1.535 (0.5)	1.535 (0.5)	1.535 (0.5)	1.535 (0.5)
γ	0.053	0.209	0.304	0.430	0.532	0.586
$\dot{\lambda}^{z}_{ss}$	1.570	1.640	1.658	1.653	1.645	1.641
U^{r}_{el}	1.535 (0.5)	1.535 (0.5)	1.535 (0.5)	1.535 (0.5)	1.535 (0.5)	1.535 (0.5)
γ	0.053	0.216	0.332	0.413	0.526	0.589
$\dot{U}^{r}_{ss}$	1.590	1.661	1.674	1.676	1.666	1.661
U^{r}_{el}	0.948 (1.0)	0.948 (1.0)	0.948 (1.0)	0.948 (1.0)	0.948 (1.0)	0.948 (1.0)
γ	0.086	0.157	0.263	0.371	0.420	0.495
$\dot{U}^{r}_{ss}$	0.792	0.835	0.840	0.837	0.836	0.831
τ_{ss}	-	$\propto$ 3.7	$\propto$ 2.5	$\propto$ 2.4	$\propto$ 2.3	$\propto$ 2.2
Note : Locations given in brackets are along the r-axis						

Table 7.5 : Pipe (X_o = 0.5) ; maximum non-dimensional stresses and strains

The stationary state stresses and strain rates compare well with the analytical solutions derived by Bailey (1935), namely :

$$\Sigma^{z}_{ss} = \left[\frac{(2-m)/m \; (r_o/r)^{2/m} + 1}{(r_o/r_1)^{2/m} - 1} \right] \alpha \qquad (7.1)$$

and

$$\dot{\lambda}^{z}_{bore} = \left(\frac{3}{4}\right)^{(m+1)/2} \left(\frac{r_o}{r_i}\right)^{2} \left[\frac{2}{m} \frac{\alpha}{(r_o/r_i)^{2/m} - 1}\right] \qquad (7.2)$$

The case of $X_o = 0.7$ will be examined further in Case Study 3 where a complete stationary state/creep rupture exercise will be followed through, including the calculation of inspection intervals based on the failure criteria.

7.5 PRESSURE VESSEL

An axisymmetric pressure vessel containing a radial branch was tested by Penny and Marriott (1973). Stationary state deformations were predicted using a finite difference scheme. The geometry and mesh details are shown in Figure 7.13. Table 7.6 lists maximum stresses and strain measures for the pressure vessel. Figure 7.14 shows a contour plot of the elastic Mises stresses and Figure 7.15 shows the stationary state Mises stresses. The complicated stress redistribution patterns can be seen from the contour plots.

Pressure vessel under internal pressure : α = 0.01385						
	m = 1	m = 3	m = 5	m = 7	m = 9	m = 11
Σ^{*}_{el}	1.909(2.01)	1.909(2.01)	1.909(2.01)	1.909(2.01)	1.909(2.01)	1.909(2.01)
Σ^{*}_{ss}	1.857(2.01)	1.252(2.01)	1.147(2.01)	1.103(2.01)	1.102(2.9o)	1.070(2.9o)
Σ^{I}_{el}	1.903(2.01)	1.903(2.01)	1.903(2.01)	1.903(2.01)	1.903(2.01)	1.903(2.01)
Σ^{I}_{ss}	1.889(2.01)	1.498(2.8o)	1.479(2.8o)	1.475(2.8o)	1.491(2.8o)	1.501(2.8o)
Σ^{θ}_{el}	1.903(2.01)	1.903(2.01)	1.903(2.01)	1.903(2.01)	1.903(2.01)	1.903(2.01)
Σ^{θ}_{ss}	1.889(2.01)	1.498(2.8o)	1.479(2.8o)	1.469(2.8o)	1.461(2.8o)	1.455(2.8o)
λ^{θ}_{el}	1.907(2.01)	1.907(2.01)	1.907(2.01)	1.907(2.01)	1.907(2.01)	1.907(2.01)
γ	-	0.095	0.155	0.232	0.280	0.328
$\dot{\lambda}^{\theta}_{ss}$	1.778	1.872	1.904	1.900	1.880	1.876
$\dot{\lambda}^{*}_{ss}$	1.857(2.01)	1.963(2.01)	1.988(2.01)	1.985(2.01)	1.970(2.01)	1.933(2.01)
Note : Locations in brackets are meriodonal angles at inner or outer surface						

Table 7.6 : Pressure vessel ; maximum non-dimensional stresses and strains

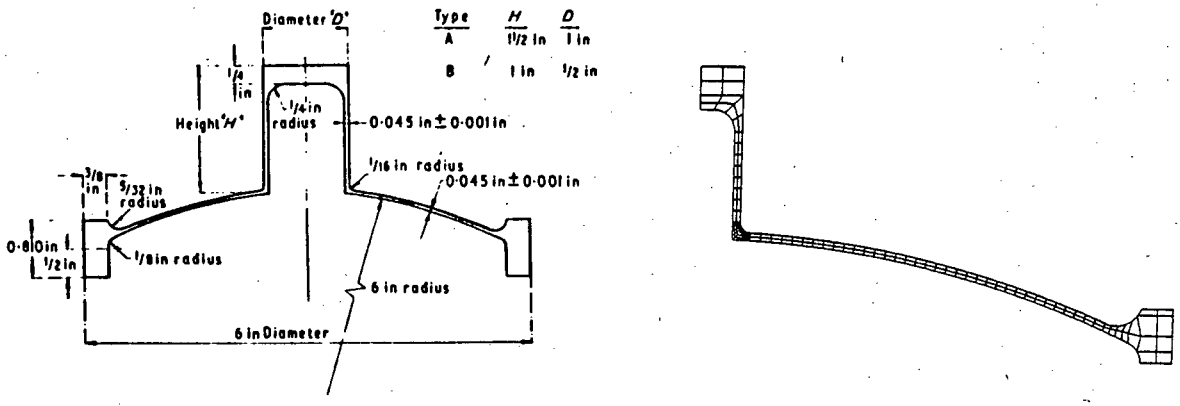

Figure 7.13 : Pressure vessel ; geometry and mesh details

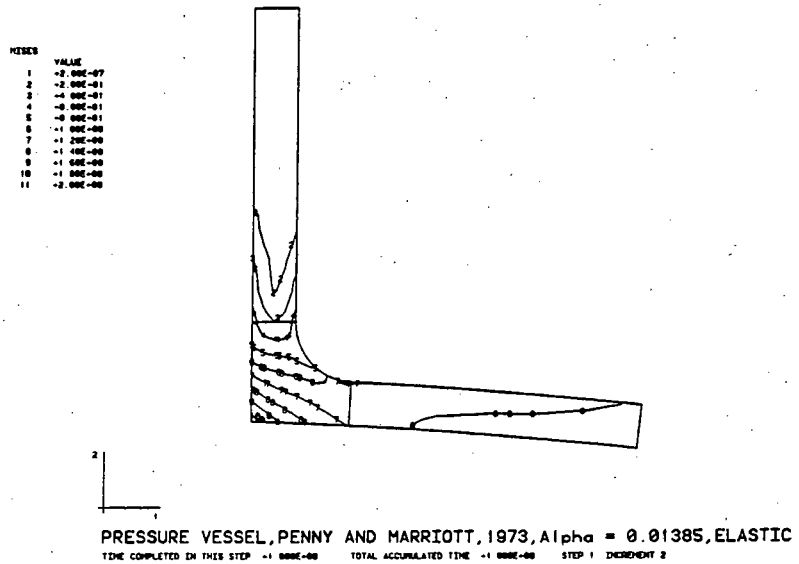

Figure 7.14 : Pressure vessel ; elastic Mises stress contour plot

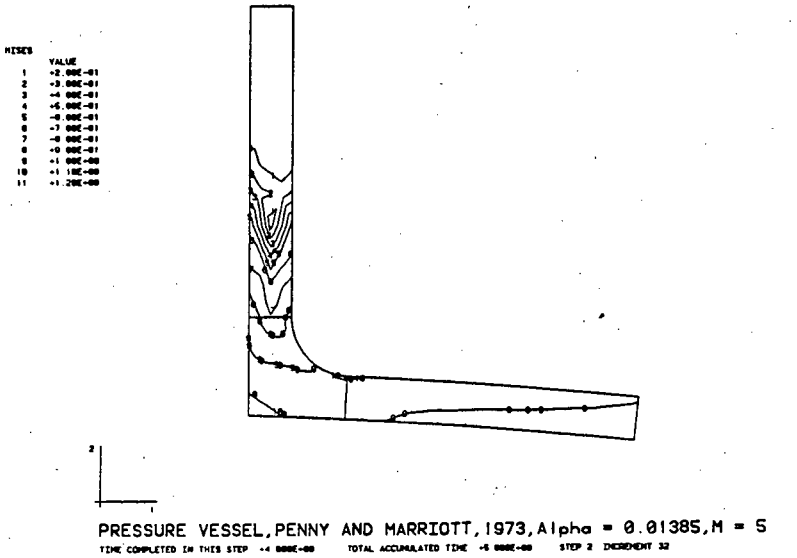

Figure 7.15 : Pressure vessel ; stationary Mises stress contour plot

8 CASE STUDIES

8.1 CASE STUDY 1 : NOTCHED ROD

A circular-cross section rod with a circumferential notch is subjected to a constant axial load of 120MPa at a temperature of 900°C. The ratio of the notch radius to the diameter of the rod is 0.15. The rod is made from a conventionally cast Nickel alloy MAR-M246. Short term experimental data from Harrison and Tilly (1973) were used by Sieburg (1989) to obtain the material parameters, listed in Table 8.1. It is required to estimate the rupture time from the maximum stationary state stresses.

m	k	n	A	B	E
8.400	8.500	1.076	$1.500\text{x}10^{-76}$	$1.720\text{x}10^{-76}$	$155\text{x}10^{9}$
Note : All units are in m/m, Nm^{-2}, and hour					

Table 8.1 : Material parameters for MAR-M246

The normalised initial and stationary state results for this problem are shown in Table 7.1. Assuming that the Hayhurst equivalent stress is the maximum principal stress, we find from Table 7.1 that the maximum stationary state principal stress, Σ^{I}_{ss}, for a stress exponent m = 8.4 is 1.799.

From the material parameters and the given loading, using equation (5.8) :

$$\bar{\sigma} = \frac{1}{\alpha} P = 169.6\text{MPa}$$

From equation (5.30) :

$$C = \frac{B\,\bar{\sigma}^{(1+k-m)}}{A\,E} = 8.35\text{x}10^{-3}$$

and

$$\tau_R = \frac{1}{C\ (1+r)\left(\Sigma^I_{ss}\right)^k} = 8.57\text{x}10^{-2}$$

From equation (5.10) :

$$t_R = \left(\frac{\tau_R}{A\ E\ \bar{\sigma}^{(m-1)}}\right)^{1/n} = 302 \text{ hours}$$

This result compares with a value of 274 hours by Sieburg (1989) who performed an analysis which coupled the creep and damage accumulation. The rupture time predicted from the maximum stationary state stress in the component will be an upper bound as the component is statically determinate : the component is not able to shed the high local stresses resulting from local damage. The result is favourable since the coupled analysis took approximately ten times as long in CPU on a Vax 6230 as the decoupled approach suggested here.

8.2 CASE STUDY 2 : PLATE WITH HOLE

A plate with a circular hole under equibiaxial tension was modeled and tested by Penny and Hayhurst (1969) and Hayhurst (1970). A similar plate was analysed using the present method and maximum initial and stationary stresses and strain measures are listed in Table 5.1.

Penny and Hayhurst (1969) studied the stationary creep behaviour of an aluminium plate under equibiaxial load of 7000 lb/in^2. The material constants for the aluminium are given in Table 8.3.

m	n	A	E
3.500	0.200	$2.090\text{x}10^{-18}$	$11.2\text{x}10^6$
Note : All units are in in/in, lb/in^2, and hours			

Table 8.2 : Material constants for aluminium plate

From Table 5.1, and using equation (5.8), the reference stress and strain are :

$$\bar{\sigma} = \frac{1}{\alpha} P = 7318 \text{ lb/in}^2$$

and

$$\bar{\varepsilon} = \frac{\bar{\sigma}}{E} = 653.4 \times 10^{-6}$$

From equation (5.24), the normalised strain-time behaviour at the hole edge is :

$$\lambda = (1 + \gamma)\, \lambda_{el} + \dot{\lambda}_{ss}\, \tau$$

where $\gamma = 0$ is the lower bound, $\gamma_{m=11}$ is the upper bound, and $\gamma_{m=3}$ is the closest to the actual problem. Rewriting the above expression in terms of real strains and times :

$$\varepsilon = \lambda\, \bar{\varepsilon} = (1 + \gamma)\, \lambda_{el}\, \bar{\varepsilon} + \dot{\lambda}_{ss}\, \bar{\varepsilon}\, \tau$$

where

$$\tau = A\, E\, \bar{\sigma}^m\, t^n$$

Substituting for the appropriate values from Table 5.1 and Table 8.2, and writing strains in terms of percent :

$$\varepsilon = 0.126\, (1 + \gamma) + 155.6 \times 10^{-4}\, t^{0.2}$$

The lower bound strain for $\gamma = 0$ is then

$$\varepsilon = 0.126 + 155.6 \times 10^{-4}\, t^{0.2}$$

and the upper bound strain for $\gamma = 0.389$ at $m = 11$ is

$$\varepsilon = 0.175 + 155.6 \times 10^{-4}\, t^{0.2}$$

while for $\gamma = 0.139$ at $m = 3$:

$$\varepsilon = 0.144 + 155.6 \times 10^{-4}\, t^{0.2}$$

These bounds are superposed on the experimental results from Penny and Hayhurst (1969) in Figure 8.1 . The best agreement occurs when $\gamma_{m=3}$ is used.

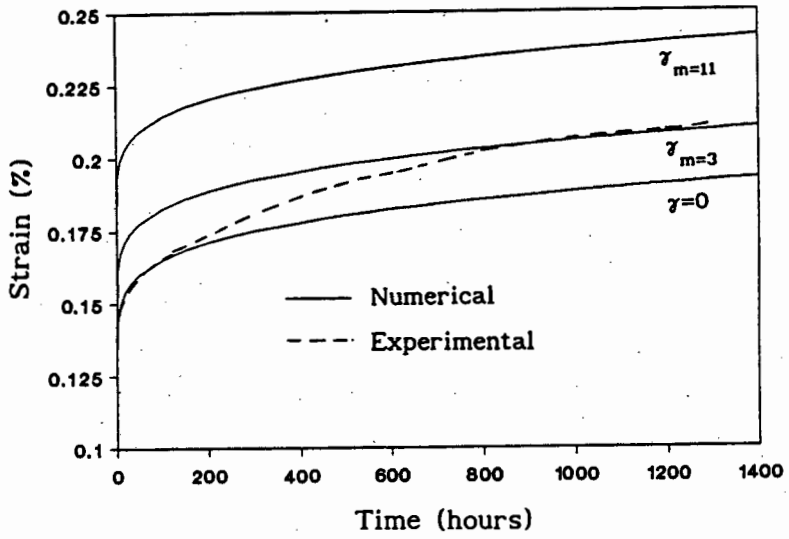

Figure 8.1 : Comparison of experimental and predicted deformations of plate with hole

Hayhurst (1970) performed rupture tests on aluminium plates and compared the experimental results with predictions from a coupled creep/damage analysis. The material constants for the aluminium are given in Table 8.3. The load on the plate was 7000 lb/in^2. From the material parameters, and using equation (5.30) the parameter C is :

$$C = \frac{B\,\bar{\sigma}^{(1+k-m)}}{A\,E} = 0.0368$$

m	k	r	n	A	B	E
3.30	5.30	2.74	0.66	5.00×10^{-18}	5.26×10^{-24}	11.2×10^{6}
Note : All units are in in/in, lb/in^2, and hours						

Table 8.3 : Material constants for aluminium plate

If the maximum stationary principal stress is used to calculate the rupture time, we obtain :

$$\tau_R = \frac{1}{C\ (1+r)\ \left(\Sigma_{ss}^{I}\right)^{k}} = 1.682$$

and

$$t_R = \left(\frac{\tau_R}{A\ E\ \bar{\sigma}^{(m-1)}}\right)^{1/n} = 256 \text{ hours}$$

If instead the stress at the skeletal point is used, then from Figure 5.11 :

$$\tau_R = 3.802 \quad \text{and} \quad t_R = 881 \text{ hours}$$

These rupture predictions are compared with Hayhurst's results in Table 8.4 :

Experimental rupture time (Hayhurst,1970)	410 hours
Computed lower bound rupture time (Hayhurst,1970)	390 hours
Computed rupture time from max stationary stress	256 hours
Computed rupture time from skeletal point	880 hours

Table 8.4 : Comparison of experimental and predicted rupture times

It can be seen that the rupture prediction from maximum stationary stresses is conservative, confirming the earlier discussion on structurally determinate components. The prediction based on the skeletal point is unconservative, and must be used with caution.

8.3 CASE STUDY 3 : PIPE UNDER INTERNAL PRESSURE

A pipe with inner and outer wall diameters of 70mm and 100mm respectively operates at 60MPa and 500°C. The material from which the pipe will be made

has already been chosen. It is required to predict the stationary state deformation at the inner and outer walls of the pipe, as well as the maximum initial and stationary state Mises and maximum principal stresses. The rupture time of the pipe based on the maximum principal stress must be calculated. Based on previous practice, the retiral life is 20,000 hours, and the predicted remaining life at that time must be calculated. A recommendation should be made whether the operating life could be safely extended beyond 20,000 hours. Lastly, the gross radial deformation of the pipe is to be monitored and safe inspection intervals must be recommended on the basis of suitable failure criteria.

The material that will be used is a chromium-molybdenum steel. Long term experimental data were obtained by Krisch (1963). Material parameters for this steel are determined in Appendix C and are listed in Table 8.5.

m	k	n	A	B	E
4.926	3.266	0.650	7.833×10^{-46}	3.402×10^{-31}	160×10^{9}
Note : All units are in m/m, Nm^{-2}, and hour					

Table 8.5 : Material parameters for chromium-molybdenum steel

The maximum non-dimensional initial and stationary state results for this problem are listed in Table 7.4, and values for m = 5 will be used here.

For the material parameters and the given loading, using equation (5.7) :

$$\bar{\sigma} = \frac{1}{\alpha} P = 146\text{MPa}$$

and

$$\bar{\varepsilon} = \frac{\bar{\sigma}}{E} = 0.913 \times 10^{-3}\text{mm/mm}$$

At the inner wall (r = 0.7), the lower and upper bound non-dimensional deformation is, from equations (5.27) and (5.29) :

$$U_l = U_e + \dot{U}_{ss}\, \tau$$

and

$$U_u = \gamma\, U_e + U_l$$

Using the values in Table 7.4, and γ at m = 5 as an upper bound :

$$U_l = 0.874 + 0.848\ \tau$$

and

$$U_u = 0.983 + 0.848\ \tau$$

The non-dimensional deformation, U, can be related to the actual deformation, u, using :

$$u = r_1\ \varepsilon\ U$$

where r_1 is the inner radius of the pipe. Then, using mm as the unit of length :

$$u_l = 35x0.913x10^{-3}\ \left(0.874 + 0.848\ \tau\right)$$

and

$$u_u = 35x0.913x10^{-3}\ \left(0.983 + 0.848\ \tau\right)$$

From the material parameters and using equation (5.7) :

$$\tau = A\ E\ \bar{\sigma}^{(m-1)}\ t^n$$

and

$$\tau = 0.0142\ t^{0.650}$$

Expressions for the lower and upper bounds on deformation at the inner wall are then :

$$u_l = 0.0279 + 383.9x10^{-6}\ t^{0.650}$$

and

$$u_u = 0.0314 + 383.9x10^{-6}\ t^{0.650}$$

Figure 8.2 shows plots of the above expressions for times up to 40,000 hours.

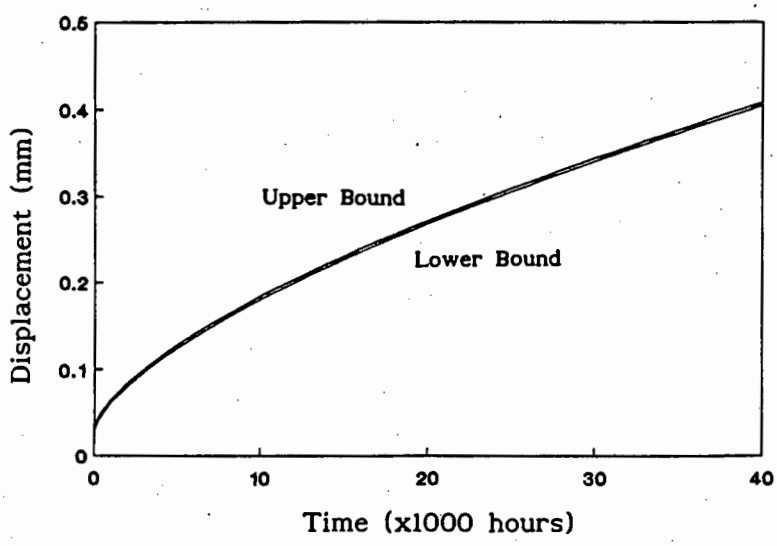

Figure 8.2 : Upper and lower bound deformation history

Similar expressions can be derived for the outer wall :

$$\dot{u}_l = 0.0225 + 269.2\text{x}10^{-6}\ t^{0.650}$$

and

$$u_u = 0.0253 + 269.2\text{x}10^{-6}\ t^{0.650}$$

The maximum stresses can be calculated from the maximum non-dimensional values using equation (5.5) :

$$\Sigma = \frac{\sigma}{\bar{\sigma}}$$

and are listed in Table 8.6.

Stress	Maximum non-dimensional stress	Maximum dimensional stress
σ^{*}_{el}	1.401 at inner wall	204.5 MPa
σ^{*}_{ss}	1.070 at inner wall	156.2 MPa
σ^{I}_{el}	1.200 at inner wall	175.2 MPa
σ^{I}_{ss}	1.086 at outer wall	158.6 MPa

Table 8.6 : Maximum initial and stationary state stresses

Using the maximum principal stress as the equivalent Hayhurst stress for rupture, then from equation (5.30) :

$$C = \frac{B\ \bar{\sigma}^{(1+k-m)}}{A\ E} = 0.0131$$

and

$$\tau_R = \frac{1}{C\ (1+k)\ \left(\Sigma^I_{ss}\right)^k} = 13.671$$

The rupture time can then be calculated using equation (5.7) :

$$t_R = \left(\frac{\tau_R}{A\ E\ \bar{\sigma}^{(m-1)}}\right)^{1/n} \simeq 39{,}000 \text{ hours}$$

The predicted rupture time exceeds the retiral life by 95% and the operation can be extended beyond the previous retiral life. Soderberg (1941) suggested that the stress at the middle of the pipe gives a better estimate of rupture times. The Mean Diameter Formula resulted from this. In this case, from Figure 7.15, the maximum principal stress at the skeletal point is $\Sigma^I_{ss} = 0.978$, from which $\tau_R = 19.243$ and $t_R \simeq 66{,}000$ hours which exceeds the retiral life by 230% . It will thus be beneficial to monitor the gross deformation of the pipe, and to retire the component only when the failure criteria are met.

If the pipe is to be retired no later than about 90% of its useful (normalised) life-time, then for failure criterion 1, and from Figure 6.4, the factor R_1 is 2.0 . This means that the pipe must be retired when the actual displacement at the bore is twice that predicted by stationary creep. For failure criterion 2, from Figure 6.5, the factor R_2 is about 1.75 . The pipe is retired when the actual displacement is 1.75 times the steady-state displacement after 39,000 hours. Lastly, for failure criterion 3, from Figure 6.6, the factor R_3 is 5.0 . The pipe is retired from service when the actual displacement rate is five times the stationary rate. As soon as any of the three criteria is achieved, the pipe must be retired from serviced, or at least subjected to an extensive investigation of the material degradation.

The gross deformation of the pipe must be monitored at regular intervals, and checked against the failure criteria. The inspection intervals must be short

enough that serious overshooting of any criterion is avoided, but not long enough for measurable creep accumulation to occur. The remaining life fraction at retirement is about 10%. If we choose, for example, one third of the remaining life fraction as a safe inspection interval to prevent late detection, then the corresponding interval, τ_{int}, is one third of 10% of the rupture time :

$$\tau_{int} = 0.033\ \tau_R = 0.456$$

and

$$t_{int} \simeq 210 \text{ hours} \simeq 9\text{days}$$

The stationary displacement accumulated in this period is about half the elastic displacement, and is too small to be measured initially. The inspection interval can thus be increased initially but should be reduced as soon as the tertiary stage is encountered.

9 CONCLUSIONS AND RECOMMENDATIONS

A creep analysis procedure has been developed which simplifies current methods, and reduces the number of computer calculations that are required to solve a problem. The analysis is based on the creep and damage laws proposed by Kachanov and Rabotnov.

The creep and damage laws are non-dimensionalised with respect to a convenient normalising stress and strain. As a consequence of this normalisation, the dependence of the creep law on the stress constant and the time and temperature functions is removed for a time hardening assumption. In addition, if the reference stress of the component is chosen as the normalising stress, the creep law becomes insensitive to the stress exponent. By similarly non-dimensionalising the load level, the dependence of the creep analysis on the load level and the actual size of the component is removed, if a geometrically similar model is used in the analysis.

After non-dimensionalising, the damage law remains dependent on the material constants and the load level, albeit not on the time function. For this reason, and to simplify the analysis, the creep and damage laws are decoupled for the purpose of the structural analysis. Consequently, only the creep law needs to be implemented in a finite element scheme, from which a stationary state analysis is extracted.

The results of the stationary state analysis, namely the stresses, strains and displacements, will be non-dimensional values, which are independent of the load level, the time and temperature function, and of the material constants except the stress exponent. However, as the analysis and, therefore, the results are insensitive to the stress exponent, only a small set of computer simulations, covering the usual range of stress exponent values, is required. The non-dimensional results can then be tabulated or otherwise compiled and stored for later use.

The stationary state analysis is unable to make predictions of rupture times directly. The Kachanov/Rabotnov damage laws can be used together with the maximum stationary stresses in the component to give estimates of rupture times. This method must be used prudently, as it will result in

unconservative estimates for statically determinate components since the method does not take high local stresses due to damage into account. For statically determinate structures on the other hand, conservative estimates will result. In this case, high stresses due to local damage can be shed to low stress and damage regions, behaviour not taken into account by the present methods.

To avoid any unconservatism, and to extend the procedure to residual life assessment and damage monitoring, several failure criteria which allow differing degrees of conservatism have been derived from the Kachanov/Rabotnov creep and damage laws. They relate coupled creep/damage strains to stationary state creep strains. The user can choose the required level of conservatism, and components are retired as soon as any of the failure criteria are met. The method is aimed at in situ monitoring of components where the gross deformation can be measured.

The non-dimensional results can be easily converted to dimensional values, without having to re-run a computer simulation. This conversion can be easily repeated over the range of temperatures and load levels applicable to the problem. The method can therefore be used in the early design stages with great economy, where the designer is faced with a large number of uncertain parameters. Usually the designer has to sort out quickly the important from the unimportant parameters. The use of design envelopes is possible using the present method. By varying the parameters of the design, the designer can swiftly focus on the best option, and then start with detailing this design. The concept is illustrated in Figure 9.1 where design 3 is the final design choice as it gives the best compromise.

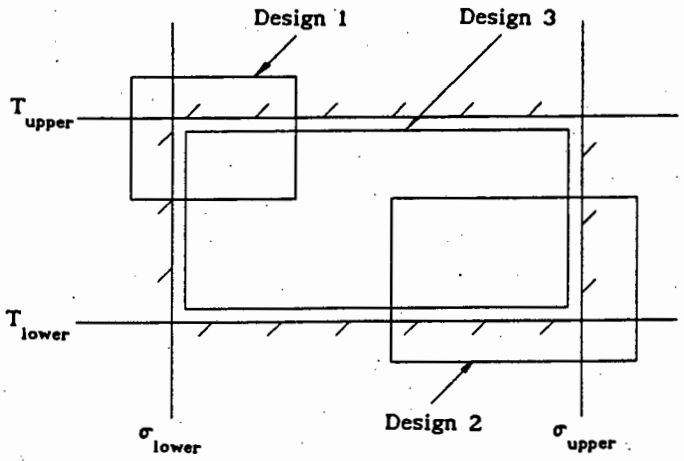

Figure 9.1 : Illustration of design envelopes

The method and procedure are illustrated in a number of simple problems for which experimental, analytical, or numerical results exist. The method is most applicable in early design studies, and in problems where structural calculations are made repetitively. The procedure is economic in terms of computer usage, and is numerically stable.

Further work should be directed towards three main areas, namely :

- To extend the procedure to include varying temperature and load patterns,

- to verify further the rupture prediction methods against experimental results, and to investigate the effects of structural determinacy, and

- to verify experimentally the proposed failure criteria in industrial applications.

10 LIST OF REFERENCES

(1) AINSWORTH, R.A. (1989). *Defect assessment procedures at high temperature*, CEGB Research, Vol. 22, pp. 1-12.

(2) ANDRADE, E.N. (1910). *The viscous flow in metals and allied phenomena*, Proc. Roy. Soc., Vol. 84, pp. 1-12.

(3) BAILEY, R.W. (1935). *The utilization of creep test data in engineering design*, Proc. I. Mech. E., Vol. 131, pp. 131-269.

(4) BENNEWITZ, J.H. (1963). *On the shape of the log stress-log time curve of long time creep-rupture tests*, Paper 69, Joint Int. Conf. on Creep, ASME/ASTM/IMechE, New York/London, pp. 5·81-5·92.

(5) BOGDANOFF, J.L. and KOZIN, F. (1984). *Probabilistic models of cumulative damage*, Wiley, New York.

(6) BOYLE, J.T. and SPENCE, J. (1980). *Some problems in the creep analysis of piping components*, Paper C189/80, Int. Conf. on Eng. Aspects of Creep, IMechE/ASME/JSME/ASTM, Sheffield, pp. 81-88.

(7) CANE, B.J., APLIN, P.F. and BREAR, J.M. (1985). *A mechanistic approach to remanent creep life assessment of low alloy ferritic components based on hardness measurements*, J. Press. Vess. Tech., Vol. 107, pp. 295-300.

(8) CALLADINE, C.R. (1963). *Stress concentration in steady creep : interpolation between solutions in elasticity and plasticity*, Paper 40, Joint Int. Conf. on Creep, ASME/ASTM/ IMechE, New York/London, pp. 2·59-2·68.

(9) CHABOCHE, J.L. (1988). *Continuum damage mechanics: Part 1 - General concepts*, J. Appl. Mech., Vol. 55, pp. 59-64.

(10) DAVIDSON, M.J., JONES, T.J., ROSARD, D.D. and SCHEIBEL, J.R. (1985). *Monitoring for life extension*, J. Press. Vess. Tech., Vol. 107, pp. 255-259.

(11) DORN, J.E. (1955). *Some fundamental experiments on high temperature creep*, J. Mech. Phys. Solids, Vol. 3, No. 2, pp. 85-116.

(12) DRUCKER, D.C. (1967). *Introduction to mechanics of deformable solids*, McGraw-Hill, New York.

(13) FAUPEL, J.H. and FISHER, F.E. (1981). *Engineering design: a synthesis of stress analysis and materials engineering*, Wiley, New York.

(14) GAROFALO, F. (1965). *Fundamentals of creep and creep rupture in metals*, MacMillan Series in Materials Science, Macmillan, New York.

(15) GOLDHOFF, R.M. (1965). *Uniaxial creep rupture behaviour of low alloy steel under variable loading conditions*, J. Basic Eng., Vol. 87, No. 2, pp. 374-379.

(16) GOOCH, D.J. (1988). *How much longer - Remanent life assessment of high temperature components*, CEGB Research, No. 21, pp. 60-67.

(17) GRAHAM, A. and WALLES, K.F.A. (1955). *Relations between long and short time properties of a commercial alloy*, J. Iron and Steel Inst., Vol. 179, pp. 105-120.

(18) GREENWOOD, G.W., JONES, H. and STRITHARAN, T. (1980). *Some mechanistic conditions affecting the extrapolation of creep data*, Paper C187/80, Int. Conf. on Eng. Aspects of Creep, IMechE/ASME/JSME/ASTM, Sheffield, pp. 77-84.

(19) HARTH, G.H. and SHERLOCK, T.P. (1985). *Monitoring the service-induced damage in utility boiler pressure vessels and piping systems*, J. Press. Vess. Tech., Vol. 107, pp. 226-229.

(20) HAYHURST, D.R. (1970). *Isothermal creep deformation and rupture of structures*, Ph. D. Thesis, Univ. Cambridge.

(21) HARRISON, G.F. and TILLEY, G.P. (1973). *Static and cyclic creep propertiesof three forms of a cast Nickel alloy*, Paper C222/73, Int. Conf. on Creep and Fatigue in Elevated Temperature Applications, IMechE/

ASME, Philadelphia, pp. 222·1-222·9.

(22) HENDERSON, J. and FERGUSON, F.R. (1980). *Assessment of the reference stress method by complex torsional creep tests*, Paper C245/80, Int. Conf. on Eng. Aspects of Creep, IMechE/ASME/JSME/ASTM, Sheffield, 1980, pp. 105-114.

(23) HEPWORTH, J.K. and WILLIAMS, J.A. (1987). *The assessment of remanent creep life estimation using full size component tests*, Paper C290/87, Conf. on Refurbishment and Life Extension of Steam Plant, IMechE, London, pp. 237-247.

(24) HIBBIT, KARLSON and SORENSEN Inc. (1988). *ABAQUS User Manual Version 4.7*, Providence, Rhode Island.

(25) HILL, R. (1964). *The mathematical theory of plasticity*, Clarendon Press, Oxford.

(26) HULT, J.A.H. (1966). *Creep in engineering structures*, Blaisdell, Waltham (Mass.).

(27) HYDE, T.H. and WEBSTER, J.J. (1980). *Assessment of some methods for predicting creep deformations and life of components*, Paper C192/80, Int. Conf. on Eng. Aspects of Creep, IMechE/ASME/JSME/ASTM, Sheffield, 1980, pp. 73-80.

(28) IWADATE, T., WATANABE, J. and TANAKE, Y. (1985). *Prediction of the remaining life oh high-temperature/pressure reactors made of Cr-Mo steels*, J. Press. Vess. Tech., Vol. 107, pp. 230-238.

(29) JASKE, C.E. (1985). *Predicting the residual life of plant equipment - Why worry?*, J. Press. Vess. Tech., Vol 107, pp. 213-216.

(30) JOHNSON, A.E., HENDERSON, J. and KHAN, B. (1963). *Multiaxial creep strain/complex stress/time relations for metallic alloys with some applications to structures*, Paper 26, Joint Int. Conf. on Creep, ASME/ ASTM/IMechE, New York/London, pp. 2·27-2·42.

(31) KACHANOV, L.M. (1958). *On rupture times under conditions of creep*, Izvestia Akademi Nauk SSR, Otd. Tekhn. Nauk, Vol. 8, pp. 26-31.

(32) KENNEDY, A.J. (1962). *Processes of creep and fatigue in metals*, Oliver and Boyd, London.

(33) KRAUS, H. (1976). *Reference stress concepts for creep analysis*, Final Report to the Subcommittee on Elevated Temperature Design of the Pressure Vessel Research Committee.

(34) KRAUS, H. (1980). *Creep analysis*, Wiley, New York.

(35) KRISCH, A. (1963). *Creep behaviour, structural changes and cracks observed in creep rupture tests lasting several years*, Paper 62, Joint Int. Conf. on Creep, ASME/ASTM/ IMechE, New York/London, pp. 1·81-1·90.

(36) MACKENZIE, A.C. (1968). *On the use of a single uniaxial test to estimate deformation rates in structures undergoing creep*, Int. J. Mech. Sci., Vol. 10, No. 5, pp. 441-453.

(37) MATSUDA, F. and FUJIKAWA, T (1980). *Reference stress approach for estimating creep strain of tapered cylindrical vessels*, Paper C241/80, Int. Conf. on Eng. Aspects of Creep, IMechE/ASME/JSME/ASTM, Sheffield, pp. 51-56.

(38) McVETTY, P.G. (1943). *Creep of metals at elevated temperatures - the hyperbolic sine relation between stress and creep rate*, Trans. A.S.M.E., Vol. 65, pp. 761-769.

(39) MILLER, A.G. (1988). *Review of limit loads of structures containing defects*, Int. J. Press. Vess. and Piping, Vol. 32, pp. 197-327.

(40) MLYNARSKI, F. and TALER, J. (1988). *Residual life assessment for boiler pressure components based on measurements of creep strains*, J. Press. Vess. Tech., Vol. 110, pp. 308-313.

(41) NADAI, A. (1963). *Theory of flow and fracture in solids*, Vol. 2, McGraw-Hill, New York.

(42) NEEDHAM, N.G. and GLADMAN, T. (1980). *The effect of stress-state on the processes controlling creep fracture in a 2.5%Cr1%Mo steel*, Paper C190/80, Int. Conf. on Eng. Aspects of Creep, IMechE/ASME/JSME/ASTM, Sheffield, pp. 49-54.

(43) NORTON, F.H. (1929). *The creep of steel at high temperatures*, McGraw-Hill.

(44) ODQVIST, F.K.G. (1966). *Mathematical theory of creep and creep rupture*, Clarendon Press, Oxford.

(45) PAYNE, C. (1979). *Numerical calculations of creep and creep rupture in axisymmetric thin shells*, Ph. D. Thesis, Univ Liverpool.

(46) PENNY, R.K. (1974). *The usefulness of engineering damage parameters during creep*, J. Metals and Materials, Vol. 8, pp. 278-283.

(47) PENNY, R.K. and HAYHURST, D. (1969), *The deformations and stresses in a stretched thin plate containing a hole during stress redistribution caused by creep*, Int. J. Mech. Sci., Vol. 11, pp. 23-39.

(48) PENNY, R.K. and MARRIOTT, D.L. (1971). *Design for creep*, McGraw-Hill, London.

(49) PENNY, R.K. and MARRIOTT, D.L. (1973). *Creep of pressure vessels*, Paper C204/73, Int. Conf. on Creep and Fatigue in Elevated Temperature Applications, IMechE/ASME/ASTM, Philadelphia, pp. 204·1-204·9.

(50) PENNY, R.K. and SIM, R.G. (1967). *Time-dependent creep of plates and pressure containers*, Paper 11/67, Int. Conf. on Pressure Vessel Design, KIVI/ASME, Delft, pp. 845-859.

(51) PRANDTL, L. (1924). Proc. 1st Int. Cong. App. Mech., Delft, Vol. 43, pp. 89-95.

(52) PRICE, A.T. and ALBERRY, P.J. (1988). *Welding - the critical link*, CEGB Research, No. 21, pp. 15-25.

(53) RABOTNOV, Yu.N. (1969). *Creep problems in structural members*, North-Holland Publ. Co., Amsterdam.

(54) SCHULTE, C.A. (1960). *Predicting creep deflections of plastic beams*, Proc. A.S.T.M., Vol. 60, pp. 895-904.

(55) SESHADRI, R. (1988). *Design and life prediction of fired heater tubes in the creep range*, J. Press. Vess. Tech., Vol. 110, pp. 322-328.

(56) SIEBURG, H. (1989). *Creep predictions for turbomachinery components*, M. Sc. Thesis, Univ Cape Town.

(57) SIM, R.G. (1968). *Creep of structures*, Ph. D. Thesis, Univ Cambridge.

(58) SIM, R.G. and PENNY, R.K. (1971). *Plane strain creep behaviour of thick-walled cylinders*, Int. J. Mech. Sci., Vol. 13, pp. 987-1009.

(59) SIMONEN, F.A. and JASKE, C.E. (1985). *A computational model for predicting the life of tubes used in petrochemical heater service*, J. Press. Vess. Tech., Vol. 107, pp. 239-246.

(60) SODERBERG, C.R. (1936). *The interpretation of creep tests for machine design*, Trans. A.S.M.E., Vol. 58, pp. 733-741.

(61) SODERBERG, C.R. (1941. *Interpretation of creep tests on tubes*, Trans. A.S.M.E., Vol. 63, pp. 737-748.

(62) SULLY, A.H. (1949). *Metallic creep and creep resistant alloys*; Butterworths Scientific Publ., London.

(63) *Superalloys II* (1984), Ed. Sims, C.T., Stolloff, N.N. and Hagel, W.C., Wiley, New York.

(64) TAIRA, S. (1973). *Relationship between thermal fatigue and low cycle fatigue at elevated temperatures*, Special Technical Publication, A.S.T.M.

(65) VISWANATHAN, R. (1985). *Dissimilar metal weld and boiler creep damage evaluation for plant life extension*, J. Press. Vess. Tech., Vol. 107, pp. 218-225.

(66) VISWANATHAN, R., DOOLEY, R. and SAXENA, A. (1988). *A methodology for evaluating the integrity of longitudinally seam-welded steam pipes in fossil plants*, J. Press. Vess. Tech., Vol. 110, pp. 283-290.

(67) WICKENS, A., STRANG, A. and OAKES, G. (1980). *High temperature properties of creep resistant 12Cr steam turbine blading steels*, Paper C217/80, Int. Conf. on Eng. Aspects of Creep, IMechE/ASME/JSME/ASTM, Sheffield, pp. 11-18.

(68) WOODFORD, D.A. (1973). *A critical assessment of the life fraction rule for creep-rupture under nonsteady stress or temperature*, Paper C180/73, Int. Conf. on Creep and Fatigue in Elevated Temperature Applications, IMechE/ASME/ASTM, Philadelphia, pp. 180·1-180·6.

(69) ZIENKIWICZ, O.C. (1977). *The finite element method*, McGraw-Hill, London.

APPENDIX A : SUMMARY OF THE FINITE ELEMENT METHOD

This Appendix will give a summary of the finite element method (F.E.M.) as applied to a stationary state creep analysis. The discussion assumes that the reader is familiar with the usual F.E.M. terminology and will describe the various steps in the matrix displacement method. The matrix terminology is the same as used in Zienkiwicz (1977).

The initial loading problem must be solved first. The existence of any initial strains due plasticity, creep, thermal variation and so on is taken into account in the formulation by the matrix $\{\varepsilon_1\}$. In the notation that follows it should be carefully noted that :

Superscript e refers to element quantities.
Subscript e refers to elastic quantities.
Primed quantities refers to local element coordinates.

The procedure is as follows :

(a) Relate element strains $\left\{ \varepsilon^e \right\}$ to element nodal displacements $\left\{ \delta^{e'} \right\}$ using a convenient local set of coordinates $\left\{ x' \right\}$:

$$\left\{ \varepsilon^e \right\} = \left[B \right] \left\{ \delta^{e'} \right\} \tag{A.1}$$

where $\left[B \right]$ is the strain-displacement matrix.

(b) Relate element stresses $\left\{ \sigma^e \right\}$ to element strains :

$$\left\{ \sigma^e \right\} = \left[D \right] \left\{ \varepsilon_e \right\} = \left[D \right] \left(\left\{ \varepsilon^e \right\} - \left\{ \varepsilon_1 \right\} \right) \tag{A.2}$$

where $\left\{ \varepsilon_1 \right\}$ are any initial strains, and $\left[D \right]$ is the stress-strain matrix.

(c) Construct element force/displacement equations in local coordinates :

$$\left\{ F^{e'} \right\} = \left[k^{e'} \right] \left\{ \delta^{e'} \right\} - \left\{ F'_1 \right\} \tag{A.3}$$

where $\left\{ F^{e'} \right\}$ are the nodal forces,

$$\left[k^{e'} \right] = \int_{element} \left[B \right]^T \left[D \right] \left[B \right] d(vol.)$$

is the element stiffness matrix, and

$$\left\{ F^{e'} \right\} = \int_{element} \left[B \right]^T \left[D \right] \left\{ \varepsilon_1 \right\} d(vol.)$$

(d) Construct a transformation matrix $\left[T \right]$ to relate local to global coordinates :

$$\left\{ x' \right\} = \left[T \right] \left\{ x \right\} \qquad (A.4)$$

The same transformation holds for forces and displacements,

$$\left\{ F^{e'} \right\} = \left[T \right] \left\{ F^{e} \right\} ; \left\{ \delta^{e'} \right\} = \left[T \right] \left\{ \delta^{e} \right\}$$

(e) Transform element force/displacement equations into global coordinates

$$\left\{ F^{e} \right\} = \left[k^{e} \right] \left\{ \delta^{e} \right\} - \left\{ F_1^{e} \right\} \qquad (A.5)$$

where

$$\left[k^{e} \right] = \left[T \right]^T \left[k^{e'} \right] \left[T \right]$$

(f) Combine element equations to form force/displacement equations for element assembly :

$$\left\{ F \right\} = \left[k \right] \left\{ \delta \right\} - \left\{ F_1 \right\} \qquad (A.6)$$

where

$\left[k \right]$ is the sum of all the $\left[k^{e} \right]$

(g) Specify the boundary conditions and reduce the global force/displacement equations as far as possible.

(h) Solve the reduced form of equation (A.6) to find :

$$\left\{ \delta \right\} = \left[k \right]^{-1} \left(\left\{ F \right\} + \left\{ F_1 \right\} \right) \qquad (A.7)$$

(i) From equations (A.1), (A.3), and (A.7) find the stresses in terms of the nodal displacements for each element :

$$\left\{ \sigma^e \right\} = \left[D \right] \left(\left[B \right] \left[T \right] \left\{ \delta^e \right\} - \left\{ \varepsilon_1 \right\} \right) \qquad (A.8)$$

Equations (A.7) and (A.8) are the solutions to the initial loading problem

(j) To begin the rate problem, first calculate the creep strain rates, $\left\{ \dot{\varepsilon}_c \right\}$, using the usual multiaxial creep laws.

(k) Calculate deflection and stress rates using steps (a) to (i), with replacement of all terms with their rates. In particular, for creep $\left\{ \varepsilon_1 \right\}$ becomes $\left\{ \dot{\varepsilon}_c \right\}$.

(l) Solve the resulting load rate/displacement rate equation :

$$\left\{ \dot{\delta} \right\} = \left[k \right]^{-1} \left\{ \dot{F} \right\} \qquad (A.9)$$

(m) Calculate the strain rates and stress rates from :

$$\left\{ \dot{\varepsilon}^e \right\} = \left[B \right] \left[T \right] \left\{ \dot{\delta}^e \right\} \qquad (A.10)$$

$$\left\{ \dot{\sigma}^e \right\} = \left[D \right] \left(\left[B \right] \left[T \right] \left\{ \dot{\delta}^e \right\} - \left\{ \dot{\varepsilon}_1 \right\} \right) \qquad (A.11)$$

(n) Choose a small time interval $\Delta\tau$ and calculate quantities at the end of the interval, for instance :

$$\left\{ \sigma^e \right\}_{\tau+\Delta\tau} = \left\{ \sigma^e \right\}_{\tau} + \left\{ \dot{\sigma}^e \right\} \Delta\tau, \text{ etc.} \qquad (A.12)$$

(o) Repeat steps (i) to (n) for successive time increments until a stationary state is achieved.

APPENDIX B : DERIVATION OF NORMALISED MULTIAXIAL CREEP EQUATIONS

The multiaxial mixed hardening creep rate equation is, from equation (3.34) :

$$\frac{d\varepsilon_{ij,c}}{dt} = n\, K^a\, e^{-Qa/RT}\, \sigma^{*ma}\, t^{na-1}\, \varepsilon^{*1-a}\, \frac{d\sigma^*}{d\sigma_{ij}} \qquad (B.1)$$

Normalise the stresses and strains in the usual manner :

$$\Sigma = \frac{\sigma}{\sigma} \quad ; \quad \lambda = \frac{\varepsilon}{\varepsilon} \quad ; \quad E = \frac{\sigma}{\varepsilon} = \frac{\sigma_o}{\varepsilon} \qquad (B.2)$$

where σ_o is a conveniently chosen reference stress. Then :

$$\frac{d\lambda_{ij,c}}{dt} = n\, K^a\, E^a\, e^{-Qa/RT}\, \sigma_o^{(m-1)a}\, t^{na-1}\, \Sigma^{*ma}\, \lambda^{*1-a}\, \frac{d\Sigma}{d\Sigma_{ij}} \qquad (B.3)$$

Transforming the time measure from t to τ :

$$\frac{d\lambda_{ij,c}}{d\tau}\,\frac{d\tau}{dt} = n\left(K\, E\, e^{-Q/RT}\, \sigma_o^{m-1}\right)^a t^{na-1}\, \Sigma^{*ma}\, \lambda^{*1-a}\, \frac{d\Sigma^*}{d\Sigma_{ij}} \qquad (B.4)$$

Letting

$$\frac{d\tau}{dt} = n\left(K\, E\, e^{-Q/RT}\, \sigma_o^{m-1}\right)^a t^{na-1} \qquad (B.5)$$

whence, integrating (B.5) :

$$\tau = a\left(K\, E\, e^{-Q/RT} \sigma^{m-1}\, t^n\right)^a \qquad (B.6)$$

Substituting (B.5) into (B.4)

$$\frac{d\lambda_{ij,c}}{d\tau} = \Sigma^{*ma}\, \lambda^{*1-a}\, \frac{d\Sigma^*}{d\Sigma_{ij}} \qquad (B.7)$$

APPENDIX C : CALCULATION OF MATERIAL CONSTANTS FROM EXPERIMENTAL DATA

The procedure for extracting material constants from experimental results is an iterative one and usually only a *best fit* of the constants is possible. In this appendix a possible procedure is proposed and is illustrated by determining material parameters from long term experimental results from Krisch (1963). The material parameters are used in Case Study 3.

Krisch gives creep and rupture curves for a chromium-molybdenum steel at temperature 500°C over a range of stresses. The region of interest is confined to the range 15 to 18 kg/mm^2. In these calculations though, the units are in m/m for strain, Nm^{-2} for stress and hour for time, and the data in Krisch are adjusted as appropriate.

The uniaxial creep and coupled creep/damage equations are given in equations (4.4), (4.5), and (4.6) :

$$\frac{d\varepsilon_c}{dt} = n\, A\, \sigma_N^m\, t^{n-1} \qquad (C.1)$$

$$\frac{d\varepsilon_{cd}}{dt} = n\, A\, \frac{\sigma_N^m}{(1-\omega)^p}\, t^{n-1} \qquad (C.2)$$

and

$$\frac{d\omega}{dt} = n\, B\, \frac{\sigma_N^k}{(1-\omega)^r}\, t^{n-1} \qquad (C.3)$$

where A, B, m, p, k, r, and n are material constants and σ_N is the nominal stress. As a first assumption, let p = k = r in order to reduce the number of unknowns. This simplification is used by many workers (Penny,1974; Payne,1979; Sieburg, 1989). Equations (C.2) and (C.3) then become :

$$\frac{d\varepsilon_{cd}}{dt} = n\, A\, \frac{\sigma_N^m}{(1-\omega)^k}\, t^{n-1} \qquad (C.4)$$

and

$$\frac{d\omega}{dt} = n\ B\ \frac{\sigma_N^k}{(1-\omega)^k}\ t^{n-1} \qquad (C.5)$$

Integrate (C.5) to obtain :

$$t_R = \left(\frac{1}{B\ (1+k)\ \sigma_N^k} \right)^{1/n} \qquad (C.6)$$

Rewrite (C.6) to obtain :

$$\log \sigma_N = \frac{1}{k} \log \left(\frac{1}{B\ (1+k)} \right) - \frac{n}{k} \log t_R \qquad (C.7)$$

Equation (C.7) predicts a linear relationship between log(nominal stress) and log(rupture time), behaviour found in most experimental data, although usually only over limited stress ranges.

From equation (C.1) an expression for the minimum creep rate can be found :

$$\left(\frac{d\varepsilon_c}{dt} \right)_{min} = n\ A\ \sigma_N^m\ t_{ss}^{n-1} \qquad (C.8)$$

where t_{ss} is the time to reach stationary state. Equation (C.8) can be rewritten :

$$\log \sigma_N = -\frac{1}{m} \log \left(n\ A\ t_{ss}^{n-1} \right) + \frac{1}{m} \log \left(\frac{d\varepsilon_c}{dt} \right)_{min} \qquad (C.9)$$

Figure C.1 from Krisch can be used to calculate minimum creep strain rates. When log(nominal stress) versus log(minimum creep strain rate) is plotted, as in Figure C.2, a straight line results. The slope of the line can be found whence a value for m can be calculated using equation (C.9). Here the slope is :

$$\frac{1}{m} = \frac{\log 181.5\times10^{6} - \log 113.8\times10^{6}}{\log 10\times10^{-7} - \log 1\times10^{-7}} = 0.203$$

whence

$$m = 4.926$$

Krisch gives a plot of log(nominal stress) versus log(rupture time). Figure C.3 superposes a straight line on Krisch's results over the region of interest. Using equation (C.7) the slope of this line is :

$$-\frac{n}{k} = \frac{\log 131.5\times10^{6} - \log 392.4\times10^{6}}{\log 100000 - \log 400} = -0.199$$

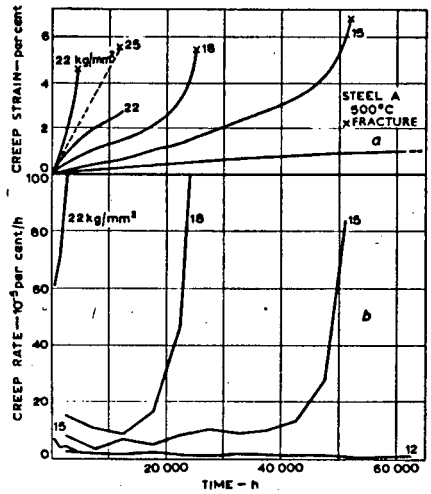

Figure C.1 : Creep experimental data from Krisch (1963)

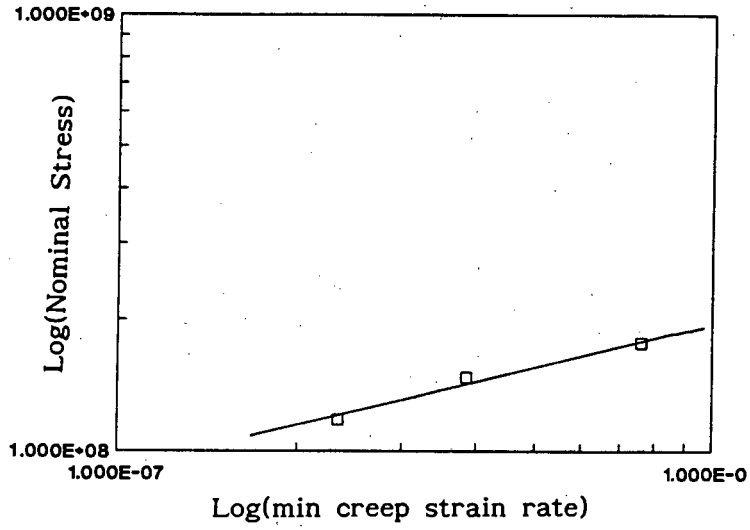

Figure C.2 : Plot log(min creep strain rate) versus log(rupture time)

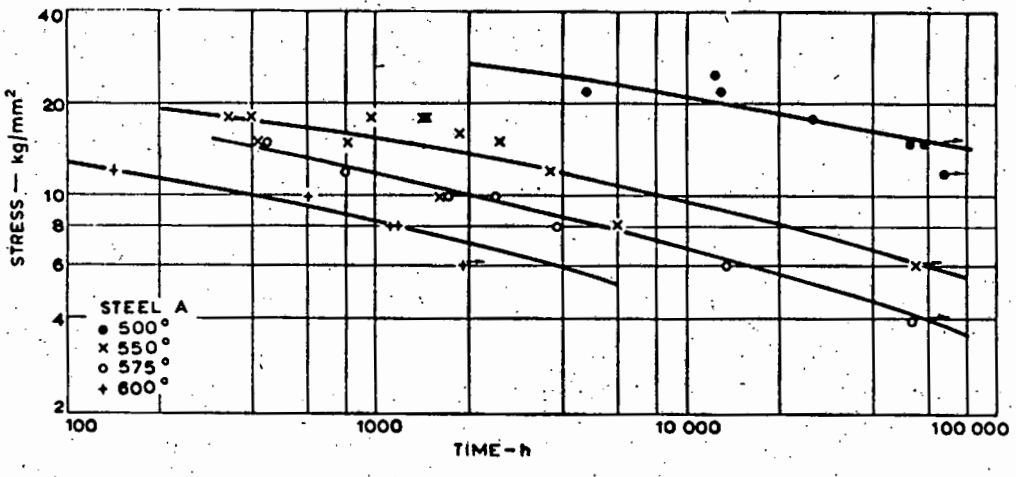

Figure C.3 : Plot log(stress) versus log(rupture time) from Krisch (1963)

At this point the iterative process starts. In this method a value for n is chosen, and values for A, k, and B are calculated using equations (C.7) and (C.9). These values are then used to predict stationary creep curves and rupture times, which are compared to measured curves and rupture times. A new value for n is chosen, and the process is repeated until the predicted values compare best with the measured values.

Bailey (1935) found that usually $\frac{1}{3} \leq n \leq \frac{1}{2}$, so the process was started with n = 0.3. It was found however that for the stress range 150MPa to 200MPa, the best result occurred at n = 0.650 . This gave that k = 3.266, from which :

$$\frac{k}{m} = 0.663$$

which is consistent with Penny (1974). The actual values for m and k are consistent with Odqvist (1966). The resulting constants from Krisch's data are shown in Table C.1 :

m	k	n	A	B	E
4.926	3.266	0.650	7.833×10^{-46}	3.402×10^{-31}	160×10^{9}
Note : All units are in m/m, Nm^{-2}, and hour					

Table C.1 : Material parameters for chromium-molybdenum steel at 500°C and stress range 150 - 200 MPa

These values are substituted in the creep and damage equations, and the predicted and measured minimum creep strain rates and rupture times are shown in Table C.2 .

Load (kg/mm^2)	Predicted		Measured	
	$\dot{\varepsilon}_{min}$ ($hour^{-1}$)	t_R (hour)	$\dot{\varepsilon}_{min}$ ($hour^{-1}$)	t_R (hour)
15	3.483×10^{-7}	56,720	3.841×10^{-7}	51,600
18	8.541×10^{-7}	22,717	7.589×10^{-7}	25,000

Table C.2 : Comparison of predicted and measured rupture times

The predictions are in error by about 10% and are the best predictions from a number of trials where the relationship between m and k is allowed to vary between the bounds given above.

APPENDIX D : RESULTS TO COURSES COMPLETED

Courses completed in partial fulfillment of the M.Sc. Degree

COURSE	DATE	SYMBOL	CREDITS
AMA363F Numerical Analysis	1988	2+	3
AMA367F Continuum Mechanics	1988	2+	3
CIV540F Finite Element Analysis	1988	2+	4
CIV588F Applied Mechanics I	1988	2+	3
CIV589S Applied Mechanics II	1988	2+	3
END500Z Technology & Development	1988	2+	5
END524Z Engineering Software Design & Devel	1989	2+	3
		TOTAL	24

Minimum number of course credits required : 20

Course Descriptions

AMA363F Numerical Analysis

Numerical methods of solution of ordinary differential equations ; approximations to functions ; eigenvalue methods. Modeling examples.

AMA367F Continuum Mechanics

Tensor algebra and analysis ; fluid and solid mechanics ; Navier-Stokes equations ; the partial differential equations of elasticity ; examples.

CIV540F Finite Element Analysis

Generalised displacement method of analysis. Elastic energy theorems leading to basic procedures of the finite element method. Approximation and interpolation of functions. Isoparametric formulation of elements. 2-D and 3-D elements of structural mechanics. Equation solving in the computer and the structure of the finite element program. Introduction to finite element

packages for practical applications. Some advanced topics in finite element analysis.

CIV588F Applied Mechanics I

Concepts of stress, strain, compatibility. Equilibrium equations and constitutive relationships. Applications to beams, rods, plates and two-dimensional elasticity. Solutions of simple boundary value problems on plane stress/strain and plates. Energy concepts in mechanics.

CIV589S Applied Mechanics II

Variational calculus and variational principles in mechanics ; virtual work, minimum potential energy, Reissner. Methods of approximation leading to the finite element method applied to plates and shells. Potential problems. Topics in nonlinear mechanics - plasticity, geometric nonlinearity, creep.

END500Z Technology and Development

Introduction to theory of economic development and technological change ; concept of appropriate technology, critique ; neo-classical theory of of choice of technique ; growth and modernisation theories, Rostow's stages of growth ; structuralists and dependency schools, technological dependence ; Marxist theories of technology and development ; basic needs and AT ; endogenous technological innovation ; impact of aid programs on the choice of technology ; country and project case studies.

END524Z Engineering Software Design & Development

Microcomputer hardware components, DOS operating system, software design methodologies, modularity and information hiding, logic and decision tables, data abstraction and file handling. Testing and debugging. Man-machine interface and computer graphics. Project management and documentation. Software tools and packages. Numerical representation and accuracy